Titre: Title:	Uncertainty Estimation in Indirect Calibration of Five-Axis Machine Tools
Auteur: Author:	Anna Los
Date:	2017
Type:	Mémoire ou thèse / Dissertation or Thesis
Référence: Citation:	Los, A. (2017). Uncertainty Estimation in Indirect Calibration of Five-Axis Machine Tools [Thèse de doctorat, École Polytechnique de Montréal]. PolyPublie. https://publications.polymtl.ca/2559/

UNIVERSITÉ DE MONTRÉAL

UNCERTAINTY ESTIMATION IN INDIRECT CALIBRATION OF FIVE-AXIS MACHINE TOOLS

ANNA LOS

DÉPARTEMENT DE GÉNIE MÉCANIQUE

ÉCOLE POLYTECHNIQUE DE MONTRÉAL

THÈSE PRÉSENTÉE EN VUE DE L'OBTENTION

DU DIPLÔME DE PHILOSOPHIAE DOCTOR

(GÉNIE MÉCANIQUE)

MAI 2017

UNIVERSITÉ DE MONTRÉAL

ÉCOLE POLYTECHNIQUE DE MONTRÉAL

Cette thèse intitulée :

UNCERTAINTY ESTIMATION IN INDIRECT CALIBRATION OF FIVE-AXIS MACHINE TOOLS

présentée par : LOS Anna

en vue de l'obtention du diplôme de : Philosophiae Doctor

a été dûment acceptée par le jury d'examen constitué de :

M. BARON Luc, Ph. D., président

M. MAYER René, Ph. D., membre et directeur de recherche

M. KHAMENEIFAR Farbod, Ph. D., membre

M. ARCHENTI Andreas, Ph. D., membre externe

DEDICATION

“Normal people... believe that
if it ain't broke, don't fix it.

Engineers believe that
if it ain't broke, it doesn't have enough features yet.”

Scott Adams

ACKNOWLEDGEMENTS

Firstly, I would like to express my deepest gratitude to my advisor Prof. René Mayer for the continuous support of my Ph. D. study and related research, for his patience, motivation, and immense knowledge.

My sincere thanks goes to my thesis committee: Prof. Andreas Archenti, Prof. Luc Baron, Prof. Farbod Khameneifar and Prof. Guillaume-Alexandre Bilodeau, for their time, insightful comments and their acceptance to join the jury.

I would like to thank Guy Gironne and Vincent Mayer, CNC technicians, and François Ménard, CMM technician, for their assistance at Virtual Manufacturing Research Laboratory (LRFV) in Polytechnique Montréal.

I am also grateful to the NSERC Canadian Network for Research and Innovation in Machining Technology (CANRIMT) for funding this PhD research.

I would like to thank my fellow doctoral students for their feedback, cooperation and of course friendship: Tibet Erkan, Najma Alami-Mchichi, Maryam Aramesh, Michal Rak, Mehrdad Givi and Elie Bitar-Nehme.

I would like to express my gratitude to my family and friends, with special thanks to Anna and Marek Balazinski, for always being there for me.

Last but not the least, I would like to thank my friend and love Xavier Rimpault for his endless support and always believing in me.

RÉSUMÉ

La calibration de machine-outil est un processus critique qui vise à maintenir la précision de la machine et, par conséquent, la qualité d'usinage aux niveaux requis. Différentes méthodes de mesures et instruments sont utilisés pour acquérir l'information de la géométrie de la machine. Les résultats de calibration sont exploités pour corriger et compenser les erreurs de la machine. Ainsi, ils devraient être évalués par rapport à leur incertitude.

Dans cette thèse, la méthode de calibration de l'artefact de l'échelle et des billes de référence (SAMBA) est estimée au travers de son incertitude. L'exécution de SAMBA nécessite de palper l'artefact non-calibré sous différentes indexations des axes de rotation de la machine et la barre d'échelle au moins une fois. Le calcul du centre des billes, introduit au sein du modèle cinématique de la machine, permet d'estimer les paramètres d'erreur géométrique de la machine (grandeur de sortie). La méthode proposée de l'estimation d'incertitude prend en compte que la calibration analysée a un modèle à entrées multiples et sorties multiples ainsi qu'une solution itérative. Ainsi, le Guide pour l'Expression de l'incertitude de mesure Supplément 2 (GUM S2) est suivi.

L'incertitude du palpage (grandeur d'entrée) est évaluée au travers de mesures répétées, ce qui permet de calculer les incertitudes types, la covariance et la fonction de densité de probabilité (PDF). Cette incertitude inclue la machine (mesurandes), le palpeur et les incertitudes de l'artefact. De sorte à inclure la performance de la machine dans le bilan d'incertitude, les mesures répétées sont effectuées avec différentes conditions préalables de calibration (avec et sans cycle de réchauffement) sur 24 heures. À l'étape suivante de la recherche, les variations à court et moyen terme dans la mesurande sont analysées en exécutant des mesures répétées de SAMBA sur cinq jours. L'incertitude d'entrée est propagée aux paramètres géométriques de la machine grâce à la méthode de Monte Carlo (MCM). L'incertitude de sortie est estimée avec la structure d'incertitude complète (incertitudes types et covariance) et avec les incertitudes estimées étendues, et avec le facteur d'élargissement approprié pour un modèle à multiples sorties. Le cadre de travail général sur l'incertitude - une alternative au long processus de la MCM - est appliqué en utilisant le Jacobien et validé avec la MCM.

Les recherches menées montrent que les résultats de calibration dépendent de la performance de la machine et de ses variations se produisant dans le temps et à cause de différentes conditions environnementales. Cet impact est montré par les différents types des incertitudes estimées. De

cette façon, le comportement de la machine est inclus dans le résultat de calibration, qui à lui seul, reflète l'état de la machine seulement au moment de la calibration.

ABSTRACT

Machine tool calibration is a critical process to maintain the machine precision and, therefore, the machining quality at the required levels. Different measuring methods and devices are used to acquire information about machine geometry. The calibration results are used to correct and compensate the machine errors. Thus, they should be evaluated through their uncertainty.

In this thesis, the scale and master balls artefact (SAMBA) calibration method is evaluated through its uncertainty. Conducting SAMBA requires probing the uncalibrated artefact in different machine rotary axes indexations and the scale bar at least one. The calculated balls centers introduced in the machine kinematic model allow estimating the machine geometric error parameters (output quantity). The proposed uncertainty estimation method takes into account that the analyzed calibration has a multi-input multi-output model and an iterative solution, which prevents from applying traditional uncertainty estimation techniques. Thus, the Guide to the Expression of Uncertainty in Measurement Supplement 2 (GUM S2) is followed.

The probing (input quantity) uncertainty is estimated through the repeated measurement, which allows calculating its standard uncertainties, covariance and probability density function (PDF). This uncertainty includes the machine (measurand), probe and the artefact uncertainties. In order to include the machine performance in the uncertainty budget, the repeated measurements are conducted with different calibration pre-conditions (with and without the warm-up cycle) over 24 hours. In the next stage of research, the short- and medium-term variations in measurand are analyzed by conducting SAMBA repeated measurement over five days. The input uncertainty is propagated on the machine geometric error parameters through the Monte Carlo method (MCM). The output uncertainty is estimated with its full uncertainty structure (standard uncertainties and covariance) and expanded uncertainties estimated with the appropriate, for a multi-output model, coverage factor. The GUM uncertainty framework (GUF) - alternative to the time-consuming MCM - is applied using the numerical Jacobian and validated with MCM.

The conducted research depicts that the calibration results depend on the machine performance and its variations occurring in time and due to the different environmental conditions. This impact is demonstrated by the different types of uncertainties estimated. That way the machine “behavior” is included in the calibration result, which alone reflects the machine state only at the moment of calibration.

TABLE OF CONTENTS

LIST OF TABLES

LIST OF FIGURES

LIST OF SYMBOLS AND ABBREVIATIONS

Abbreviations

ANOVA	Analysis of variance
ASME	American Society of Mechanical Engineers
BIMP	Bureau International des Poids et Mesures
CMM	Coordinate measuring machine
CNC	Computer numerical control
GUM	Guide to the Expression of Uncertainty in Measurement
GUM S1	Guide to the Expression of Uncertainty in Measurement Supplement 1
GUM S2	Guide to the Expression of Uncertainty in Measurement Supplement 2
GUF	GUM uncertainty framework
HTM	Homogeneous Transformation Matrices
ISO	International Organization for Standardization
JCGM	Joint Committee for Guides in Metrology
MC	Monte Carlo
MCM	Monte Carlo method
MIMO	Multi-input multi-output
PDF	Probability density function
RUMBA	Reconfigurable uncalibrated master ball artefact
SAMBA	Scale and master balls artefact

Symbols

B	Machine rotary axis around Y
b	Machine bed
b	Indexation of B-axis

C	Machine rotary axis around Z
c	Indexation of C-axis
C_1	Machine spindle
$\boldsymbol{C_x}$	Sensitivity matric associated with input quantity
$\boldsymbol{d}$	Initial dimension of artefact
d	Validation parameter
$\boldsymbol{e_v}$	Volumetric error
E_{AOB}	Out-of-squareness of the B-axis relative to the Z-axis
E_{COB}	Out-of-squareness of the B-axis relative to the X-axis
E_{XOC}	Distance between the B and C axes
E_{AOC}	Out-of-squareness of the C-axis relative to the B-axis
E_{BOC}	Out-of-squareness of the C-axis relative to the X-axis
E_{BOZ}	Out-of-squareness of the Z-axis relative to the X-axis
E_{AOY}	Out-of-squareness of the Y-axis relative to the Z-axis
E_{COY}	Out-of-squareness of the Y-axis relative to the X-axis
E_{XOC1}	X offset of the spindle relative to the B-axis
E_{YOC1}	Y offset to the spindle relative to the C-axis
E_{XX}	Positioning linear error term of the X-axis
E_{YY}	Positioning linear error term of the Y-axis
E_{ZZ}	Positioning linear error term of the Z-axis
F	Machine foundation
$\boldsymbol{J}$	Jacobian matrix
$\boldsymbol{J^+}$	Pseudoinverse Jacobian matrix
$\boldsymbol{J_{num}}$	Numerical Jacobian matrix

k_p	Coverage factor for hyper-ellipsoidal coverage region
k_q	Coverage factor for hyper-rectangular coverage region
L	Scale bar calibrated length
λ_{max}	Maximum eigenvalue of correlation matrix $\boldsymbol{R_y}$
τ	Machine geometric error parameter adjustment threshold
M	Number of Monte Carlo simulations
m	Number of output quantities
N	Number of input quantities
p	Coverage probability
p-value$_A$	p-value from ANOVA
p-value$_B$	p-value from Bartlett's test
$\boldsymbol{P}_{ball}$	Ball center position
$\boldsymbol{P}_{tip}$	Tool tip position
$\boldsymbol{R}_{AOC}$	Rotation matrix around *X*-axis
$\boldsymbol{R_y}$	Correlation matrix associated with the estimate $\boldsymbol{y}$ of output quantity $\boldsymbol{Y}$
$r(x_{i,}x_{j,})$	Correlation coefficient between the estimates x_i and x_j
$r_{all}(x_{i,}x_{j,})$	Correlation coefficient between the estimates x_i and x_j (obtained with all the data)
$r_{pooled}(x_{i,}x_{j,})$	Pooled Correlation coefficient between the estimates x_i and x_j
$\boldsymbol{s}$	Standard deviation
T	Tool
${}^{X'}\boldsymbol{T}_{B_0}$	Homogenous transformation matrix of the nominal B-axis location relative to the actual *X*-axis carriage
${}^{ball}\boldsymbol{T}_{tip}$	Homogenous transformation matrix of the tip location relative to the ball location

$\boldsymbol{U_x}$	Covariance matrix associated with estimate $\boldsymbol{x}$ of input quantity $\boldsymbol{X}$
$\boldsymbol{U_{x\,\mathrm{pooled}}}$	Pooled covariance matrix associated with estimate $\boldsymbol{x}$ of input quantity $\boldsymbol{X}$
$\boldsymbol{U_y}$	Covariance matrix associated with estimate $\boldsymbol{y}$ of output quantity $\boldsymbol{Y}$
U_p	Expanded uncertainty for the coverage probability p
u	Standard uncertainty
W	Workpiece
X	Machine linear axis
$\boldsymbol{X}$	Input quantity
$\boldsymbol{x}$	Estimate of input quantity $\boldsymbol{X}$
$\boldsymbol{x_R}$	Residual volumetric prediction error
Y	Machine linear axis
$\boldsymbol{Y}$	Output quantity
$\boldsymbol{y}$	Estimate of output quantity $\boldsymbol{Y}$
$\boldsymbol{\tilde{y}}$	Estimate of output quantity from Monte Carlo method results
Z	Machine linear axis

CHAPTER 1 INTRODUCTION

"The history of machine tools is the history of the precision of machine tools."

Lamikiz et al.(Lamikiz, López de Lacalle, & Celaya, 2009)

In the manufacturing area, material removal machining is a major process. Machining precision has been improving since the first machine tools were constructed and this progress continues. The ability to machine with narrower geometrical tolerances is a key component in terms of part and assembly design evolution. Increasing the quality of the final workpiece requires an even bigger increase in the machining precision. This parameter is crucial when a new machine is being designed and, even later, all along its life in service. The last few decades have brought significant changes in the machine tools performance and features. The computer numerical control (CNC), automated tool change, on-machine measurement etc. allow manufacturing a workpiece faster, with tighter tolerances and more complex design.

One of the most important parameters of a machine specification is its precision. It refers to the machine positioning accuracy (the ability to indicate the nominal value) and repeatability (the dispersion of the results when showing the same value). The resolution is also considered as an important factor since it represents the smallest position change that machine axis encoders can detect.

Evaluating and maintaining desired precision levels requires identifying the sources of machine inaccuracies. Among thermal, geometric, kinematic and dynamic errors, the geometric ones have the most significant impact on the machine positioning accuracy. Various calibration methods have been developed that allow testing and verifying those errors. Machine tool calibration gives the information about the machine geometry and, depending on the method and the applied model, it results in one (single-output) or a number of identified geometric error parameters (multi-ouput). Machine calibration is a subject of numerous research projects. Moreover, it has to be one step ahead of the machine precision progress.

1.1 Problem definition

The calibration of machine tool has to be performed frequently to ensure the machine ability to keep the required precision. The information about the machine performance obtained during the

calibration is later used, when the decision about error correction or compensation is made. Thus, the calibration results should be evaluated through their uncertainty as any other measurement result. The estimation of calibration uncertainty is a challenging task. The main uncertainty sources include the artefact or measuring device calibration uncertainty (if present), environmental conditions, and the machine itself (because its performance changes). In this case the machine is an uncertainty source and the measurand (measured quantity) itself. How to estimate the uncertainty on the quantities that are being estimated? Moreover, if an uncalibrated artefact is used in the calibration, it has no calibration uncertainty but its geometry variations may impact the results. How to include this influence in uncertainty budget? If the calibration method is non-linear and iterative, how the uncertainty can be propagated on the results? When applied method has a multi-output, should this be considered in data analysis? In this thesis the methodology and the experiments are presented to answer these questions since there is no available standard that would give full and comprehensive guidance to the highlighted issues.

1.2 Objectives

The main objective of this thesis is to develop a procedure that allows estimating the uncertainty of indirect calibration methods with an iterative solution and multi-output.

The secondary objectives include:

1) Estimating the measurement uncertainty of the uncalibrated artefact probing with full uncertainty structure;
2) Estimating the uncertainty on the calibration results that includes machine (measurand) performance;
3) Propagating the uncertainty on the calibration results using a method that is time-efficient and appropriate for multi-input multi-output iterative models;
4) Estimating the input and output uncertainty with the full uncertainty structure (standard uncertainties and covariance).

1.3 Hypotheses

In this thesis, the following hypotheses are presumed:

1) Machine has the rigid body kinematics;
2) The applied geometric error model is optimized. The errors model is not part of the evaluation in this thesis;
3) The probing measurement has a normal distribution - the hypothesis of normal distribution is assumed and tested using statistical normality tests;
4) The repeated calibration measurement gives the estimate of its standard uncertainty, covariance and normal distribution parameters (mean and variance).

CHAPTER 2 LITERATURE REVIEW

In this chapter, the state of the art in the machine performance testing is presented. Firstly, the machine different structures are presented. Then, the main machine errors sources are listed and various calibration methods are described. The standards for testing the machine performance and for uncertainty estimation are briefly discussed. The detailed strategies and methodology of the calibration uncertainty estimation are to be described in the articles following the literature review.

2.1 Multi-axis machines

Multi-axis machines are widely used in manufacturing for various machining operations (machine tools) and measurements (coordinate measuring machines (CMMs)). CMMs traditionally have a three-axis topology with different configuration of the linear axes. Modern machine tools, except for three linear axes (X, Y, Z), have additional two rotary axes (B, C). Examples of different topologies of five-axis machines are shown in Figure 2.1.

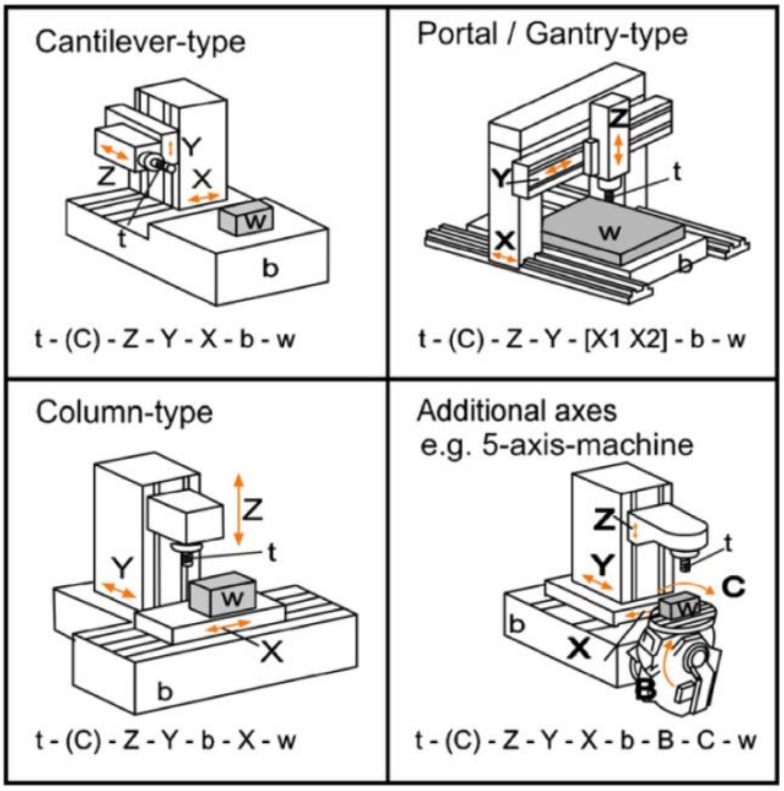

Figure 2.1: Examples of different topology of multi-axis machines (Schwenke et al., 2008)

The machine tool geometry has a kinematic structure, which includes machine components (workpiece w (or W), tool t (or T) and machine bed b (or F - foundation)) and linear (X, Y and Z) and rotary axes (B, C) (Abbaszadeh-Mir, Mayer, & Fortin, 2003; Mir, Mayer, & Fortin, 2002; Schwenke et al., 2008). Most of the machines have serial structure. It means that all the axes move independently from one another.

When the machine is about to be purchased or designed the following requirements are considered (López de Lacalle & Lamikiz, 2009): the maximum part size, workpiece main geometry (for a cylindrical shape, the lathe machine is considered in the first place), second geometry (design complexity), material removal rate and, finally, precision.

2.2 Machine performance

Machine precision is defined by its positioning accuracy (difference between the actual and nominal values) and repeatability (caused by the random sources expressed as the range of variations for the same position) (Lamikiz et al., 2009). The precision of the manufactured machine tool has been significantly increasing over the time. The evolution of machine tool accuracy in the previous century is presented in Figure 2.2.

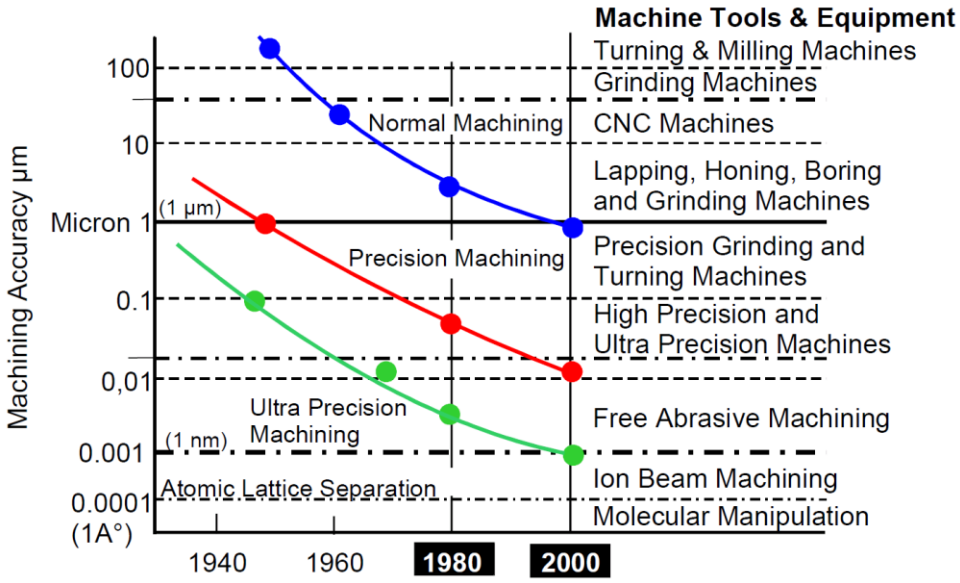

Figure 2.2: Machine tool accuracy over the past century (Byrne, Dornfeld, & Denkena, 2003)

The positioning accuracy of the tool and workpiece has a direct impact on the volumetric error (relative position of the workpiece to tool) and therefore, the quality of machined parts. The

positioning errors are influenced by many error sources which include environmental factors, machine components and assembly inaccuracies and machining process dynamics. The typical error sources are listed in Figure 2.3.

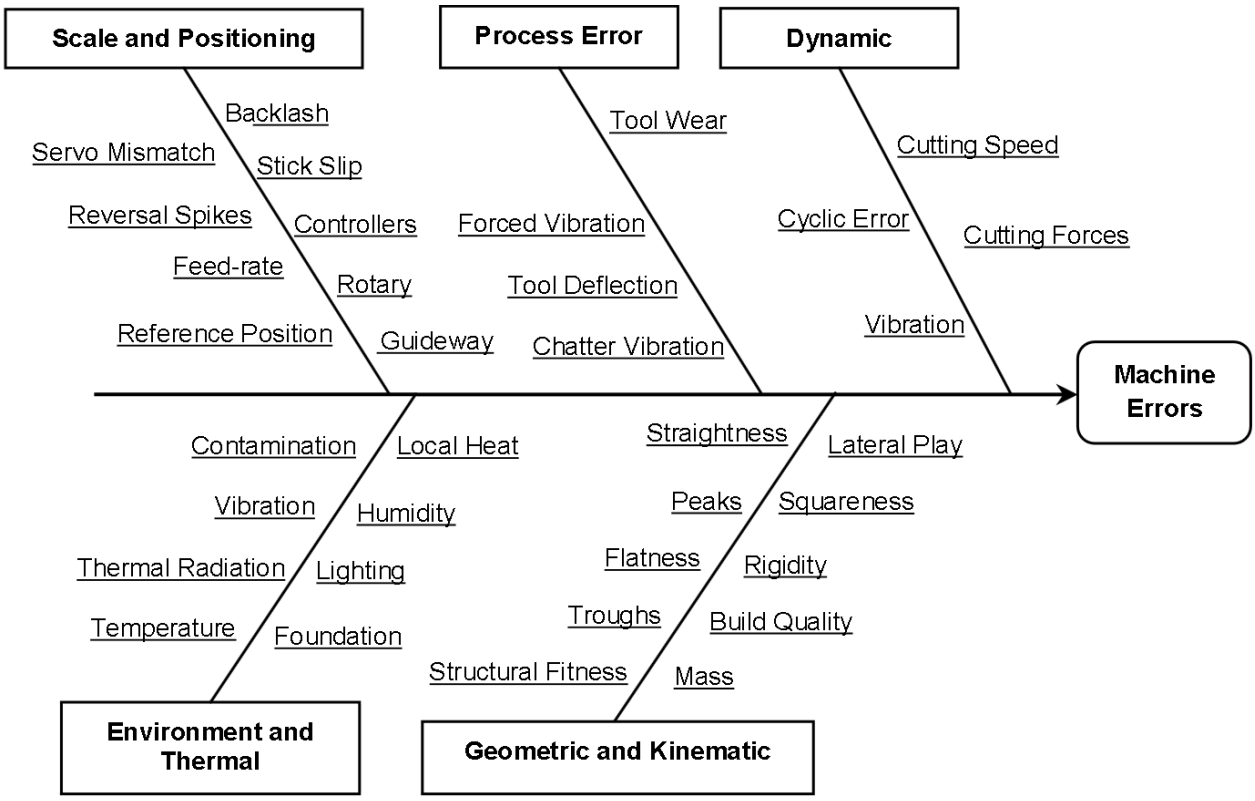

Figure 2.3: Ishikawa diagram with machine error sources (Jamshidi, Maropoulos, Chappell, & Cave, 2015) based on (Lamikiz et al., 2009)

Ramesh et al. defined two most significant error sources (Ramesh, Mannan, & Poo, 2000) as:

1) Quasi-static errors – related to the machine structure: kinematic, geometric and thermal errors
2) Dynamic errors – caused by the spindle error motion, vibrations of the machine structure, controller errors

2.2.1 Machine geometric error

Geometric errors in machine structure are the most significant error sources and result in position and orientation inaccuracies of the tool and workpiece (volumetric error) (Abbaszadeh-Mir, Mayer, Cloutier, & Fortin, 2002; Erkan, Mayer, & Dupont, 2011; Seng Khim & Chin Keong, March 17-

19, 2010). Those errors are results of the imperfection of machine components and inaccuracies that occur during the assembly (Ramesh et al., 2000). Geometric errors can be divided into two groups: link error parameters (location errors: joints misalignments, angular offsets, rotary axes separation error) and motion errors (component errors: scale error, straightness error, yaw, pitch, roll of linear axis and angular error, tilts, radial and axial errors of rotary axis) (Abbaszadeh-Mir et al., 2002; Schwenke et al., 2008). The former are position-independent geometric error parameters, the latter are position-dependent (their values change with the position of the axis).

Each axis is affected by 6 motion errors and 5 location errors (Schwenke et al., 2008). In (Ramesh et al., 2000) the link and location errors are showed for the linear and rotary axis correspondingly (Figure 2.4).

2.3 Calibration

Frequent calibrations are crucial for testing and controlling machine precision all along its life in service. Monitoring of machine performance is fundamental for avoiding machining parts that would be rejected after the quality check. Calibration process allows estimating machine geometric errors. They can be used for machine compensation or error correction (Givi & Mayer, 2014), which ensures that the machine is working with the required precision.

For the identification of mentioned geometric errors, different methods and devices are applied. The measurement of geometric errors can be provided using direct and indirect methods (Schwenke et al., 2008). The former gives more detailed information about one of the geometric errors, the latter leads to more complex identification.

2.3.1 Direct methods

Direct methods allow measuring the axis errors without the influence of the other axes and are commonly conducted using laser interferometry techniques (Castro, 2008; Chen, Kou, & Chiou, 1999; Okafor & Ertekin, 2000) or calibrated gauges. When the machine positioning errors are checked, the artefact (e.g., gauge blocks, step gauges) or the laser beam are aligned with the machine axis.

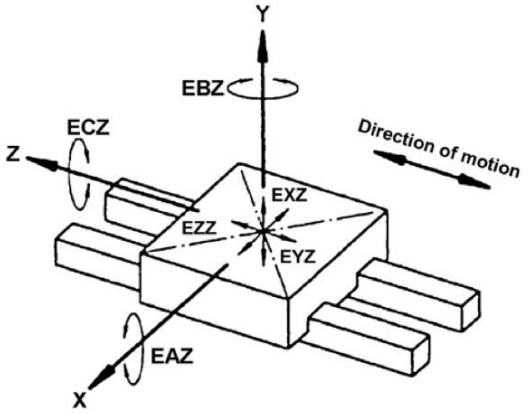

EXZ: horizontal straightness error motion of Z (straightness error motion of Z in X direction)
EYZ: vertical straightness error motion of Z (straightness error motion of Z in Y direction)
EZZ: positioning error
EAZ: pitch error motion of Z (tilt error motion around X)
EBZ: yaw error motion of Z (tilt error motion around Y)
ECZ: roll error motion

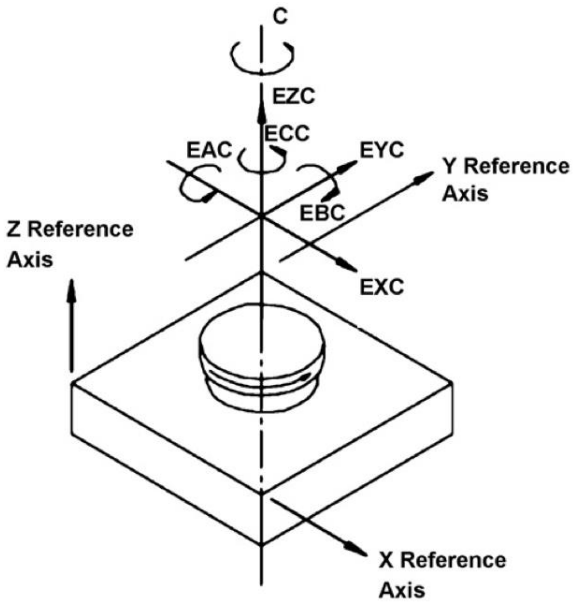

EXC: radial error motion of C in X direction
EYC: radial error motion of C in Y direction
EZC: axial error motion of C
EAC: tilt error motion around X of C
EBC: tilt error motion around Y of C
ECC: angular positioning error

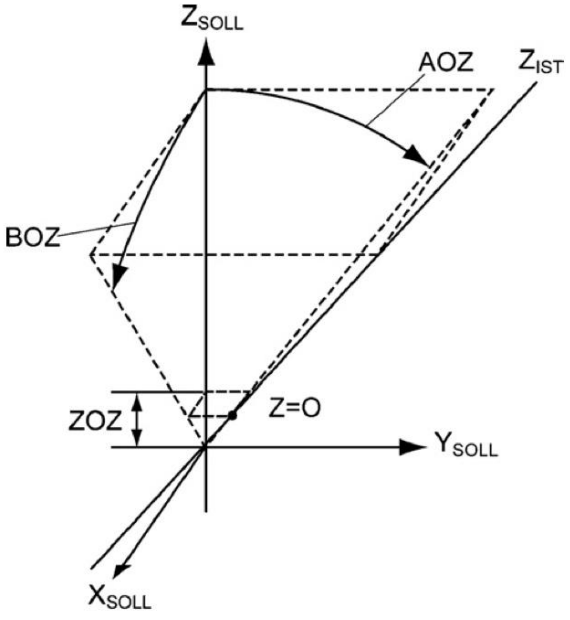

Z0Z: zero position of Z
A0Z: squareness of Z to Y
B0Z: squareness of Z to X

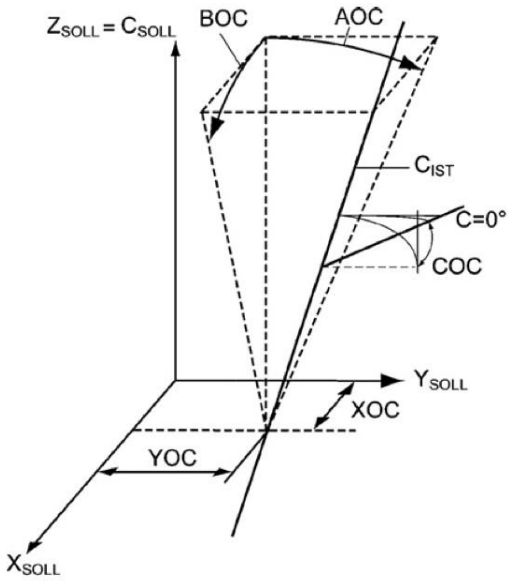

X0C: X position of C, Y0C: Y position of C
A0C: squareness of C to Y, B0C: squareness of C to X
C0C: zero angular position of C

Figure 2.4: Link and location errors of linear and rotation axes (Schwenke et al., 2008)

Laser interferometry is one of the most accurate methods but requires expensive equipment, trained operator and may be time consuming. Through direct measurements, the positioning, straightness, angular and squareness errors can be measured separately. Figure 2.5 shows the laser interferometer alignment for the measurement of the Y-axis positioning error. The laser head is situated outside the machine, the interferometer is set on the machine table and reflector is attached to spindle. During the measurement X and Z axes are locked. The readings from the CNC machine and laser interferometer are registered for the same positions and then compared. The difference between them is used to calculate the positioning error.

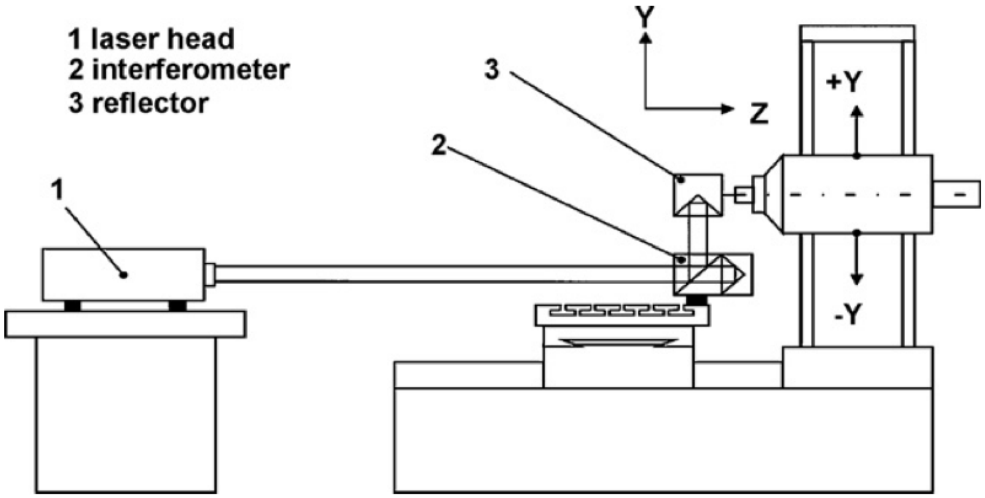

Figure 2.5: Y-axis position error measurement using laser interferometry (Schwenke et al., 2008)

2.3.2 Indirect methods

Indirect methods identify errors using different measuring devices, such as ball-bar (Jae Pahk, Sam Kim, & Hee Moon, 1997), various calibrated 2- and 3-D artefacts (Bringmann, Kung, & Knapp, 2005; Lei & Hsu, 2003), laser trackers (Aguado, Samper, Santolaria, & Aguilar, 2012; Linares et al., 2014) and laser-tracer (Moustafa, Gerwien, Haertig, & Wendt, 2009; Schwenke, Schmitt, Jatzkowski, & Warmann, 2009), “chase the ball” calibration (Bringmann & Knapp, 2006; Zargarbashi & Mayer, 2009) or an uncalibrated artefact probing (Mayer, 2012).

In order to identify geometric errors using indirect methods, the machine kinematic model needs to be built. The detailed procedure of error modeling and identification is presented in (Mir et al., 2002). The main steps are:

1) Building a direct kinematic model of the machine

The kinematic model represents the relative location of a workpiece W and tool T to the machine frame F. It can be described by using the homogenous transformation matrices (HTM) (Mir et al., 2002).

2) Generating Jacobian matrix

The sensitivity Jacobian matrix **J** represents the changes in the tool position $\delta\boldsymbol{\tau}$ relative to the workpiece (volumetric error (Seng Khim & Chin Keong, March 17-19, 2010)) caused by the small changes in the machine error parameters $\delta\boldsymbol{y}$:

$$\delta \boldsymbol{e}_v = \boldsymbol{J} \cdot \delta \boldsymbol{y} \tag{2.1}$$

The Jacobian matrix can be obtained from the HTMs.

3) Identifying unknown geometric error parameters geometric

To identify the parameters the Jacobian matrix $\boldsymbol{J}$ is calculated for different workpiece and tool position. Therefore the eq. (2.1) becomes:

$$\delta \boldsymbol{y} = \boldsymbol{J}^{+} \cdot \delta \boldsymbol{e}_v \tag{2.2}$$

where $\boldsymbol{J}^{+}$ is a pseudoinverse matrix of $\boldsymbol{J}$.

One of the devices that allow efficient volumetric error measurement and estimating machines errors is the ball-bar (Abbaszadeh-Mir et al., 2003; Jamshidi et al., 2015; Lee & Yang, 2013). Pahk et al. (Jae Pahk et al., 1997) used the kinematic ball-bar (Figure 2.6) to measure the volumetric error. The circular error measurement were conducted on the machine tool and the variations of the ball-bar length were registered. The authors developed a model that allowed identifying machine parametric errors: positional, straightness, angular, and backlash.

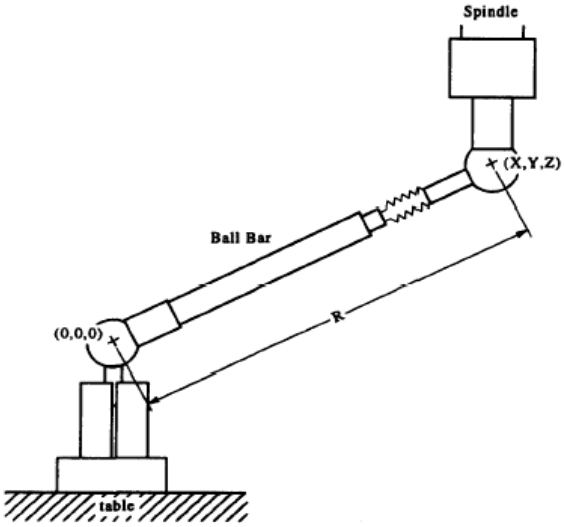

Figure 2.6: Error measurement using the kinematic ball-bar (Jae Pahk et al., 1997)

Bringmann et al. (Bringmann et al., 2005) proposed a calibrated pseudo-3D-artefact (Liebrich, Bringmann, & Knapp, 2009) for a calibration of a three-axis machine tool, a CMM or a robot. The artefact was obtained from the 2D-ball plate placed on the kinematic coupling mounted on the base plate or on a spacer (Figure 2.7 left). The measurement of the ball positions with the four linear probes system (Figure 2.7 right) in different configurations of the artefact allowed eliminating the CMM errors that were not influencing the calibration of the artefact.

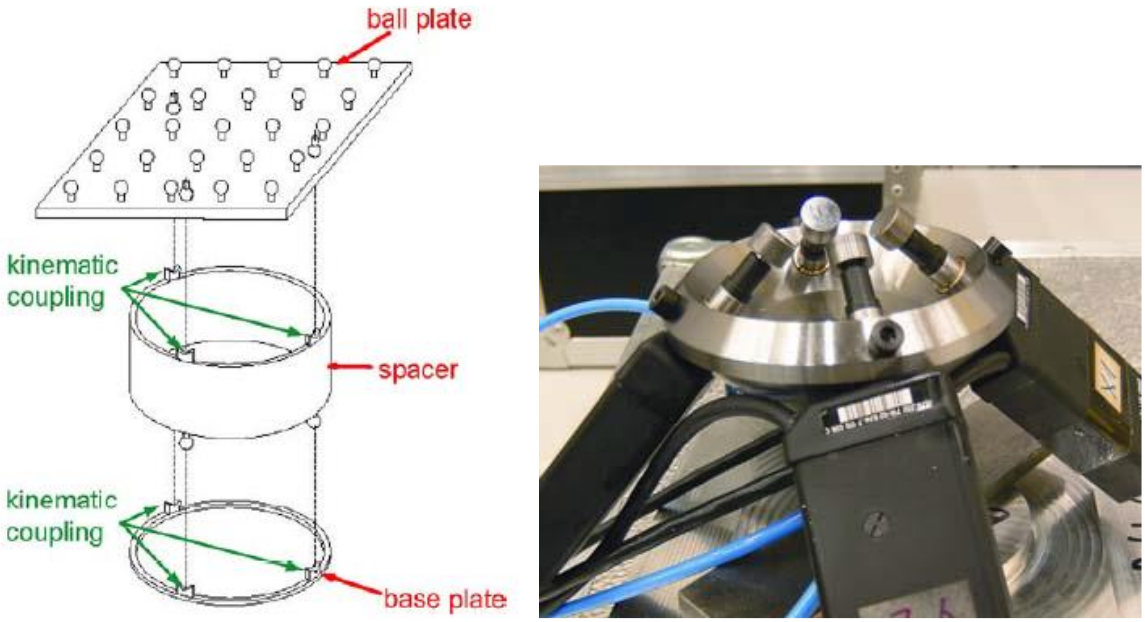

Figure 2.7: left: Schematic configuration of the pseudo-3D-artefact; right: linear displacement measurement system with four sensors(Bringmann et al., 2005)

The indirect methods can be conducted using the laser techniques. Schwenke et al. (Schwenke et al., 2009) used a tracking interferometer (laser tracer), which beam tracks the reflector (mounted on the machine head). It allowed registering the length measurements and comparing them to the nominal ones. Those differences introduced in the machine kinematic model led to the machine linear and rotary axes errors estimation.

"Chase the ball" or cap-ball model based calibration was performed by Bringmann et al. (Bringmann & Knapp, 2006) and (Zargarbashi & Mayer, 2009). This method requires mounting the ceramic ball in the machine spindle and measuring its position changes during the axes movement with the trajectory that maintains the same nominal position of the tool and workpiece. The tool and workpiece position differences are measured using four linear sensors (Bringmann & Knapp, 2006) or three capacity sensors (Zargarbashi & Mayer, 2009). The latter configuration is presented in Figure 2.8.

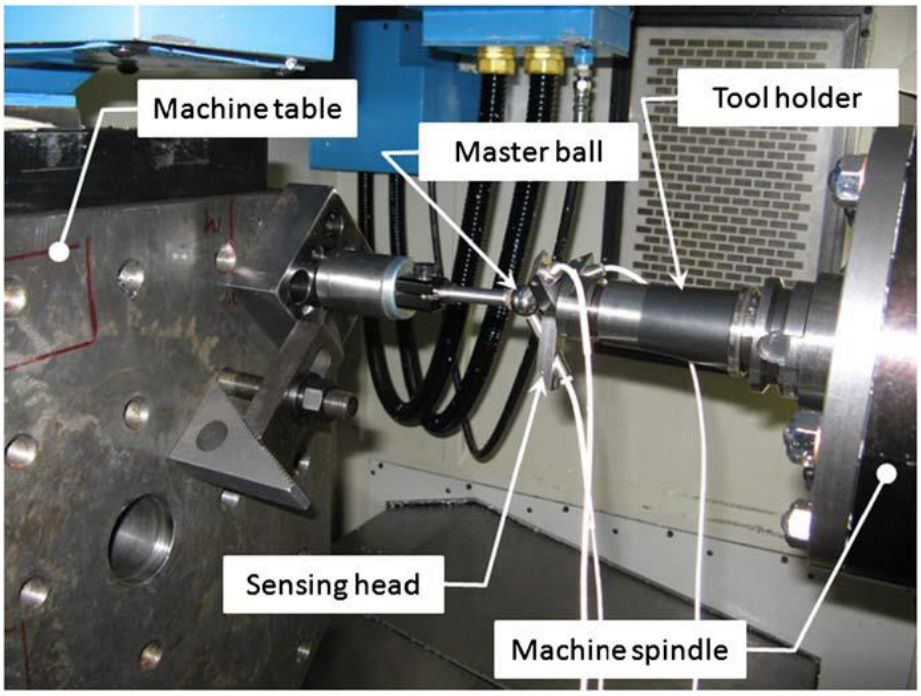

Figure 2.8: Cap-ball measurement system (Zargarbashi & Mayer, 2009)

Viprey et al. (Viprey, Nouira, Lavernhe, & Tournier, 2016) designed a calibrated multi-feature bar that consists in a repetition of a pattern (four flat surfaces and three cylinders). Aligning the artefact with the linear axes of a three-axis machine tool and measuring features of the proposed bar led to the estimation of twenty one geometric errors.

However, the machine tool calibration can be performed with an uncalibrated artefact. Erkan et al. (Erkan, 2010; Erkan et al., 2011) used uncalibrated master ball artefact (RUMBA) to identify machine geometric error parameters. The proposed artefact consists of master balls mounted at the tips of rods, with different lengths, screwed onto the machine table (Figure 2.9). The artefact is reconfigurable and does not need calibration, what makes the measurement faster and easier to conduct. During the test, the balls centers are measured in different angular axes indexations in order to obtain the value of the volumetric error. The analysis of the position measurement of each ball and the whole artefact allows separating the impact of the rotary and linear axes on the volumetric error.

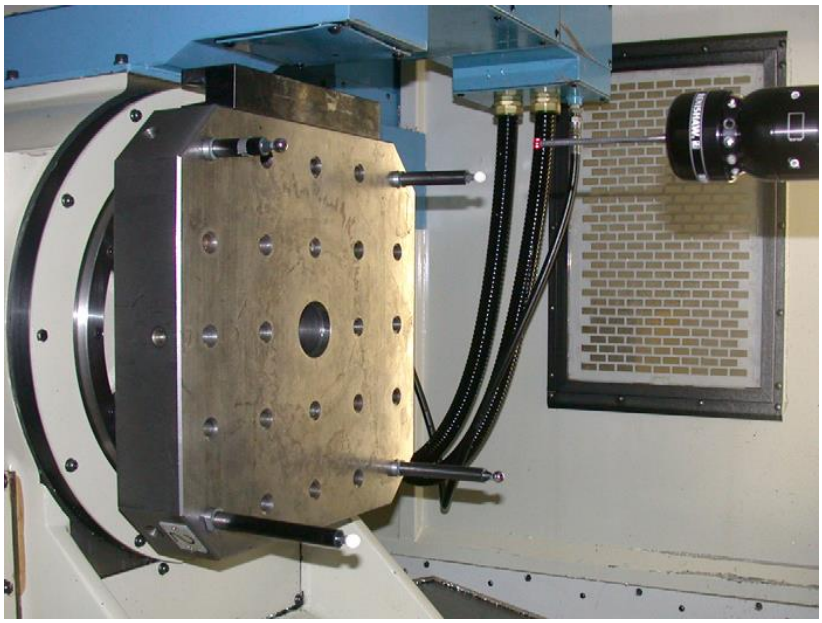

Figure 2.9: Artefact configuration on five-axis machine (Erkan et al., 2011)

Scale enriched master ball artefact (SAMBA) (Mayer, 2012) method is very similar to the RUMBA and can be conducted for various number of master balls (up to twenty four - Figure 2.10) with different calibration strategies (Mchichi & Mayer, 2014). The presence of a calibrated scale bar (which has to be measured at least once) allows estimating the scale errors of the linear axis. In (Mayer, 2012), SAMBA method was used to identify ten location errors (Figure 2.11) and three scale errors. The estimated machine geometric error parameters are listed in Table 2.1. along with their descriptions and both symbols used in (Mayer, 2012) and in this thesis.

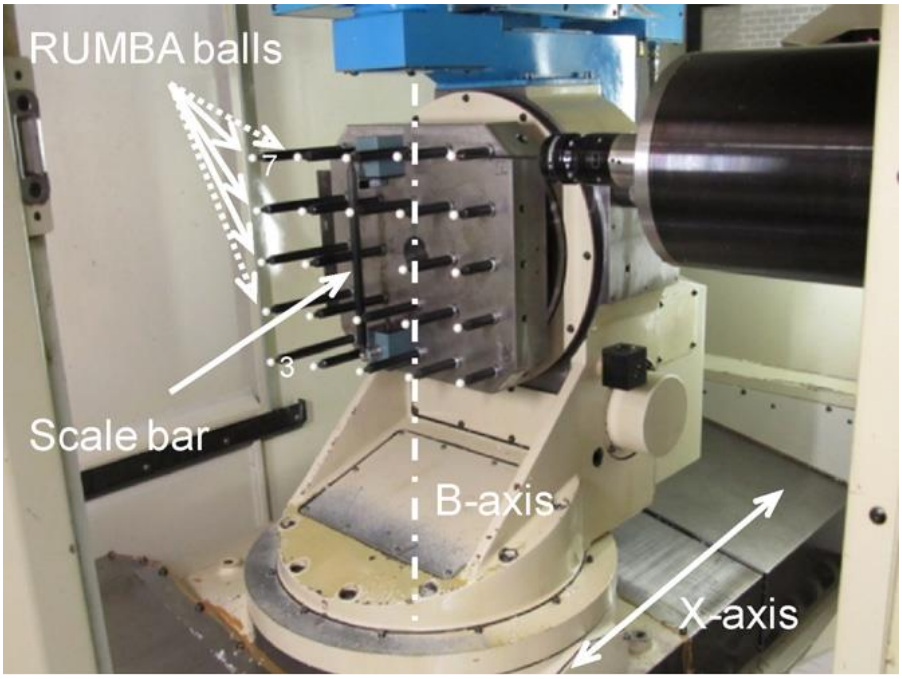

Figure 2.10: SAMBA artefact with twenty four master balls mounted on the machine tool (Mayer, 2012)

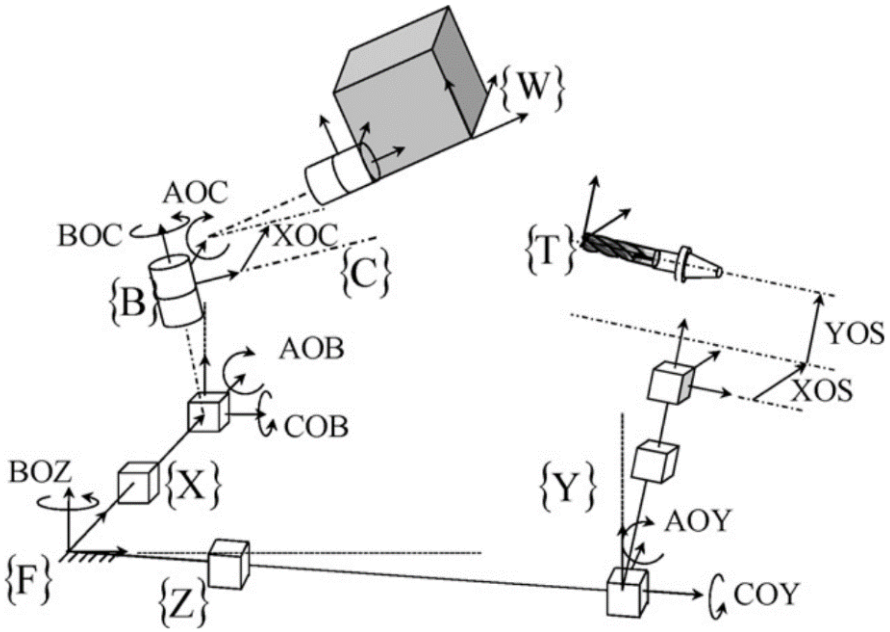

Figure 2.11: Axis location errors of a machine tool with WCBXFZYT topology (Mayer, 2012)

Table 2.1: Estimated machine geometric error parameters (Mayer, 2012)

Symbol (Mayer, 2012)	**Symbol in this thesis**	**Description**
AOB	E_{AOB}	out-of-squareness of the B-axis relative to the Z-axis (μrad)
COB	E_{COB}	out-of-squareness of the B-axis relative to the X-axis (μrad)
XOC	E_{XOC}	distance between the B and C axes (μm)
AOC	E_{AOC}	out-of-squareness of the C-axis relative to the B-axis (μrad)
BOC	E_{BOC}	out-of-squareness of the C-axis relative to the X-axis (μrad)
BOZ	E_{BOZ}	out-of-squareness of the Z-axis relative to the X-axis (μrad)
AOY	E_{AOY}	out-of-squareness of the Y-axis relative to the Z-axis (μrad)
COY	E_{COY}	out-of-squareness of the Y-axis relative to the X-axis (μrad)
XOS	E_{XOC1}	X offset of the spindle relative to the B-axis (μm)
YOS	E_{YOC1}	Y offset to the spindle relative to the C-axis (μm)
EXX	E_{XX}	positioning linear error term of the X-axis (μm/m)
EYY	E_{YY}	positioning linear error term of the Y-axis (μm/m)
EZZ	E_{ZZ}	positioning linear error term of the Z-axis (μm/m)

Another example of a calibration without a calibrated artefact was presented in Figure 2.12 (Mayer, Rahman, & Los, 2015). This method uses an uncalibrated cylindrical indigenous artefact (machine table) and allows estimating machine inter-axis errors. It requires mounting a touch probe in the spindle head and probing a number of points on around and on the machine table in different rotary axis indexations.

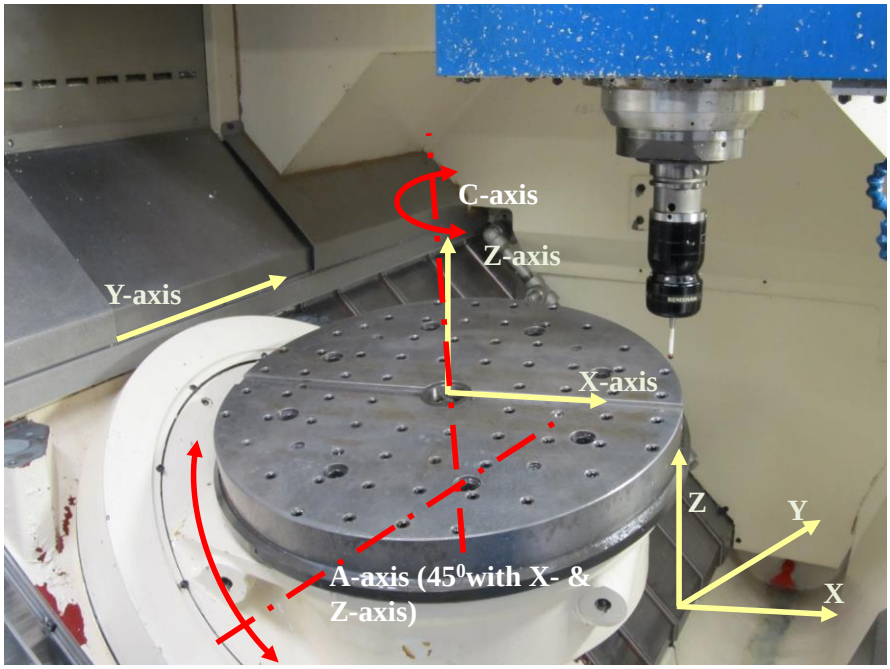

Figure 2.12: Indigenous artefact probing on the wCAYFXZ(C1)t machine tool (Mayer et al., 2015)

2.3.3 Standards

The available standards for the machine tool testing give the guidance on the machine testing using the direct methods and the measuring equipment with a high precision, e.g., laser interferometer. ISO 230-2 (ISO, 230-2:2014) and ASME B5.54 (ASME, B5.54:2005) standards describe procedures for the measurement of the machine geometric errors and their repeatability of the results through the repeated uni- and bi-directional tests. The significant difference of testing the machine according to those standards is that ISO 230-2 requires a warm-up test before the measurement, while ASME B5.54 excludes it. However, both standards do not consider the indirect calibration methods.

2.4 Calibration results evaluation

Once the information about the machine geometry is known and the calibration results are estimated, a decision to/not to use them for compensation or apply a software correction has to be made. This decision has a direct impact on the machine precision, thus the calibration results should be evaluated.

In the literature, examples of calibration results evaluation through the predicted volumetric error (Liang, Chen, Chen, Sun, & Chen, 2013) or the workpiece feature errors (Bringmann, Besuchet, & Rohr, 2008) can be found. However, this thesis focuses on the calibration as a measurement process, therefore the calibration uncertainty estimation is studied.

2.4.1 Uncertainty estimation

The uncertainty is a "non-negative parameter characterizing the dispersion of the quantity values being attributed to a measurand, based on the information used" (GUM, Joint Committee for Guides in Metrology, JCGM 200:2012). Every measurement result should be presented with its uncertainty. The direct calibration methods results uncertainty is typically estimated as the uncertainty of, for example, the laser displacement measurement. The indirect methods, due to their complex models, usually lead to the application of the Monte Carlo method (MCM) for the uncertainty assessment. In general, Monte Carlo method requires sampling the input quantity possible values, using obtained samples to compute the results and aggregating the results. In uncertainty estimation, the input quantity samples are obtained from their distribution and the calculated output values give the estimate of the result distribution. Thus, the uncertainty can be calculated.

Lira et al. (Lira & Grientschnig, 2010) proposed a method that estimates the uncertainty of positional deviations of a machine tool when the calibration is performed according to the ISO 230-2 standard (ISO, 230-2:2014). This approach included in the uncertainty budget: the measurand (position) variations, temperature, measuring device alignment and resolution. Those uncertainties were propagated on the estimate machine positional accuracy results using the law of propagation of uncertainties.

The test conditions and their impact on the positioning measurement used for direct calibration was analyzed by Knapp (Knapp, 2002). The author pointed out that, in practice, the calibration is performed in a workshop not in laboratory conditions, and the test uncertainty should not be propagated only from the measuring device uncertainty. The non-optimal conditions were amplified in the uncertainty propagation in order to demonstrate that uncertainty results, obtained for example, only from the laser interferometer displacement, may not reflect the reality.

Santolaria et al. (Santolaria & Ginés, 2013) applied MCM to estimate the uncertainty on the robot arm calibration results. The input uncertainty includes the length measurement uncertainty. The calibration uncertainty is later propagated on the position and orientation results.

Schwenke et al. (Schwenke, Franke, Hannaford, & Kunzmann, 2005) estimated the uncertainty of six parametric errors from the uncertainty of the laser tracking interferometer measurements modeled as the interferometric length measurement and propagated to the calibration results using MCM. This method included only the uncertainty of the measuring device (laser interferometer).

In (Jokiel Jr, Ziegert, & Bieg, 2001) the uncertainty on the calibration of parallel kinematic machines was analysed. The authors pointed the main sources of positioning accuracy errors as the external instrument and the machine itself through the variation of the strut length due to the thermal, geometric and controller influence.

The machine performance changes over the time and their influence on the calibration error were depicted by Parkinson et al. in (Parkinson, Longstaff, & Fletcher, 2014) for the squareness measurement. The authors included, not only the measuring device uncertainty, but also the variations of the straightness errors due to temperature changes. That allowed estimating the uncertainty on the squareness error and developing a calibration automated planning that reduced the uncertainty.

One of the most essential research on the calibration uncertainty was conducted by Bringmann et al. (Bringmann & Knapp, 2009). Through the indirect calibration method the authors showed that machine tool performance has an impact on the calibration results and, including only the uncertainty of the measuring device in the environmental conditions is not sufficient. The Monte Carlo method was applied. The machine performance impact was tested through the introduction in the machine model the geometric errors and simulating the calibration results. The noise added to each error was a random value generated from the uniformly distributed range, which were taken from similar measurements, machine specification or standard values. Thus, the *a priori* information about the machine tool performance (which is being tested) is required. This methodology for calibration uncertainty estimation was later followed by Ibaraki et al. (Ibaraki, Iritani, & Matsushita, 2013) in a calibration with an artefact of a square column geometry fixed on the machine table.

Presented methods of calibration uncertainty estimation show that, when it comes to machine tool calibration, there is no common procedure. The Monte Carlo method is widely used for various type of calibration methods and kinematic models (multi-axis machine tools, parallel kinematic machines and robots) uncertainty propagation. However, the necessity for including the machine performance variations in the uncertainty budget has been demonstrated. In all cases of indirect calibration, the uncertainty estimation was performed without considering correlations between the input data, which Haesslbrath et al. (Haesselbarth & Bremser, 2004) consider significant, when similar procedure or an object are measured, and especially when the repeated measurement is being performed. Not including the correlations between the input quantities while using the Monte Carlo method results in sampling the input quantity without considering the interdependencies between them. Thus, it gives less accurate resemblance of the reality. Correlations between the calibration results are not considered either, thus there is no information about the interdependencies between the results. Despite the multi-output calibration model types, the coverage factor for expanded uncertainty is estimated as for a single-output model.

2.4.2 **Standards**

Estimations of the uncertainty of calibration methods are presented in the ISO 230-2 standard (ISO, 230-2:2014). However, it is only for the indirect calibration method shown in the standard using a calibrated component (laser interferometer). In this case, the law of propagation of uncertainty can be adapted and applied.

Joint Committee for Guides in Metrology (JCGM) is one of the international organizations of *Bureau Interantional des Poids et Mesures* (BIMP). JCGM produced a series of documents "Evaluation of measurement data". The "Guide to the expression of uncertainty in measurement" (GUM) JCGM 100:2008 (GUM, Joint Committee for Guides in Metrology, JCGM 100:2008) states the general rules of the measurement uncertainty and the GUM Supplement 1 (GUM S1) JCGM 101:2008 (GUM, Joint Committee for Guides in Metrology, JCGM 101:2008) allows calculating the uncertainty of measurements with an arbitrary model through the Monte Carlo method (MCM). Both of those approaches (GUM and GUM S1) are limited to single output models. The uncertainty on multi-output models can be propagated using the MCM or GUM uncertainty framework (GUF) as described in the GUM Supplement 2 (GUM S2) JCGM 102:2011 (GUM, Joint Committee for Guides in Metrology, JCGM 102:2011).

Finally, the JCGM 107 (GUM, Joint Committee for Guides in Metrology, JCGM 107:In preparation) as it is described in JCGM 104 (GUM, Joint Committee for Guides in Metrology, JCGM 104:2009) provides guidance in the evaluation of the uncertainty when least-square models are used to estimate parameters of the calibration function. The necessity of evaluating and taking into account the uncertainty structure (the standard uncertainties and covariances of the measured quantities) is expressed. Unfortunately, according to the latest JCGM Working Group 1 News brochure ((BIPM), 2017), JCGM 107 is not available yet and should be developed at a later stage.

The standards for machine performance testing and uncertainty estimation show the need, complexity and challenges of the calibration uncertainty estimation but has yet to give the specific guidance when least-square model is used in an indirect calibration with uncalibrated artefact.

2.4.2.1 Adaptive Monte Carlo method

The Monte Carlo method described in GUM S2 (GUM, Joint Committee for Guides in Metrology, JCGM 102:2011) allows propagating the uncertainty sources on the measurement result without the analytical representation of a measurement model. In general, the MCM requires sampling the distributions of the input quantity and introducing these sets of random (with the distribution) values into the model, so that the range of the output values can be calculated. The detailed (adaptive) Monte Carlo approach for SAMBA method applied in the presented research is to be described in Chapter 4.

MCM method according to GUM S2 has been applied by Eichstadt et al. (Eichstadt, Link, Harris, & Elster, 2012) in an uncertainty evaluation of a dynamic measurement, in which the knowledge about the measuring system is limited. Conducting the MCM allowed avoiding linearization of the model, which could significantly influence the magnitude of the errors, and calculating the coverage regions for a multi-output model.

2.4.2.2 GUM uncertainty framework

GUM S2 gives the opportunity to estimate the uncertainty of a multi-output model using the GUM uncertainty framework (GUF). This approach requires calculating the partial derivatives of the output quantities to the input quantities. When the measurement models have the iterative solution or cannot be expressed analytically, the partial derivatives may be estimated experimentally or

numerically. The detailed GUF methodology is to be presented in Chapter 6 and its validation with MCM in Chapter 7.

CHAPTER 3 GENERAL PRESENTATION

The introduction (Chapter 1) and the literature review (Chapter 2) shaped the thesis subject. This chapter presents the overall structure with the article overview. The following three chapters corresponds to three (two journal and one conference) articles. In Chapter 7 additional results are presented. Those chapters show the main doctoral research. The thesis dissertation ends with a general discussion (Chapter 8) and conclusion (Chapter 9).

All tests and calculations presented in this thesis were conducted on a five-axis machine tool using the SAMBA calibration method, which has a multi-input, multi-output model with iterative solution and (scale enriched) uncalibrated artefact.

The article entitled “Uncertainty estimation of a five-axis machine tool calibration using the adaptive Monte Carlo method”, which was submitted in March 2017 to Precision Engineering Journal, is in Chapter 4. The research work, presented therein, is exploring the possibility of calculating the uncertainty of the calibration method that uses the uncalibrated artefact. Moreover, the machine performance and its variations due to the different environmental conditions are analysed. The following uncertainty sources are considered: the artefact variations occurring during the test, the probe repeatability and the machine itself. Thus, the measurand (machine geometry) is, at the same time, the source of the calibration uncertainty. In order to include all those factors, the repeated measurements (over 24 hours) are proposed as the estimation of the probing uncertainty (input quantity). That way, standard deviations, covariance and distributions are obtained and propagated through the (adaptive) MCM method on the calibration results (output quantity). The results with their expanded uncertainties are compared for different environmental conditions.

Chapter 5 is constituted of the article “Machine geometry time dependent variations and their effect on calibration results”, which was submitted in March 2017 to Measurement. In this paper, the machine performance changes are analysed. However, this time the focus is on short- and medium-term variations. In the previous paper, it was established that the machine changes occur during one day. But do the machine tool varies between the days? To answer this question, the SAMBA calibration was repeated on the machine four times a day over five days. That allows comparing the mean and variances obtained for each day. Moreover, the trend in the probing and calibration results is discussed.

Chapter 6 presents the paper “Application of GUF for a multi-output iterative measurement model estimation according to GUM S2 in indirect five-axis CNC machine tool calibration”, which was presented during the XI LAMDAMAP 2015 conference and published in the proceedings Laser Metrology and Machine Performance XI, in March 2015. MCM has many advantages. It does not require the analytical function of the measurement model or its linearization. Moreover, distributions of the estimated parameters are obtained. However, depending on the number of MC trials and based on a single trial running time, it can be time-consuming. GUF allows estimating the uncertainties faster but it requires the sensitivity Jacobian matrix of the output quantity to the input quantity. Since SAMBA has an iterative solution to the least square method the Jacobian cannot be established analytically. Thus, it is estimated with the numerical Jacobian. Then, the GUF method is used to calculate the uncertainties on the calibration results for different number of master balls present in the artefact.

Finally, in Chapter 7 the validation of time-efficient GUF with the MCM is presented. The estimated parameters, their uncertainties, covariance matrices and the coverage factors are compared for both methods. The MCM simulation results are calculated for different numbers of MC trials in order to show its impact on the obtained values.

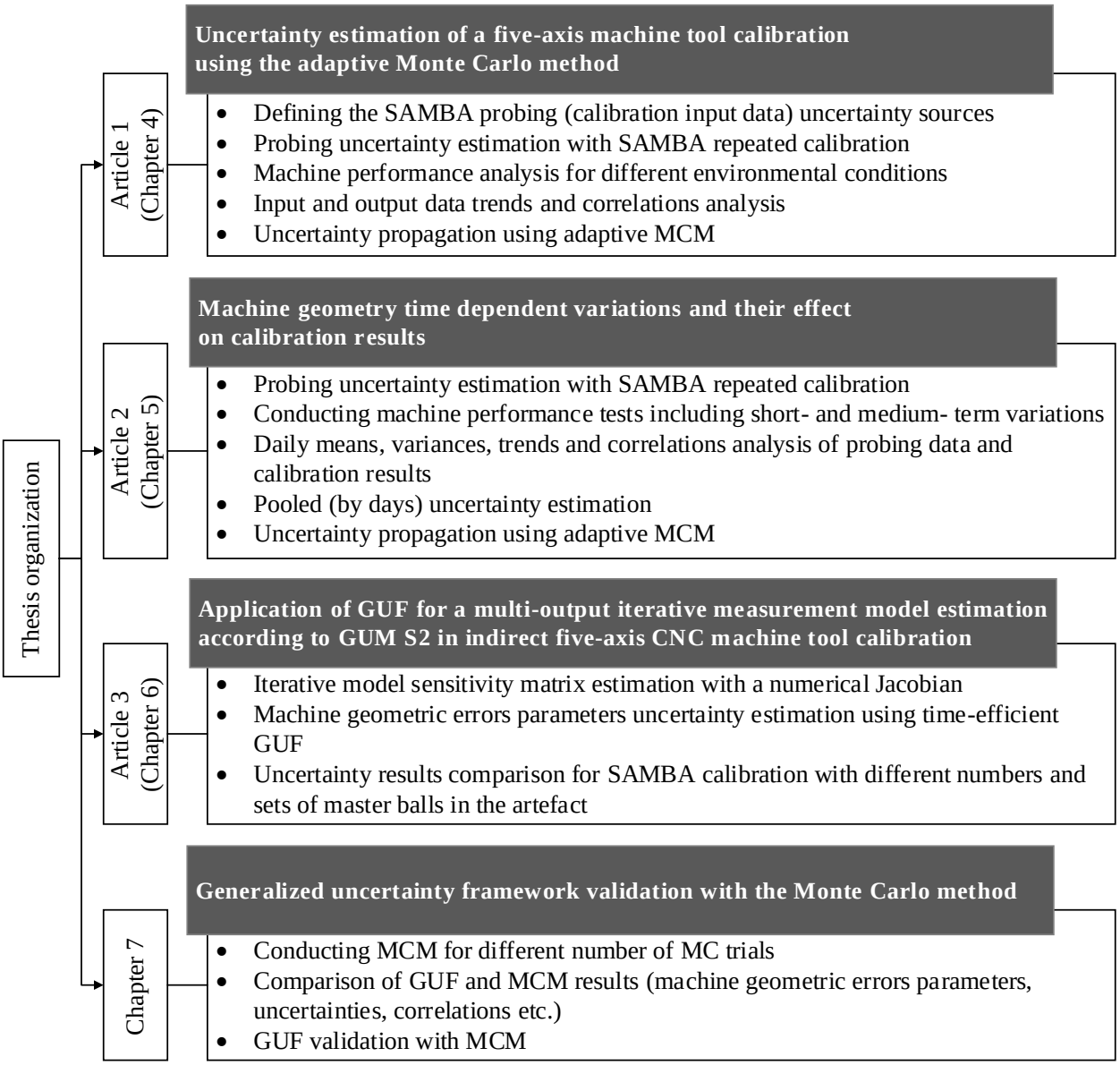

Figure 3.1: Thesis organization chart

CHAPTER 4 ARTICLE 1: UNCERTAINTY ESTIMATION OF A FIVE-AXIS MACHINE TOOL CALIBRATION USING THE ADAPTIVE MONTE CARLO METHOD

A. Los, J.R.R. Mayer

Department of Mechanical Engineering, Polytechnique Montreal, Montreal, QC, Canada

* Submitted to *Precision Engineering* in March 2017

4.1 Abstract

Calibration of the geometry of five-axis machine tools needs to be performed periodically since the machine accuracy has a direct impact on machined parts. Because mechanical adjustment and a software correction may be done using calibration results, the measurement results must be evaluated. In this paper, the scale and master ball artefact (SAMBA) method is evaluated through the estimation of the uncertainty of the identified machine geometric error parameters. This approach has the multi-input multi-output (MIMO) model and an iterative solution that makes it challenging to apply commonly used uncertainty calculation methods. The Guide to the Expression of Uncertainty in Measurement Supplement 2 (GUM S2) gives the opportunity to estimate the uncertainty of a MIMO model through the adaptive Monte Carlo method (MCM). The uncertainty is propagated from the repeated calibration tests conducted in different conditions. The uncertainties are calculated for each of the identified machine geometric error parameters along with their covariance. The correlations between the output variables and the impact of the machine conditions before and during the calibration are analyzed. The results demonstrate machine tool performance impact on the calibration results.

Keywords: machine tool, calibration, SAMBA, Monte Carlo, uncertainty.

4.2 Introduction

The calibration of a machine tool requires estimating the geometric error parameters of its linear and angular axes. Schwenke et al. [1] described and classified different methods for machine tool calibration into two groups: direct and indirect methods. The former allow measuring the axis

errors without the influence of the other axes and are commonly conducted using laser interferometry techniques [2, 3]. The latter identify errors using different measuring devices, such as ball-bar [4], various 2- and 3-D artefacts [1, 5-7], laser trackers [8] and laser tracer [9] or an uncalibrated artefact probing [10].

Once the estimates of the geometric error parameters have been obtained, the decision of using them for a correction and/or compensation must be made. That is why the calibration results should be evaluated. One of the evaluation methods can be conducted through the predicted (with and without calibration) workpiece feature errors as Bringmann et al. proposed in [11], that allowed choosing the most optimal calibration method. The estimated calibration results can also be evaluated through their uncertainty as any other kind of measurement result. Since the measurement models used in the indirect methods are complex and are multi-input multi-output, the GUM uncertainty framework (GUF) for a single output presented in GUM [12] cannot be conducted.

Bringmann et al. [13] estimated the uncertainties on the machine geometric error parameters of the model-based indirect calibration method, called “chase the ball”, using general Monte Carlo method (MCM). This approach requires adding noise to the geometric errors in the simulated machine model. The noise values are chosen arbitrarily from standards or machine specifications without considering correlations between them or the obtained calibration results. The authors also depicted that the machine performance has a significant impact on the calibration results. Other researchers also applied MCM based on GUM Supplement 1 (GUM S1) [14]. Andolfatto et al. [15] used the adaptive MCM to estimate uncertainty on machine tool axis location errors with the confidence intervals. Santolaria et al. [16] conducted robot kinematic calibration and estimated, through simulation, the uncertainty on the calibration results. Schwenke et al. [17] estimated the uncertainty on six parametric errors of the Y-axis of a coordinate measuring machine (CMM) and on a milling machine. The machine errors are identified using a laser tracer. The displacement measurements noise is estimated as normally distributed random numbers without considering the correlation between the input data. All of the previously mentioned approaches use the MCM for a multi-output model but do not consider the full uncertainty structure (standard uncertainties and covariance of the measured data) (JCGM 104:2009 6) [18], nor the coverage factor associated with the number of the estimated parameters.

The indirect calibration methods allow estimating many geometric errors simultaneously. That is why the covariance between them should also be considered when the uncertainties are calculated. Moreover, the coverage factor should be based not only on the desired coverage probability but on the number of output values as well. The opportunity of calculating the uncertainty on the multi-output model results is given in GUM S2 [19]. It has been applied by Eichstadt et al. [20] to an efficient uncertainty estimation in a challenging case of dynamic measurement. The MCM uncertainty estimation results are compared with two other memory-efficient approaches.

In this paper, the machine geometric errors are identified using the SAMBA [10] method, whereby the volumetric observations are gathered using an uncalibrated artefact made of a number of spheres, a calibrated fixed length ball bar (scale bar) and a touch trigger probe mounted in the machine tool spindle. The machine, with its axis location and linear axis positioning error gains, is modeled using rigid body kinematics so that its geometric error parameters can be estimated. This method is based on a multi-output model – all the machine geometric errors are calculated simultaneously from the volumetric measurement indications (probing data). In this paper, since the SAMBA method is based on multistage and iterative calculations, analytical procedures are not easily conducted. Thus the adaptive MCM [19] is followed. The uncertainties for the probing data are estimated from the repeated measurement conducted under different measurement conditions (with and without the warm-up cycle). The warm-up cycle performed before the measurement allows simulating the machine working conditions [21] and is required when the calibration (using direct methods) is following the ISO 230-2 standard [22]. However, the ASME B5.54 standard [23] (for indirect methods) do not require a warm-up cycle and the errors due to machine heat sources are not present prior to the tests [21]. Conducting the calibration series with and without the warm-up cycle allows demonstrating the machine performance influence on calibration results depending on the calibration pre-conditions.

4.3 SAMBA calibration method

4.3.1 Artefact probing

The SAMBA method allows estimating the machine geometric error parameters from the probing (using a touch probe mounted in the spindle) of a number of master balls (mounted on rods with different lengths) in different machine rotary axis indexations and a scale bar (probed at least once).

The SAMBA artefact with the four master balls and the scale bar (which is the only calibrated component) mounted on the machine table is depicted in Figure 4.1 (right). For each indexation, each of the balls is probed in five points, which allows calculating the X-, Y- and Z-axis readings corresponding to positioning the stylus tip at the ball center and comparing it with its nominal position.

Herein, the experimental data is collected using a HU40-T model five-axis machine tool made by Mitsui Seiki. Its topology is depicted in Figure 4.1 (left). The analyzed machine is modeled using eleven joint link errors with values estimated during previous calibration [10].

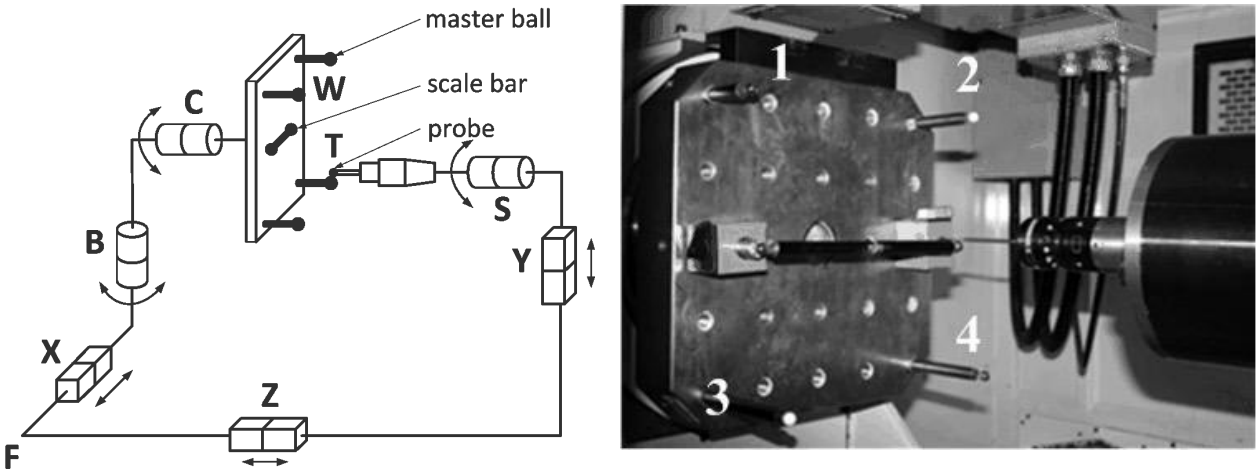

Figure 4.1: left: Five-axis CNC machine model with the topology WCBXFZY(C1)T; W - workpiece, T - tool, F - machine foundation, B, C – rotary axes around the Y and Z axes respectively, X, Y, Z – machine linear axes, S – spindle; right: SAMBA artefact being probed using the Renishaw probe MP700 on a Mitsui Seiki HU40-T machine tool

4.3.2 **Parameters identification**

The identification of the geometric error parameters, presented in Figure 4.2, requires building the kinematic model of the machine, that allows calculating the predicted tool position $\boldsymbol{P}_{tip}$ [24] relative to the probed ball center position $\boldsymbol{P}_{ball}$ using the measured axis positions. At measurement, the two positions coincide virtually (not physically since the probe tip cannot be positioned at the center of the ball):

$$\left(\boldsymbol{P}_{tip} - \boldsymbol{P}_{ball}\right)_{actual} \equiv [0, \quad 0, \quad 0]^T \tag{4.1}$$

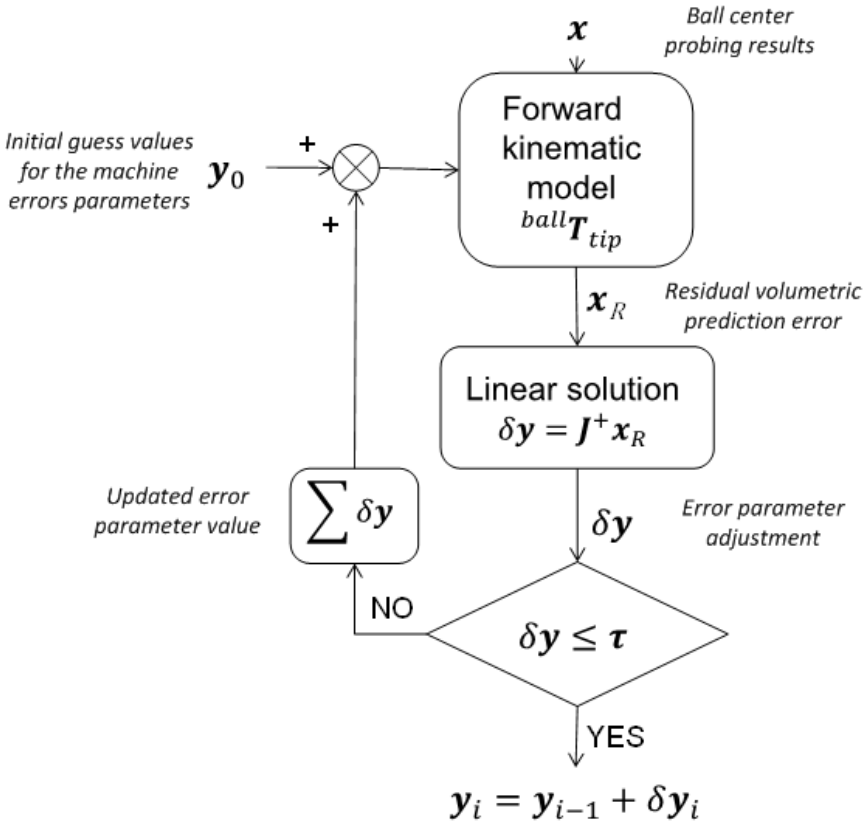

Figure 4.2: SAMBA identification flow chart

The Newton-Gauss approach is used to estimate the changes to the machine geometric error parameters in order to reduce the error between the prediction of the model and the observation:

$$\left(\boldsymbol{P}_{tip} - \boldsymbol{P}_{ball}\right)_{predicted} + \boldsymbol{J} \cdot \delta\boldsymbol{y} = 0 \tag{4.2}$$

where:

$\boldsymbol{J}$ is the sensitivity Jacobian matrix (of the residuals $\boldsymbol{x}_R$ to $\delta\boldsymbol{y}$) and $\delta\boldsymbol{y}$ is the column matrix of the adjustment in machine parameters and the artefact geometry and dimension.

With:

$$\left(\boldsymbol{P}_{tip} - \boldsymbol{P}_{ball}\right)_{predicted} = \boldsymbol{x}_R \tag{4.3}$$

Equation 4.2 can be solved for $\delta\boldsymbol{y}$:

$$\boldsymbol{J} \cdot \delta \boldsymbol{y} = -\boldsymbol{x}_R \tag{4.4}$$

Finally, we obtain:

$$\delta \boldsymbol{y} = \boldsymbol{J}^{+} \cdot (-\boldsymbol{x}_R) \tag{4.5}$$

where $\boldsymbol{J}^{+}$ is a pseudoinverse matrix of $\boldsymbol{J}$ and $\boldsymbol{x}_R$ is predicted and extracted from the homogenous transformation matrix ${}^{ball}\boldsymbol{T}_{tip}$:

$$\boldsymbol{x}_R = {}^{ball}\boldsymbol{T}_{tip} \begin{bmatrix} 0 \\ 0 \\ 0 \\ 1 \end{bmatrix} \tag{4.6}$$

keeping only the top three components. For the analyzed five-axis machine,

$$\begin{aligned} {}^{ball}\boldsymbol{T}_{tip} = \left({}^{F}\boldsymbol{T}_{X_0}\, {}^{X_0}\boldsymbol{T}_{X}\, {}^{X}\boldsymbol{T}_{X'}\, {}^{X'}\boldsymbol{T}_{B_0}\, {}^{B_0}\boldsymbol{T}_{B}\, {}^{B}\boldsymbol{T}_{B'}\, {}^{B'}\boldsymbol{T}_{C_0}\, {}^{C_0}\boldsymbol{T}_{C}\, {}^{C}\boldsymbol{T}_{C'}\, {}^{C'}\boldsymbol{T}_{ball} \right)^{-1} \cdot \\ \cdot\ {}^{F}T_{Z_0}\, {}^{Z_0}\boldsymbol{T}_{Z}\, {}^{Z}\boldsymbol{T}_{Z'}\, {}^{Z'}\boldsymbol{T}_{Y_0}\, {}^{Y_0}\boldsymbol{T}_{Y}\, {}^{Y}\boldsymbol{T}_{Y'}\, {}^{Y'}\boldsymbol{T}_{S_0}\, {}^{S_0}\boldsymbol{T}_{S}\, {}^{S}\boldsymbol{T}_{tip} \end{aligned} \tag{4.7}$$

where, for example:

$${}^{X'}\boldsymbol{T}_{B_0} = \boldsymbol{I} \tag{4.8}$$

is the homogenous transformation matrix of the nominal *B*-axis location relative to the actual *X*-axis carriage, while:

$${}^{B_0}\boldsymbol{T}_{B} = \begin{bmatrix} cos\ b & 0 & sin\ b & 0 \\ 0 & 1 & 0 & 0 \\ -sin\ b & 0 & cos\ b & 0 \\ 0 & 0 & 0 & 1 \end{bmatrix} \tag{4.9}$$

is the HTM of the nominal rotary motion of the *B*-axis by an angular rotation b. Finally,

$$ {}^{B}\boldsymbol{T}_{B'} = \begin{bmatrix} (\boldsymbol{R}_{COC} \cdot \boldsymbol{R}_{BOC} \cdot \boldsymbol{R}_{AOC})_{3x3} & \begin{matrix} E_{XOBC} \\ E_{YOBC} \\ E_{ZOBC} \end{matrix} \\ \begin{matrix} 0 & 0 & 0 \end{matrix} & 1 \end{bmatrix} \tag{4.10} $$

is the HTM of the error in the location of the following axis and $\boldsymbol{R}_{AOC}$, $\boldsymbol{R}_{BOC}$, $\boldsymbol{R}_{COC}$ are rotation matrices around *X*-, *Y*- and *Z*- axis, respectively.

After the first parameters' estimation vector $\delta \boldsymbol{y}_1$ is used directly, since all error parameters values are initially null (perfect machine) and the uncalibrated artefact is introduced in the model with its initial dimensions $\boldsymbol{d}$ (which includes the rods lengths, the distances between them and position on the machine table) $\boldsymbol{y}_0 = [0, \dots, 0, \boldsymbol{d}]$, to calculate new predictions of volumetric errors $\delta \boldsymbol{x}_{R,1}$. Those values are used to estimate $\delta \boldsymbol{y}_2$ and added to the last estimated values until $|\delta \boldsymbol{y}_i - \delta \boldsymbol{y}_{i-1}|$ is smaller than a predefined permissible threshold τ.

4.4 Adaptive Monte Carlo method

The analyzed calibration method has a multi-output and an iterative solution which is why the (adaptive) MCM presented in GUM S2 [19] has been selected to propagate the probing uncertainty on the calibration result. Because it generates multiple output, the described identification method of machine geometric error parameters precludes from using traditional methods of uncertainty estimation that are designed for single-output measurements and which do not allow analyzing the results covariance [12, 14]. The multi-output model requires calculating and analyzing the uncertainty on each calibration result with respect to all results. This opportunity is given by GUM S2 [19].

4.4.1 Input uncertainty

The input data of the SAMBA calibration are the probing results (the machine axis position readings or indications) and the calibrated scale bar length. The contributors to the probing uncertainty are the probe, the scale bar calibrated length when on the machine tool, the artefact (only the drift occurring during one cycle) and, as it has been demonstrated by Bringmann et al. [25], the machine performance. The probe uncertainty can be evaluated through its repeatability. However, the readings uncertainty depends on the machine as well. The artefact is uncalibrated (except for the scale bar) and it is being co-calibrated during SAMBA identification along with the

machine geometric error parameters. The standard uncertainty of the scale bar is estimated as its calibration uncertainty since it is a calibrated component, made of temperature insensitive carbon fiber and mounted on a kinematic seat that does not constrain its length.

Application of the adaptive MCM requires estimating the probability density functions (PDFs) of the input quantities as well as their joint PDF. To include all the uncertainty sources and reflect the machine performance in the uncertainty, the indirect calibration test measurement procedure is repeated many times. Repeated tests allow calculating the covariance matrix of the input data, estimating their PDFs and building the joint PDF (including the correlations), which is used for sampling the simulated probing results. Moreover, to demonstrate the machine performance impact on the calibration results, the tests are conducted in two different conditions: with and without the warm-up cycle before the calibration measurements.

4.4.2 **Output uncertainty**

The MCM method allows estimating uncertainties without calculating partial derivatives of the model. Furthermore, the adaptive MCM allows adjusting the number of MC trials while ensuring the results' required stability. Figure 4.3 presents the adaptive MCM for SAMBA. M arrays of the N input data are created by sampling their PDFs (and/or joint PDF) obtained using, e.g., a Gaussian copula [26]. For each of the M vectors, the m output quantities are calculated. M vectors of the output quantity are used to calculate the output value vector by calculating its average:

$$\tilde{\boldsymbol{y}} = \frac{1}{M}(\boldsymbol{y}_1 + \cdots + \boldsymbol{y}_M) \tag{4.11}$$

The associated covariance matrix is estimated by:

$$\boldsymbol{U}_{\tilde{\boldsymbol{y}}} = \frac{1}{M-1}\left((\boldsymbol{y}_1 - \tilde{\boldsymbol{y}})(\boldsymbol{y}_1 - \tilde{\boldsymbol{y}})^T + \cdots + (\boldsymbol{y}_{\mathrm{M}} - \tilde{\boldsymbol{y}})(\boldsymbol{y}_{\mathrm{M}} - \tilde{\boldsymbol{y}})^T\right) \tag{4.12}$$

The mean and covariance matrix are used to calculate the coverage factors k_q and k_p [19], which are the hyper-rectangular and hyper-ellipsoidal coverage regions factors, respectively.

The number of MCM trials can be set before conducting calculations. However, in order to ensure the results stability, the adaptive MCM is performed herein.

The first step of the adaptive MCM consists in performing $h = 10$ times $M = 10^4$ MC trials. For each $r = 1, \dots, h$ subsets, the output quantity estimate $\boldsymbol{y}^{(r)}$ and its standard deviation $\boldsymbol{s_y}^{(r)}$, the maximum eigenvalue ${\lambda_{max}}^{(r)}$ of the correlation matrix $\boldsymbol{R_y}^{(r)}$, and coverage factors ${k_p}^{(r)}$ and ${k_q}^{(r)}$ are calculated.

The set of $h = 10$ estimates of the output quantities is used to calculate the standard deviations (for $j = 1, \dots, m$) as one of the stability parameters:

$$\boldsymbol{s}^2_{\boldsymbol{y}_j} = \frac{1}{h(h-1)} \sum_{r=1}^{h} \left(\boldsymbol{y}_j^{(r)} - \boldsymbol{y}_j \right)^2 \tag{4.13}$$

In a similar way, the remaining stability parameters standard deviations (of results variances $\boldsymbol{s}_{\boldsymbol{u}_{\boldsymbol{y}_j}}$, correlation matrix $\boldsymbol{R}$, maximum eigenvalue $\boldsymbol{s}_{\lambda_{max}}$ and coverage factors $\boldsymbol{s}_{k_p}$ and $\boldsymbol{s}_{k_q}$, for ellipsoidal and rectangular coverage factors, respectively) are estimated. The obtained values are multiplied by two and compared with their corresponding required numerical tolerances. If at least one of the doubled standard deviations is greater than its numerical tolerance, the value of h is increased by 1 and a new set of M output data is calculated. The procedure is repeated until the results reach the demanded stability.

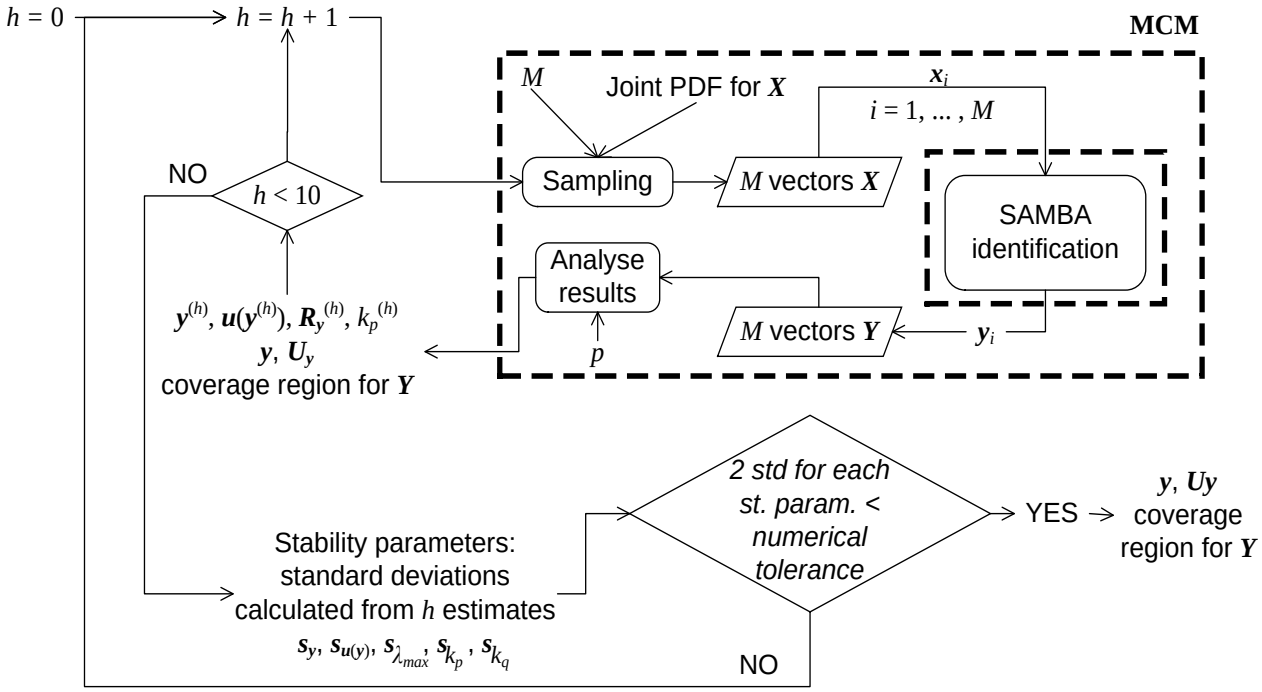

Figure 4.3: Adaptive MCM scheme applied to the SAMBA calibration method

4.5 Measurement and simulation

4.5.1 SAMBA artefact probing

The SAMBA artefact used for the study is depicted in Figure 4.1 (right) and consists of four master balls 12.7 mm in diameter mounted on rods with different lengths and a scale bar with a calibrated length of 304.6686 mm.

The probing of the artefact is performed experimentally repeatedly, and later numerically simulated for MCM purposes, for seven different rotary axis indexations pairs ([b, c] = [90, 270], [60, 180], [30, 90], [0, 0], [-90, -270], [-60, -180], and [-30, -90] deg) and the scale bar is measured once for [b, c] = [0, 0] deg.

4.5.2 Uncertainty propagation

In order to estimate the distribution and associated uncertainty of the input data, repeated SAMBA measurements were performed on the test machine over a 24-hour period. That allowed calculating the covariance matrix of the input data, its PDFs and the joint PDF. The model input quantity $\boldsymbol{X}$ has the estimate $\boldsymbol{x} = \left(x_1, y_1, z_1, \dots, x_{(N-1)/3}, y_{(N-1)/3}, z_{(N-1)/3}, L\right)$ where x_i, y_i, z_i are the X-, Y- and Z-axis position readings corresponding to the touch probe stylus tip position at the ball center, L is the calibrated scale bar length and N is the number of input quantities. The identified machine geometric error parameters and the predicted volumetric errors are m model output quantities $\boldsymbol{Y}$ with estimate $\boldsymbol{y} = (y_1, \dots, y_m)$. The identified machine geometric error parameters, the measurand, are listed in Table 4.1.

Table 4.1: Identified machine geometric error parameters

Symbol	Description	Calibration result
E_{AOB}	out-of-squareness of the B-axis relative to the Z-axis (μrad)	0.9
E_{COB}	out-of-squareness of the B-axis relative to the X-axis (μrad)	-1.5
E_{XOC}	distance between the B and C axes (μm)	-102.2
E_{AOC}	out-of-squareness of the C-axis relative to the B-axis (μrad)	3.9
E_{BOC}	out-of-squareness of the C-axis relative to the X-axis (μrad)	19.9
E_{BOZ}	out-of-squareness of the Z-axis relative to the X-axis (μrad)	-37.5
E_{AOY}	out-of-squareness of the Y-axis relative to the Z-axis (μrad)	-8.8
E_{COY}	out-of-squareness of the Y-axis relative to the X-axis (μrad)	23.9
E_{XX}	positioning linear error term of the X-axis (μm/m)	-45.2
E_{YY}	positioning linear error term of the Y-axis (μm/m)	5.3
E_{ZZ}	positioning linear error term of the Z-axis (μm/m)	-20.5

4.6 Results

4.6.1 Probing

The measured input quantities are the probing results and the scale bar length. The latter has the standard uncertainty $u(L) = \pm 0.0012$ mm (from calibration). The probing uncertainty was estimated from conducting repeated tests (44 times) over a period of 24 hours with a preceding warm-up cycle (*Hot-Cold*), when the temperature decreased from 27 to 23 degrees Celsius, and also without the warm-up cycle (*Cold-Cold*). This resulted in two sets of probing uncertainty estimates.

Figure 4.4 shows the *X*-, *Y*- and *Z*-axis readings for the center of master ball 1 for the *Cold-Cold* and *Hot-Cold* repeated measurements. Trends can be observed for all three coordinates for both measurement conditions. Similarly, the probing comparison of master balls 3 and 4 (Figure 4.5), exhibits a strong correlation between the corresponding coordinates *Y* and *Z*, and for *X* in *Cold-Cold*. A similar trend for all the *X*, *Y* and *Z* coordinates can be observed for those coordinates when different balls are compared for different indexations with stronger correlations for the *Hot-Cold* measurement, which maybe as a result of thermal drift. The estimated input quantity uncertainty corresponds to the 24 hours results variation which could be due to changes of the measurand (machine geometric error parameters) and/or changes in the geometry and size of the machine table

which, in association with the ball/stem assemblies, constitute the SAMBA artefact. However, the data acquisition period is 44 times longer (for 44 repetitions) than a single SAMBA test. So, it is expected that the $\boldsymbol{U_x}$ obtained this way contains information about machine and artefact variation through 24 hours as opposed to what takes place during a single measurement cycle (half an hour). The estimated standard uncertainties vary for *Cold-Cold* test between 0.77 and 3.1 μm for *X*, 0.77 and 2.1 μm for *Y* and 2 and 4.7 μm for the *Z* coordinates. The *Hot-Cold* measurement resulted in larger values of standard uncertainties: from 0.8 to 7.3 μm for *X*, from 8.7 to 14 μm for *Y* and from 6.4 to 11 μm for the *Z* coordinates.

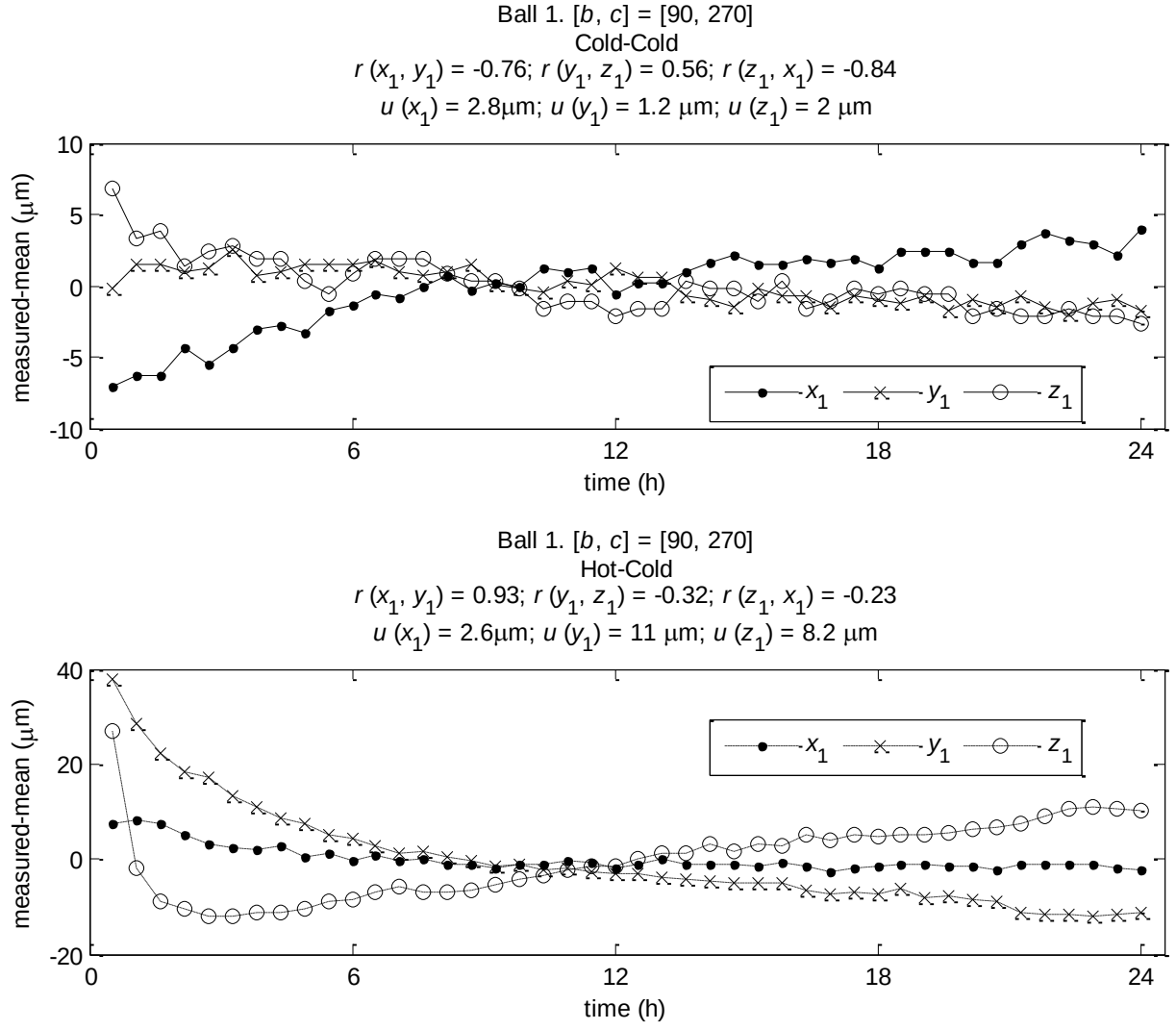

Figure 4.4: *X*-, *Y*- and *Z*- coordinates of ball 1 obtained from the repeated measurements in [*b*, *c*] = [90°, 270°] with (bottom) and without (top) the warm-up cycle

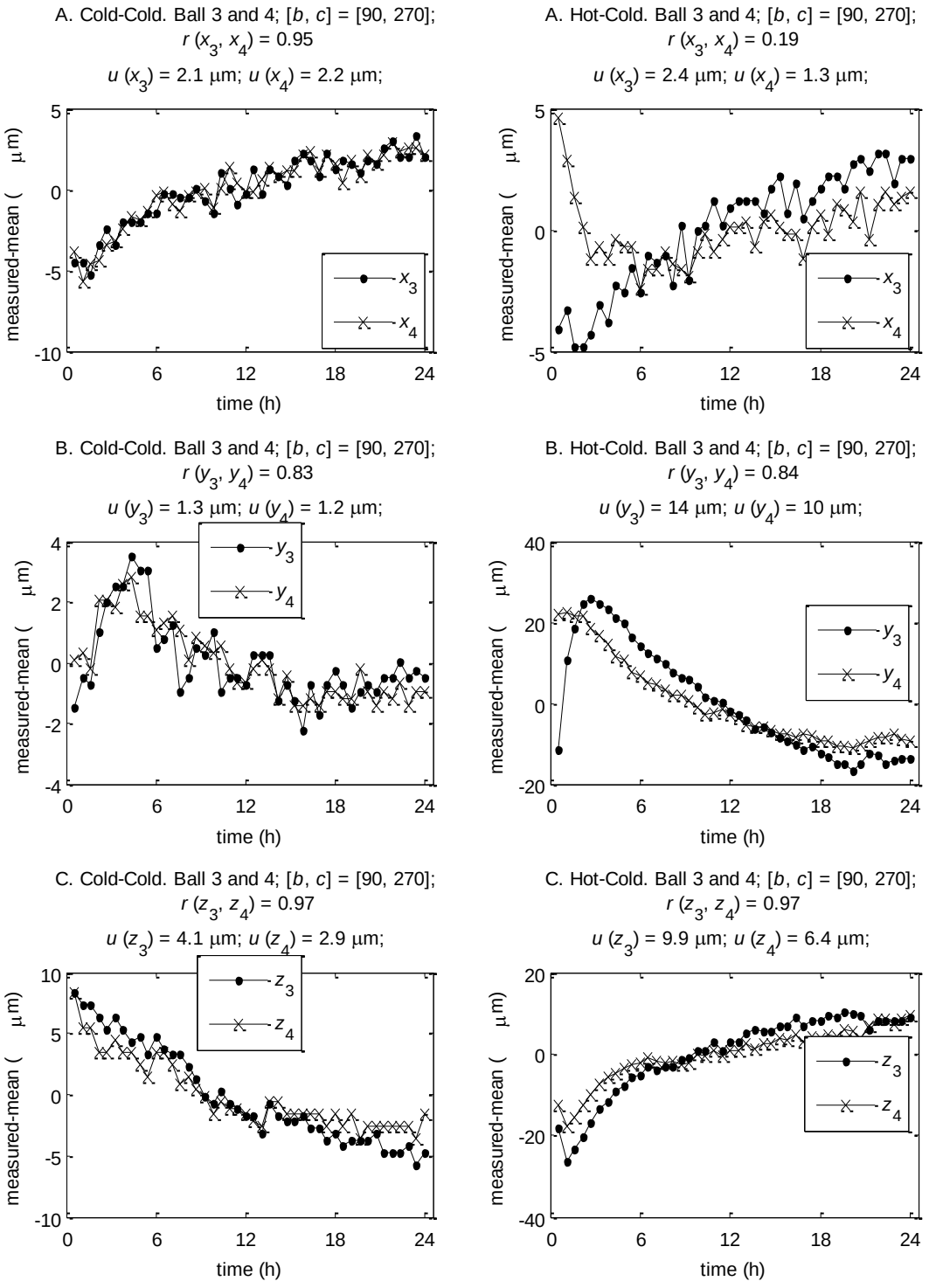

Figure 4.5: Probing results of balls 3 and 4 obtained from the repeated measurements in [*b*, *c*] = [90°, 270°] with (right) and without (left) the warm-up cycle

The experimental SAMBA repeated measurements are used to calculate the covariance $\boldsymbol{U}_x$ of the probing data, which includes their standard uncertainties and correlations between them (which are not depicted for all the gathered data due to their large amount).

The calculated correlation coefficients along with the probing standard deviations are used to estimate the joint PDF of the input data, which is later used to sample the input data vectors for MCM using the $\boldsymbol{U}_{\boldsymbol{x}}$ obtained from the *Cold-Cold* test and from *Hot-Cold* in the independent MC simulations.

4.6.2 **Machine errors**

The calibration results are presented for the eleven output quantities representing the machine geometric error parameters. The other output quantities (artefact estimated geometry) are also considered when the adaptive MCM stabilizing parameters are calculated but are not presented here since they are a byproduct that is not used. In all the presented adaptive MCM cases, the results reached the required stability after $hM = 10^5$ MC trials. For the coverage probability p = 0.95 the estimated rectangular regions coverage factor k_q = 2.9 (for a single output the coverage factor for p = 0.95 is k = 2). In Figure 4.6, the repeated SAMBA calibration results, obtained with and without the warm-up cycle, are depicted with their expanded uncertainties:

$$U_p(y_i) = \pm k_q u(y_i) \tag{4.14}$$

where $u(y_i)$ is the standard uncertainty of y_i calculated from the covariance matrix $U_{\boldsymbol{y}}$.

Performing the warm-up cycle before measurements led to significant machine geometry changes. However, over time and with the temperature decreasing, the geometry converges to the same state as in the *Cold-Cold* and, for most of the parameters, reached stability after a few hours. A similar trend (with the significant value changes at the beginning of the test series) could be observed in the probing results (Figure 4.4 and Figure 4.5). The uncertainties of *Cold-Cold* and *Hot-Cold* measurands were estimated from the corresponding probing data. For the test with the warm-up (*Hot-Cold*), additional adaptive MCM simulation was conducted that included the probing data from the same *Hot-Cold* cycle but without the results obtained during the first 6 hours (*Hot-Cold**) in order to exclude the period when the machine geometry appears to be changing significantly as can be observed in the calibration results (Figure 4.6). The calibration pre-conditions had the least

impact on E_{COY}, regarding its variations as well as its uncertainties. For the remaining parameters, the Hot-Cold uncertainty intervals are significantly wider than the Cold-Cold ones. Removing the early test data, where the machine geometry changes the most, allows reducing the uncertainty and depicts the machine performance impact on the calibration results when the calibration is performed only a few hours after the warm-up cycle. In the case of E_{AOB}, E_{AOY} and E_{AOC} their *Hot-Cold** uncertainties have smaller values than the *Cold-Cold* ones.

Figure 4.7 depicts the adaptive MCM simulation results for *Hot-Cold* (top graphs) and *Cold-Cold* (bottom graphs) with three uncertainties. The *Hot-Cold* MCM results are more dispersed, which is reflected by the uncertainties. The estimated correlation coefficients differ between the *Hot-Cold*, *Cold-Cold* and *Hot-Cold** results. The highest correlations can be observed when the *Hot-Cold* covariance is used (similarly to the probing data). E_{AOB} and E_{AOY} are strongly correlated in all three cases while the correlation between E_{COB} and E_{XOC} decreases significantly when *Cold-Cold* data is analyzed.

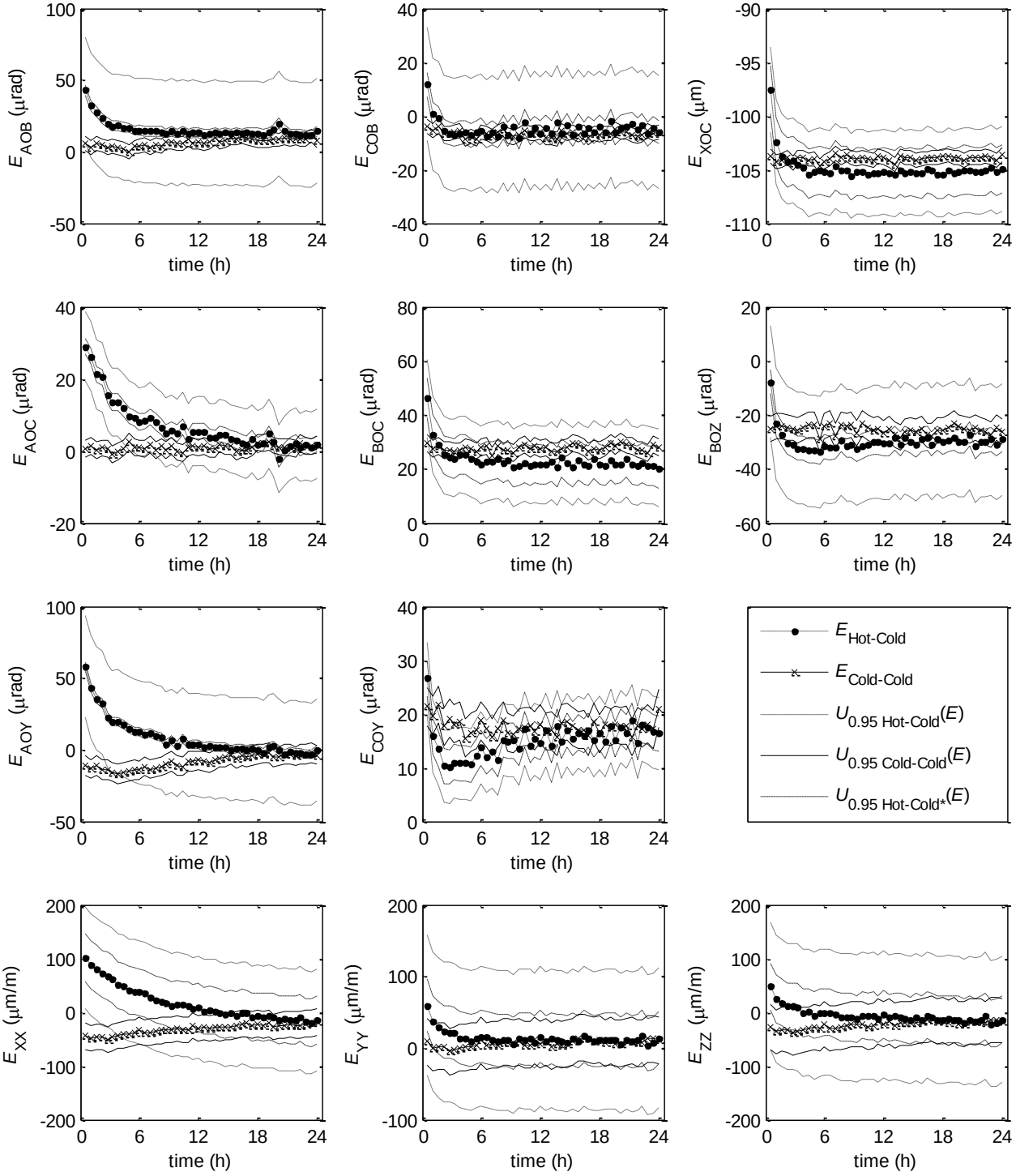

Figure 4.6: Repeated SAMBA calibration results for *Cold-Cold* and *Hot-Cold* test with three uncertainties for $p = 0.95$

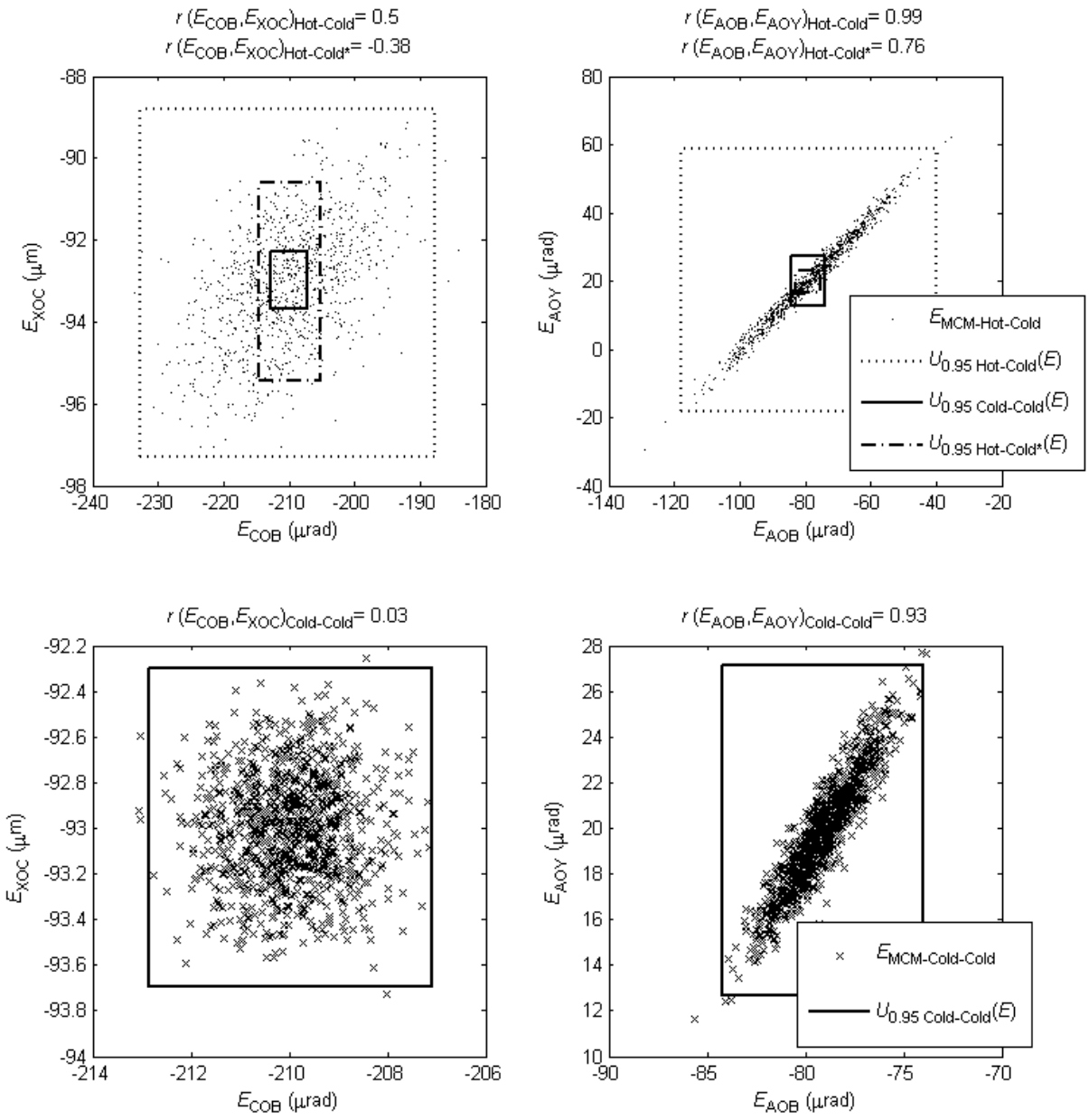

Figure 4.7: MCM results for *Cold-Cold* (bottom) and *Hot-Cold* (top) with the estimated expanded rectangular uncertainties for $p = 0.95$ for E_{XOC} vs. E_{COB} (left) and E_{AOY} vs. E_{AOB} (right) (only 1% of the results are depicted for graph clarity reasons)

When all the data is analyzed, the most correlated are the scale errors E_{xx}, E_{yy} and E_{zz}. The strong correlations between those three parameters are probably due to thermal effects due to the whole machine either cooling down, for the *Hot-Cold* test, or slightly warming up, for the *Cold-Cold* test. It is also observed that the correlations are significantly stronger for *Hot-Cold* data than for *Cold-Cold* probably due to the larger thermal drift in the probing results.

Since strong covariances are present, whenever the calibration results are used in further calculations, e.g., for predicting the volumetric error, and their uncertainty is propagated, it is crucial to include such covariance since the rectangular uncertainty regions (2D projections of the hyper-rectangular coverage regions of the dimension *m*) are covering a vast area where there are no results (as in Figure 4.7 – right). Sampling the results PDFs without including their correlations would result in generating the input vectors with the values covering the whole hyper-volume of the hyper-rectangular uncertainty coverage regions. This is not likely to occur when a correlation between the parameters is observed and would not reflect the machine geometry behavior.

4.7 Conclusion

A single calibration test reflects the machine geometric state at the moment and conditions of the measurement. The conducted research shows that changes in the machine geometry can be observed during a 24-hour period. The calibration pre-conditions significantly impact the calibration result. A method for evaluating the uncertainty on the calibration results that includes machine performance has been proposed.

The adaptive MCM (Monte Carlo method) was used to calculate the machine geometric error parameters (output quantity) uncertainties for the indirect, iterative and multi-output calibration method SAMBA. Although time-consuming (100 000 MC trials take around 28 hours to simulate), this uncertainty estimation method proved its usefulness when an iterative measurement model is being analyzed.

The uncertainty on the probing (input quantity) was estimated experimentally from 44 repetitions over a 24 hours period with (*Hot-Cold*) and without (*Cold-Cold*) warm-up cycle before the test series to demonstrate machine performance in different conditions. This input uncertainty estimation approach includes the influence of both the changing measurand and changing artefact. Their variations are visible in the probing data. A stronger trend is observed in probing in the *Hot-Cold* than in *Cold-Cold* conditions. That corresponds to the machine cooling down in the former and slightly warming up in the latter.

The input covariance matrix (estimated from the repeated probing) contains, apart from the standard uncertainties, the correlations between the input quantities – full uncertainty structure. That way the probing data interdependencies are considered and the MC sampling is performed

accordingly. Thus, the calibration results with expanded uncertainty reflect the machine daily "behavior" in terms of the interdependence of certain error sources and not only the range of variations. Including these interdependencies in uncertainty propagation may be substantial when the compensation values are to be used to correct the machine or compensate it by changing parameters in the machine controller.

The estimated machine geometric error parameters (output quantity) expanded uncertainties are calculated using the coverage factors for a multi-output model for a desired coverage probability $p = 0.95$so that the depicted coverage regions reflect this probability. The obtained expanded uncertainties reflect the machine performance. The tests performed without the warm-up cycle resulted in smaller calibration uncertainty than those performed after the warm-up test but may not reliably represent the behavior of a machine accomplishing a variety of tasks over a 24 hour period.

Finally, the correlations between the output parameters are estimated, which is crucial in a multivariate analysis, so that, for example, the uncertainty on volumetric error predictions could be confidently estimated on the basis of these machine error parameters.

4.8 Acknowledgment

This research was supported by the NSERC Canadian Network for Research and Innovation in Machining Technology (NSERC CANRIMT; www.nserc-canrimt.org).

4.9 References

[1] H. Schwenke, W. Knapp, H. Haitjema, A. Weckenmann, R. Schmitt, and F. Delbressine, "Geometric error measurement and compensation of machines-An update," CIRP Annals - Manufacturing Technology, vol. 57, pp. 660-675, 2008.

[2] H. F. F. Castro, "Uncertainty analysis of a laser calibration system for evaluating the positioning accuracy of a numerically controlled axis of coordinate measuring machines and machine tools," Precision Engineering, vol. 32, pp. 106-113, 2008.

[3] A. C. Okafor and Y. M. Ertekin, "Vertical machining center accuracy characterization using laser interferometer: Part 1. Linear positional errors," Journal of Materials Processing Technology, vol. 105, pp. 394-406, 2000.

[4] H. Jae Pahk, Y. Sam Kim, and J. Hee Moon, "A new technique for volumetric error assessment of CNC machine tools incorporating ball bar measurement and 3D volumetric

error model," International Journal of Machine Tools and Manufacture, vol. 37, pp. 1583-1596, 1997.

[5] B. Bringmann, A. Küng, and W. Knapp, "A Measuring Artefact for true 3D Machine Testing and Calibration," CIRP Annals - Manufacturing Technology, vol. 54, pp. 471-474, 2005.

[6] W. T. Lei and Y. Y. Hsu, "Error measurement of five-axis CNC machines with 3D probe ball," Journal of Materials Processing Technology, vol. 139, pp. 127-133, 2003.

[7] S. H. H. Zargarbashi and J. R. R. Mayer, "Single setup estimation of a five-axis machine tool eight link errors by programmed end point constraint and on the fly measurement with Capball sensor," International Journal of Machine Tools and Manufacture, vol. 49, pp. 759-766, 2009.

[8] S. Aguado, D. Samper, J. Santolaria, and J. J. Aguilar, "Identification strategy of error parameter in volumetric error compensation of machine tool based on laser tracker measurements," International Journal of Machine Tools and Manufacture, vol. 53, pp. 160-169, 2012.

[9] S. Moustafa, N. Gerwien, F. Haertig, and K. Wendt, "Comparison of error mapping techniques for coordinate measuring machines using the plate method and laser tracer technique," in 19th IMEKO World Congress 2009, September 6, 2009 - September 11, 2009, Lisbon, Portugal, 2009, pp. 2487-2491.

[10] J. R. R. Mayer, "Five-axis machine tool calibration by probing a scale enriched reconfigurable uncalibrated master balls artefact," CIRP Annals - Manufacturing Technology, vol. 61, pp. 515-518, 2012.

[11] B. Bringmann, J. P. Besuchet, and L. Rohr, "Systematic evaluation of calibration methods," CIRP Annals - Manufacturing Technology, vol. 57, pp. 529-532, 2008.

[12] GUM, "Evaluation of measurement data - Guide to the expression of uncertainty in measurement," ed, Joint Committee for Guides in Metrology, JCGM 100:2008.

[13] B. Bringmann and W. Knapp, "Model-based `Chase-the-Ball' Calibration of a 5-Axes Machining Center," CIRP Annals - Manufacturing Technology, vol. 55, pp. 531-534, 2006.

[14] GUM, "Evaluation of measurement data – Supplement 1 to the "Guide to the expression of uncertainty in measurement" – Propagation of distributions using a Monte Carlo method," ed, Joint Committee for Guides in Metrology, JCGM 101:2008.

[15] L. Andolfatto, J. R. R. Mayer, and S. Lavernhe, "Adaptive Monte Carlo applied to uncertainty estimation in five axis machine tool link errors identification with thermal disturbance," International Journal of Machine Tools and Manufacture, vol. 51, pp. 618-627, 2011.

[16] J. Santolaria and M. Ginés, "Uncertainty estimation in robot kinematic calibration," Robotics and Computer-Integrated Manufacturing, vol. 29, pp. 370-384, 2013.

[17] H. Schwenke, M. Franke, J. Hannaford, and H. Kunzmann, "Error mapping of CMMs and machine tools by a single tracking interferometer," CIRP Annals - Manufacturing Technology, vol. 54, pp. 475-478, 2005.

[18] GUM, "Evaluation of measurement data – An introduction to the "Guide to the expression of uncertainty in measurement" and related documents," ed, Joint Committee for Guides in Metrology, JCGM 104:2009.

[19] GUM, "Evaluation of measurement data – Supplement 2 to the "Guide to the expression of uncertainty in measurement" – Extension to any number of input quantities," ed, Joint Committee for Guides in Metrology, JCGM 102:2011.

[20] S. Eichstadt, A. Link, P. Harris, and C. Elster, "Efficient implementation of a Monte Carlo method for uncertainty evaluation in dynamic measurements," Metrologia, vol. 49, pp. 401-410, 2012.

[21] A. Lamikiz, L. N. López de Lacalle, and A. Celaya, "Machine Tool Performance and Precision," in Machine Tools for High Performance Machining, L. N. López de Lacalle and A. Lamikiz, Eds., ed London: Springer London, 2009, pp. 219-260.

[22] ISO, "Test code for machine tools -- Part 2: Determination of accuracy and repeatability of positioning of numerically controlled axes," ed, 230-2:2014.

[23] ASME, "Methods for Performance Evaluation of Computer Numerically Controlled Machining Centers," ed, B5.54:2005.

[24] Y. A. Mir, J. R. R. Mayer, and C. Fortin, "Tool path error prediction of a five-axis machine tool with geometric errors," Proceedings of the Institution of Mechanical Engineers, Part B: Journal of Engineering Manufacture, vol. 216, pp. 697-712, 2002.

[25] B. Bringmann and W. Knapp, "Machine tool calibration: Geometric test uncertainty depends on machine tool performance," Precision Engineering, vol. 33, pp. 524-529, 2009.

[26] P. Antonio, "Copulas for uncertainty analysis," Metrologia, vol. 47, p. 262, 2010.

CHAPTER 5 ARTICLE 2: MACHINE GEOMETRY TIME DEPENDENT VARIATIONS AND THEIR EFFECT ON CALIBRATION RESULTS

A. Los, N. Alami Mchichi, J. R. R. Mayer

Department of Mechanical Engineering, Polytechnique Montreal, Montreal, QC, Canada

* Submitted to *Measurement* in March 2017

5.1 Abstract

Machine geometry is changing over time and requires frequent calibration. The calibration results reflect the machine state during the performed procedure. It can be suspected that the geometry is changing between days and even over a day. The question is how significant are those changes and whether they are time dependent. In order to observe the machine performance changes, the scale and master balls artefact (SAMBA) calibration method is repeatedly conducted on a five-axis machine tool. This indirect calibration method allows estimating simultaneously a number of the geometric error parameters (output quantity) from the measurements performed in the machine working volume (input quantity). When an uncalibrated artefact is used the machine readings are the main contributor of the measurement process. Thus, the machine geometry changes are, both, the measurand and the uncertainty source. In this paper, a method for estimating the calibration pooled uncertainty, including the machine-probe-artefact measuring system and its changes over time is proposed. The uncertainty sources of the method are listed. The measurement variations and trend occurring during the test, the random and systematic errors are discussed. The measurement uncertainty is estimated from the repeated measurements. The strategy for performing the test (considering its duration and the pre-test machine conditions) and computing the covariance matrix are discussed. The experimentally estimated correlations between the input data are analyzed. The estimated probing data uncertainty is then used to calculate the calibration results uncertainty through the adaptive Monte Carlo method (MCM). Three methods of uncertainty estimation considering short- and medium-term changes are proposed. The results show that the machine performance changes over time and has an impact on the calibration results. The obtained uncertainties explain the measurand variation over time. The proposed uncertainty

estimation method allows including machine performance variations in the calibration evaluation and would be beneficial to the machine user after the calibration results are obtained and the compensation is about to be applied. Results highlight the necessity of including the machine performance along with its changes occurring over time in the calibration uncertainty estimation.

Keywords: machine tool, calibration, SAMBA, Monte Carlo, uncertainty, GUM S2.

5.2 Introduction

The calibration of multi-axis machine tools is a demanding task. Its aim is to allow estimating the machine geometric error so that the machine's positioning accuracy can be evaluated and corrected. Various methods are used in industry, which are usually classified into direct (measuring an error source of one axis without the influence of the other axes) and indirect (estimating the errors by error separation from measurement resulting from errors superposition) [1]. The former are usually realized with laser interferometry [2]. The latter use instruments such as ballbar, laser trackers [3] or Lasertracer [4] measurements or the probing of various calibrated or uncalibrated 2- and 3-D artefacts [5, 6].

The choice of the calibration method and the action taken based on its result should consider their quality since it has a direct impact on the machined workpiece geometric and dimensional errors [7]. In the case of the direct methods, the quality of the calibration results can be quantified by the uncertainty of the estimated errors that can be propagated from the uncertainty of the performed measurement (e.g., laser interferometer displacement measurement). The indirect methods often require specific uncertainty evaluation methods, usually based on the Monte Carlo method (MCM) [1]. Schwenke et al. [8] estimated the uncertainty of six parametric errors from the uncertainty of the laser tracking interferometer measurements modeled as the interferometric length measurement and propagated to the calibration results using MCM. This method only includes the uncertainty of the measuring device (laser interferometer), which Bringmann et al. [5] demonstrated to be insufficient and showed that the machine performance may be the main contributor to the calibration uncertainty. In order to evaluate this influence the machine was modeled with all its geometrical errors and this model was used in MCM simulation (the typical noise range taken from the standards or machine specification was added to the modeled errors without considering the correlation between them) to generate the R-test [9] results and to identify from four parametric

errors. The obtained sets of identified errors were used to calculate their standard deviations as uncertainties. However, the machine geometry not only has an impact on the calibration results, but also changes over time. This issue is investigated by Parkinson et al. [10] for the direct squareness measurement performed using a mechanical square and indicator. The authors show that the calibration result changes due to temperature drift and propose an automated scheduling method that minimizes the calibration uncertainty due to the measurand change which occurs between the performed squareness measurements. When the machine performance is considered in the uncertainty estimation its variation should be included, not only with the typical ranges specified by the manufacturer, but also those occurring in the daily and/or weekly machine working period.

This research focuses on the short- and medium-term measurand (machine geometric error parameters) variations and their impact on the calibration results obtained using the scale and master balls artefact (SAMBA) method probing data uncertainty estimation. The machine tool geometry changes, due to apparently random and systematic error, caused for example by the thermal drift of the machine and the artefact, occurring during each day, between days, as well as during the entire test procedure. In order to estimate the input data uncertainty (covariance) and analyse the measurand variation, repeated SAMBA measurements are performed over a few days. The calibration results uncertainties are estimated using the adaptive MCM according to GUM S2 [11].

5.3 Calibration method

Calibration of the machine tool using the SAMBA [6] method requires probing an artefact, consisting of a number of master balls (typically four) and a scale bar (Figure 5.1), using the machine touch probe mounted on the spindle, for different machine B- and C-axis indexations. The probing data (input data) and a machine kinematic model are used to identify the machine geometric error parameters (output data).

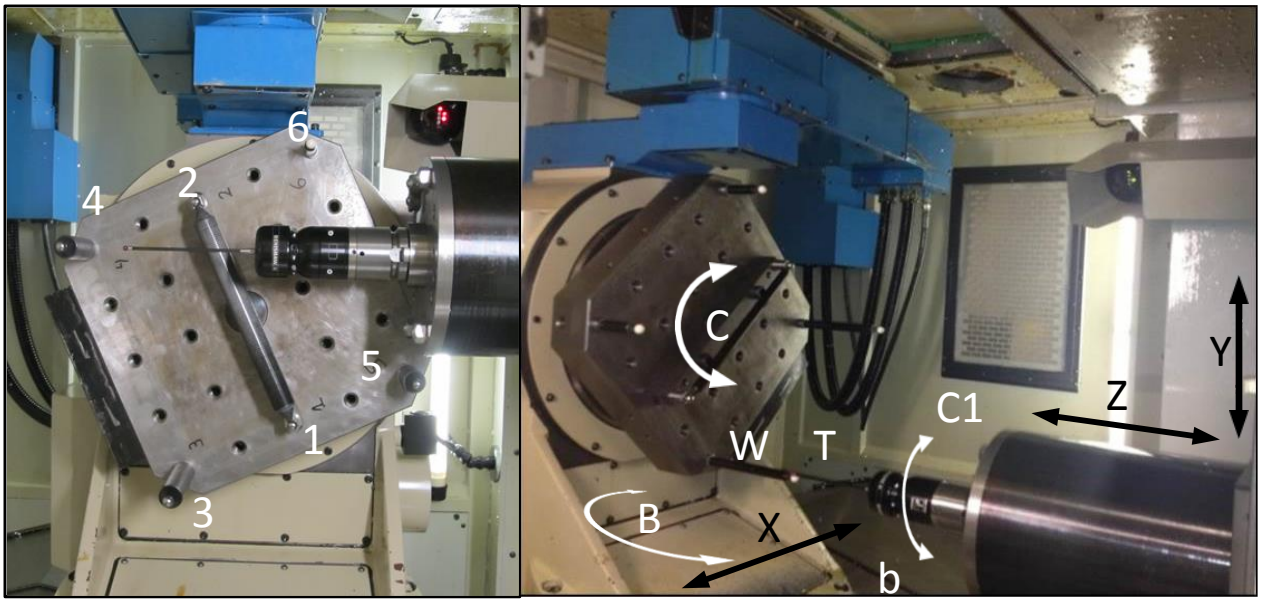

Figure 5.1: SAMBA artefact being probed using the touch trigger probe on the Mitsui Seiki HU40-T machine tool with the topology WCBXbZY(C1)T; W – workpiece, T – tool, b – machine bed, B, C – rotary axes around the Y and Z axes respectively, X, Y, Z – machine linear axes, C1 – spindle

During calibration each master ball is probed in five points and the probe tip and the master ball virtually coincide (physically the probe cannot reach inside the master ball), thus their actual positions are virtually the same. When the X-, Y- and Z-axis probing readings are introduced in the (nominal) machine kinematic model and used to predict the tip and the ball center position, the difference between those vectors is the initial prediction error $\boldsymbol{x}_R$. In order to minimize $\boldsymbol{x}_R$ (residuals) the Newton-Gauss approach is used to estimate the changes in the machine geometric error parameters y:

$$\boldsymbol{x}_R + J \cdot \delta \boldsymbol{y} = 0 \tag{5.1}$$

Where J is the sensitivity Jacobian matrix of the $\boldsymbol{x}_R$ to the machine geometric error parameters.

Equation 5.1 is solved for $\delta \boldsymbol{y}$, which in the next step is introduced in the machine kinematic model and the new $\boldsymbol{x}_R$ is calculated. That allows estimating a new adjustments $\delta \boldsymbol{y}$. This procedure is repeated until $\delta \boldsymbol{y}$ is smaller than a specific threshold which indicates insignificant changes adjustments in $\boldsymbol{y}$.

5.4 Input quantity uncertainty

The input data (probing) uncertainty results from systematic and apparently random causes, such as thermal drift, changes in the machine and artefact geometry, such as the artefact deflection and geometry change due to thermal effects. However, when we consider the artefact geometry variations, only those occurring within one measurement cycle will influence the calibration results. The measuring equipment used in the SAMBA calibration method are the touch probe and the artefact. During such a measurement process the machine indications are gathered because they cannot be predicted in advance. This is different from a measurement process, as is used for example when conducting a laser interferometer or laser tracking test, in which the machine is programmed to reach a specific commanded position. In such cases the machine readings are not independently gathered, they are assumed. In both approaches the machine variability is present. As a result, depending on the measuring process used, the machine variability manifests itself either in the instrument readings or in the machine readings. In order to include the impact of the machine performance and the calibration scheduling in the calibration uncertainty, the repetition of test measurements is proposed for input data uncertainty estimation. The uncertainty estimated this way includes the variation of the geometry and performance occurring over time in the probe, artefact and machine. However, it does not include repeatable errors such as the probe lobing errors, stem bending and repeatable components of the motion errors.

The repeated measurement allows calculating the N input data covariance matrix:

$$\boldsymbol{U}_{\mathrm{x}} = \begin{bmatrix} u(x_1, x_1) & \dots & u(x_1, x_{N-1}) & \\ \vdots & \ddots & \vdots & 0 \\ u(x_N, x_1) & \dots & u(x_{N-1}, x_{N-1}) & \\ & 0 & & u(x_N, x_N) \end{bmatrix} \tag{5.2}$$

where each element (i, j) equals:

$$u(x_i, x_j) = r(x_i, x_j)u(x_i)u(x_j) \tag{5.3}$$

where $u(x_i)$ and $u(x_j)$ are the uncertainties of x_i and x_j and $r(x_i, x_j)$ is the correlation between them. The first N-1 elements correspond to the coordinates of probing data and the N-th element is the uncertainty of the scale bar length as an uncorrelated component.

In order to analyze the differences between short- and medium-term variation, the uncertainties are estimated in three ways: for each day u, from all of the performed cycles u_{all} and pooled by the days u_{pooled} (including variation occurring during each day, but removing variation between the days). The pooled covariance $\boldsymbol{U}_{\text{x pooled}}$ is calculated as the weighted average of each day covariance $\boldsymbol{U}_{\text{x}}$:

$$\boldsymbol{U}_{\text{x pooled}} = \frac{\sum_{i=1}^{k}\left((n_i-1)\boldsymbol{U}_{\text{x}i}\right)}{\sum_{i=1}^{k}(n_i-1)} \tag{5.4}$$

where n_i is the number of repetitions of the i-th day, k is the number of days and $\boldsymbol{U}_{\text{xi}}$ is the covariance of the i-th day.

5.5 Output quantity uncertainty

The SAMBA calibration method has a multi-input multi-output model with an iterative solution that makes the analytical uncertainty calibration methods not feasible. Thus, the uncertainty of the geometric error parameters is calculated from the probing uncertainty through (adaptive) MCM according to GUM S2 [11] which allows adjusting the number of the MCM trials M depending on the required results stability. The minimum value of M is 10^5. The standard deviations, correlations and the probability density functions (PDFs) of the input quantity are estimated from the performed SAMBA measurements.

5.6 Measurements and simulation

In order to estimate the covariance matrix of the input quantity the repeated measurement was performed over five days (with a break between the 4$^{\text{th}}$ and 5$^{\text{th}}$ day) with four SAMBA cycles each day. The tests were performed in the laboratory with the temperature varying during most of the time between 21.5 and 22.5 degrees Celsius with short spikes at 23.5 and 24.5 degrees Celsius.

Four master balls, with a diameter of 19.05 mm mounted on rods with the lengths: 178.8, 153.4, 102.6 and 77.2 mm were probed at $c_1 = 0$ (spindle indexation angle) and [b, c] = [-60, -235], [0, -135], [0, 0], [0, 90], [30, 175], [90, 270], [50, 170], [0, 135], [15, 0], [0, -50], [-45, -90], [-90, -270] deg and at [b, c] = [0, 0] for c_1 = 90, 180 and 270 deg. The scale bar of length 304.98923 mm was probed at [c_1, b, c] = [0, 0, 0]. This strategy takes around 65 minutes for each measuring cycle.

The measurement results are used to identify thirteen machine geometric error parameters listed in Table 5.1. The analyzed machine is modeled in MATLAB with the geometric error parameters obtained from the performed SAMBA measurement so that the MCM simulations can be implemented. The input quantity joint PDF is modeled using a Gaussian copula that includes correlations between the input data. The parameters of this copula are estimated from the repeated measurement covariance. This estimation of the input data joint PDF allows keeping the measurement data variations occurring over time and with the correlations between them, which reflects the machine performance variations when the samples are drown for the MCM simulation.

Table 5.1: Identified machine geometric error parameters

Symbol	Description
E_{AOB}	out-of-squareness of the B-axis relative to the Z-axis (μrad)
E_{COB}	out-of-squareness of the B-axis relative to the X-axis (μrad)
E_{XOC}	distance between the B and C axes (μm)
E_{AOC}	out-of-squareness of the C-axis relative to the B-axis (μrad)
E_{BOC}	out-of-squareness of the C-axis relative to the X-axis (μrad)
E_{BOZ}	out-of-squareness of the Z-axis relative to the X-axis (μrad)
E_{AOY}	out-of-squareness of the Y-axis relative to the Z-axis (μrad)
E_{COY}	out-of-squareness of the Y-axis relative to the X-axis (μrad)
E_{XOC1}	X offset of the spindle relative to the B-axis (μm)
E_{YOC1}	Y offset to the spindle relative to the C-axis (μm)
E_{XX}	positioning linear error term of the X-axis (μm/m)
E_{YY}	positioning linear error term of the Y-axis (μm/m)
E_{ZZ}	positioning linear error term of the Z-axis (μm/m)

5.7 Results

5.7.1 Input quantity

Example results of the probing changes and of their estimated standard uncertainties are depicted in Figure 5.2. For all the analyzed balls, the systematic and random variations between the cycles and between the days can be observed. The probing results are changing with time (maybe due to what happens over that period such as the effect of the tests and the environmental conditions). For most of the coordinates, similar trends can be observed during each day, especially for the Z

coordinate. The break between days 4 and 5 does not have an observable impact on the results except that for the Z coordinate the *u* values drops on the 4th day but increases on the 5th day.

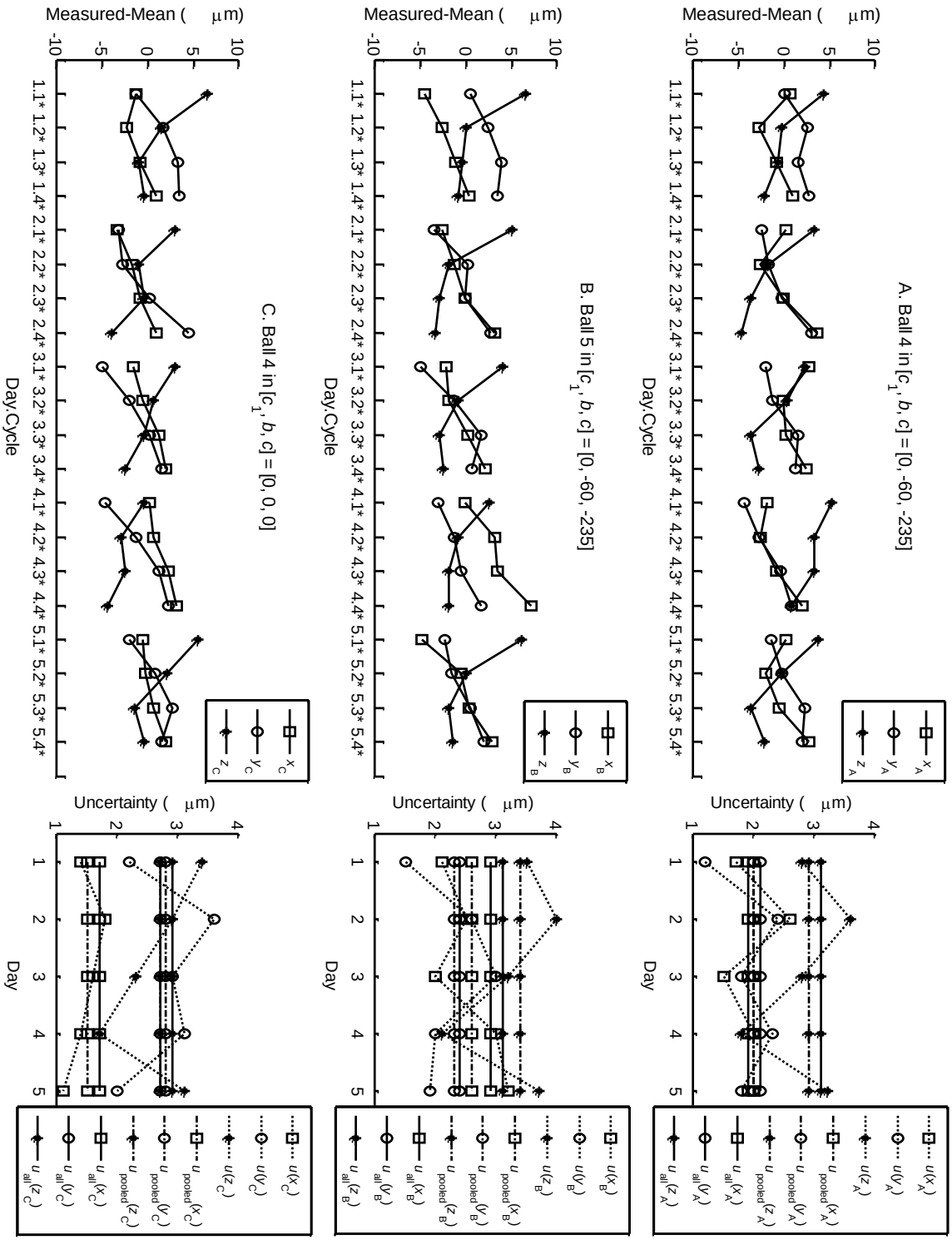

Figure 5.2: Examples (A, B, C) of X, Y and Z coordinate probing variations of master balls (left) and uncertainty calculated for each day, using all the data and pooled by days (right)

The u values vary between the days with the smallest difference occurring for the X coordinate. The values obtained for day 1 and 5 are similar in comparison with the full range of variation (except for x_B). Except for x_A, z_B, y_C, the estimated results of u_{pooled} are lower than u_{all}. When all 159 probing results are considered the maximal estimated uncertainties values are obtained for the Z coordinate: $u_{all}(x) = 3.6$ μm (for ball 3 in $[c_1, b, c] = [0, 0, -135]$), $u(x) = 4$ μm (for z_B) and $u_{pooled}(x) = 3.4$ μm (for z_B).

Figure 5.3 depicts the histograms for the Bartlett's test (testing the hypothesis of equal variances between the groups) and for one-way ANOVA (testing the hypothesis of equal means between the groups) including all the input data probing coordinates. For both statistical tests used, each day is a separate group. The p-values not bigger than 0.05 suggest that at least for one of the days the variance/mean is not equal to the others. For all of the input data, the variances can be considered equal while the means are equal for 25% of the probing data, which may indicate the changes in the artefact and/or machine geometry occurring between the days.

For the coordinates depicted in Figure 5.2 p-values$_B$ (Bartlett's test) and p-values$_A$ (one-way ANOVA) are bigger than 0.05, which means that the daily means and variances are equal for each coordinate. The equal means and variances and the number of degrees of freedom $\upsilon_{all} = 19$ and $\upsilon_{pooled} = 15$ explains, as mentioned before, the u_{all} being higher than u_{pooled} for x_A, z_B, y_C (the pooled covariance is calculated as the mean of the each day covariance – the standard uncertainty is the square root of the mean of the each day standard deviation).

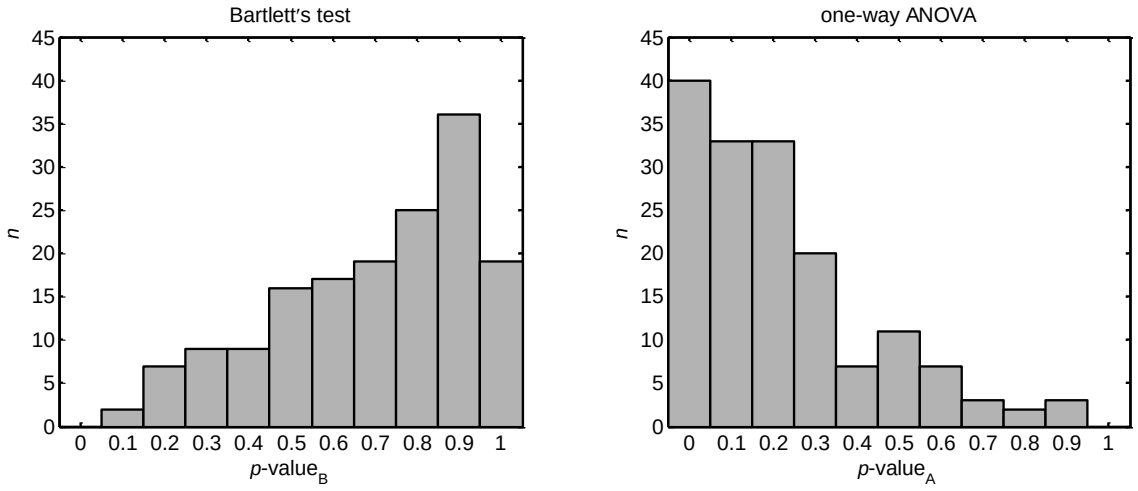

Figure 5.3: Histograms of the p-values for the Bartlett's test and one-way ANOVA estimated for all the probing data

The correlation coefficients between the coordinates for the balls probing examples depicted in Figure 5.2 using two covariance calculation methods are presented in Table 5.2 and Table 5.3.

Correlations between the X, Y and Z coordinates can be observed. Furthermore, the X and Y coordinates values are increasing during the day while the Z are decreasing, which resembles machine's axis and/or artefact drift effect. When all measurements are used to calculate the covariance, the most correlated with each other are Y and Z coordinates. The X coordinates have relatively small correlation coefficients when paired with Y and Z. That results from the machine topology – Y-axis slides on the Z-axis (some of the Z-axis motion errors are directly influencing the motion of Y-axis). Variations in the Z-axis error influence the Y-axis. Thus, the axis readings are correlated [12].

The pooled correlations for X (except for x_A), Y and Z have higher absolute values than those calculated from all the measurements. For all of the correlation coefficients, the sign remains the same for r_{all} and r_{pooled}. That shows that pooling does not change the character of the measurements interdependencies, only its magnitude, which results from similar measurement trend for each day. Pooling causes data separation into the five groups (days) so that the daily measurement sequence plays a bigger role than when the covariance is estimated from all the measurement results (in that case the order of the results has no impact on the covariance value). Including correlation coefficients in the MCM input data sampling is necessary to reflect the actual probing interdependencies.

Table 5.2: Correlation coefficients r_{all} between the coordinates of the three master balls

x_A	0.38	-0.29	0.29	0.13	-0.04	0.38	0.24	-0.10
	y_A	-0.74	0.26	0.84	-0.50	0.35	0.90	-0.28
		z_A	-0.29	-0.63	0.76	-0.26	-0.65	0.47
			x_B	0.34	-0.70	0.83	0.48	-0.89
				y_B	-0.58	0.37	0.86	-0.43
					z_B	-0.57	-0.62	0.86
						x_C	0.51	-0.67
							y_C	-0.51
								z_C

Table 5.3: Correlation coefficients r_{pooled} between the coordinates of the three master balls

x_A	0.47	-0.17	0.53	0.29	0.00	0.61	0.39	-0.20
	y_A	-0.86	0.89	0.87	-0.79	0.85	0.95	-0.81
		z_A	-0.85	-0.89	0.95	-0.79	-0.86	0.93
			x_B	0.84	-0.79	0.86	0.88	-0.87
				y_B	-0.87	0.87	0.87	-0.87
					z_B	-0.7	-0.83	0.92
						x_C	0.85	-0.74
							y_C	-0.86
								z_C

5.7.2 **Output quantity**

The uncertainty of the identified machine geometric error parameters is estimated using adaptive MCM. In all of the cases, the results achieved the required stability thresholds after the initial $M = 10^5$ MCM trials. The estimated uncertainty is a result of the measurement uncertainty propagation and does not include the model uncertainty. However, the model itself can be evaluated through residuals obtained from the prediction using the identified machine geometric error parameters. The maximum residual predicted (including all 20 performed cycles) was 0.032 mm.

In Figure 5. three uncertainties (for each day u, from all of the performed cycles u_{all} and pooled by the days u_{pooled}) are shown for the thirteen identified parameters for the coverage probability $p = 0.95$ (the coverage factor is calculated on the basis of the output covariance $\boldsymbol{U}_y$ and in accordance with the number of output quantities). In addition, the p-values for the Bartlett's test (p-value$_B$) and one-way ANOVA (p-value$_A$) performed on the calibration results estimated from the performed measurements are computed.

The calibration results depict the machine geometry variation. The changes in machine performance can be observed for each day as well as from one day to another. For E_{AOB}, E_{XOC1}, similar trends occurring each day are present. The remaining parameters have more random characteristic and do not reflect the trend that we could observe for the probing data which may result from the uncalibrated artefact geometry changing between the calibration procedures which do not influence the machine geometric errors estimation (the algorithm is simultaneously estimating the artefact and the machine geometry). For all the parameters the daily variances and means (except for E_{BOC}) are equal (p-value > 0.05).

Stopping the machine after the 4th day seems not to have had an impact on the calibration results, except for the E_{BOC}, in which case the mean value of the 4th day significantly differs from the others (p-value$_A$ = 0). This offset was attributed to the resetting of the zero position on the B-axis which holds the C-axis and so directly acts upon $E_{BOC.}$ For all of the parameters common uncertainty bounds can be found when $U_{0.95\ all}$ and $U_{0.95\ pooled}$ (except for E_{BOC}) are considered. Relatively wide uncertainty bounds are observed for p-value$_A$ and p-value$_B$ being the closest to 1. Both, $U_{0.95\ all}$ and $U_{0.95\ pooled}$, have very close values. The changes in the measurand occurring through the 20 cycles performed during five days can be explained (common uncertainty bounds are found) by both the short- $u_{x\ pooled}$ and medium-term $u_{x\ all}$ uncertainty (except for the E_{BOC}).

The variation of E_{BOC} observed for each day is very small. However, the mean value of the fourth day is significantly different than for the remaining days. The uncertainties estimated for each day have close values to each other and to the pooled uncertainty. The common uncertainty bounds can be found for each day calibration results, so $U_{0.95}$ and $U_{0.95\ pooled}$ explain the changes occurring during each day. When all the results are considered, $U_{0.95\ all}$ explains the changes in the measurand. The E_{BOC} does not vary significantly during the day but may vary between the days. The choice of the uncertainty should reflect which variations the user wants to include. If high precision equipment is used to calibrate the machine with large medium- and/or short-term changes, the calibration results will reflect the machine state only at the moment of calibration. However, the machine geometry may change significantly after one calibration cycle, which can be observed in the calibration results. The machine changes occur over a period longer than the calibration time.

The estimated calibration results reflect variations in the machine geometry but do not include the uncalibrated artefact geometry changes from one cycle to another. However, although the latter variations are included in the input uncertainty, the geometric error parameters estimated uncertainty seems not to be overestimated. The uncalibrated artefact's dimensions changes are a disturbance only if they are occurring within one cycle. The SAMBA method uses uncalibrated ball positions which are self-calibrated during the parameters identification. The artefact's dimensions are introduced in the model along with machine geometric error parameters and they are being estimated for each cycle performed. Thus, if the changes in the dimensions occurs between the performed cycles the dimensions in the calibration model are updated. We assume that by using the input data covariances means that the trials correctly reproduced the changes that correspond to artefact geometry variation from those caused by machine geometry variation.

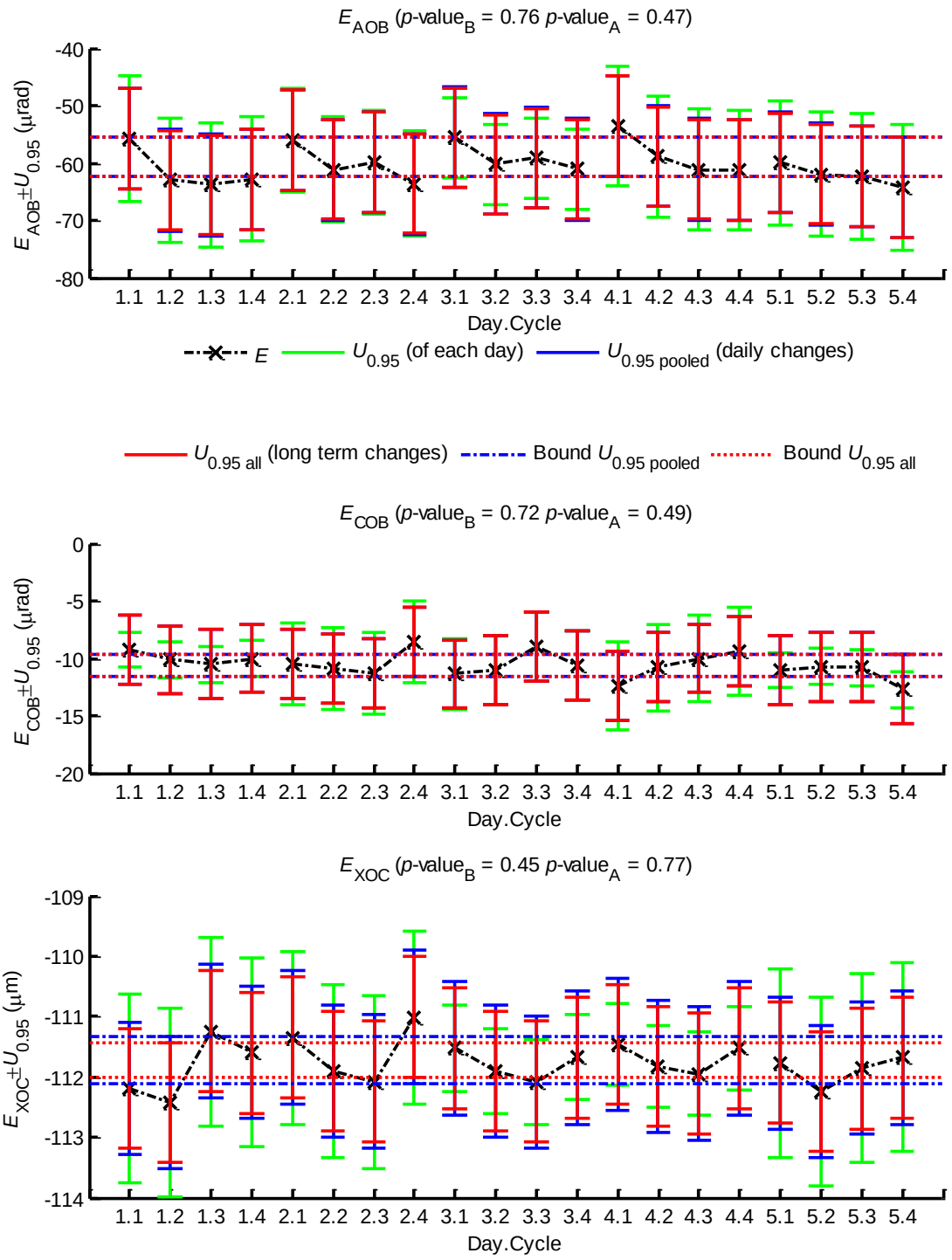

Figure 5.4: Calibration uncertainty values including short- and medium-term measurand changes for the confidence level p = 0.95 with the p-value of the Bartlett's test and one-way ANOVA

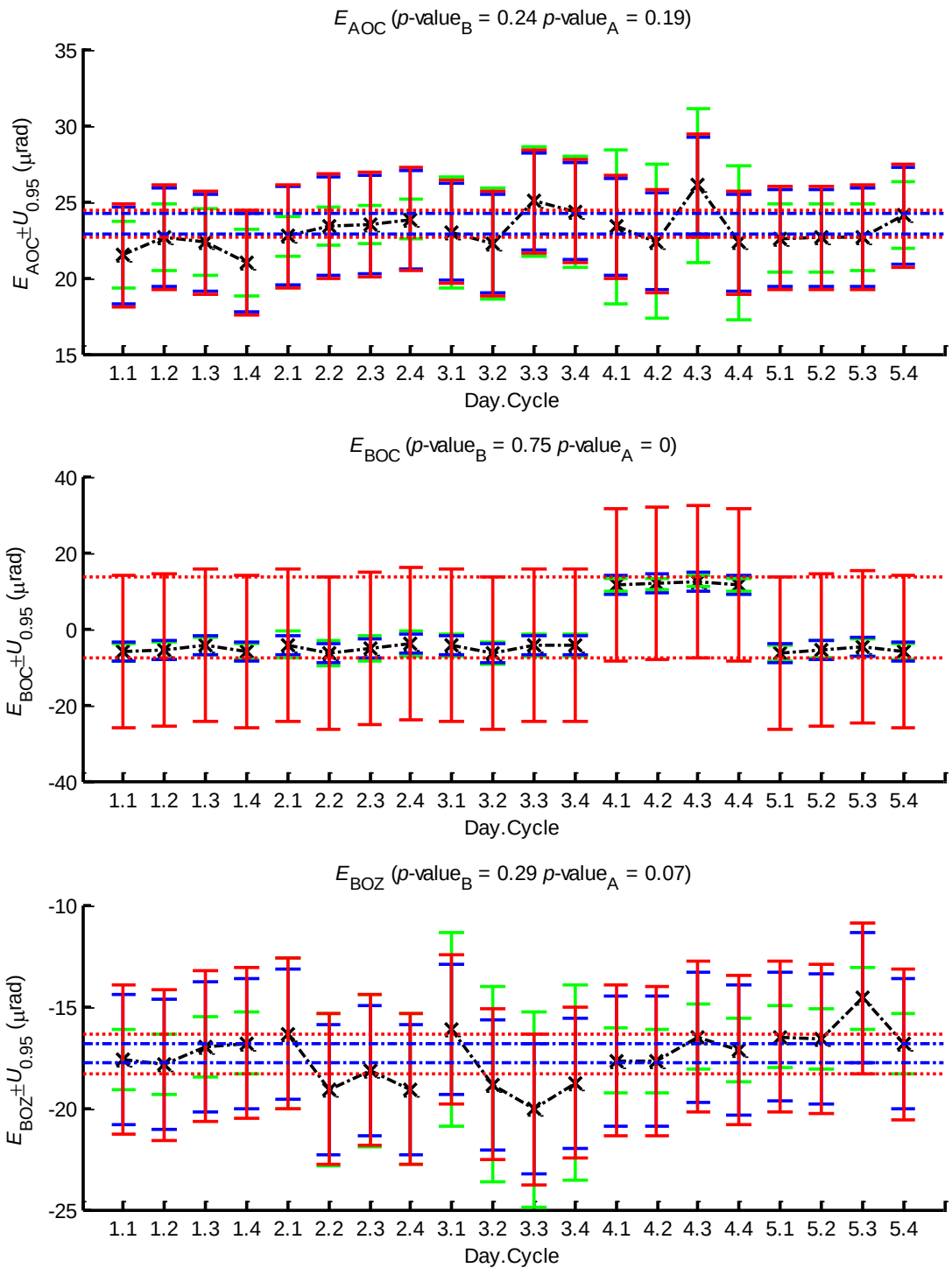

Figure 5.4 (continued): Calibration uncertainty values including short- and medium-term measurand changes for the confidence level p = 0.95 with the p-value of the Bartlett's test and one-way ANOVA

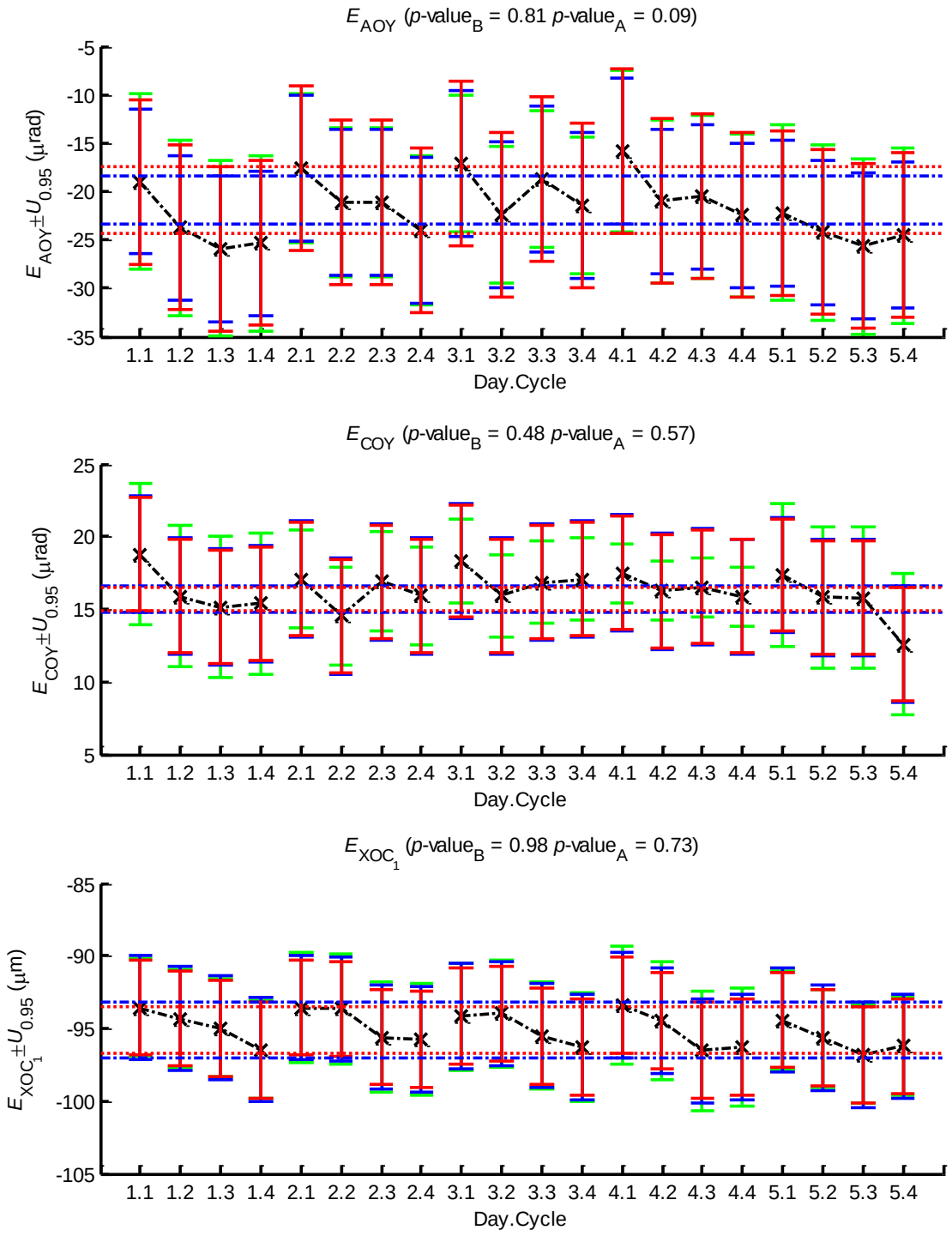

Figure 5.4 (continued): Calibration uncertainty values including short- and medium-term measurand changes for the confidence level p = 0.95 with the p-value of the Bartlett's test and one-way ANOVA

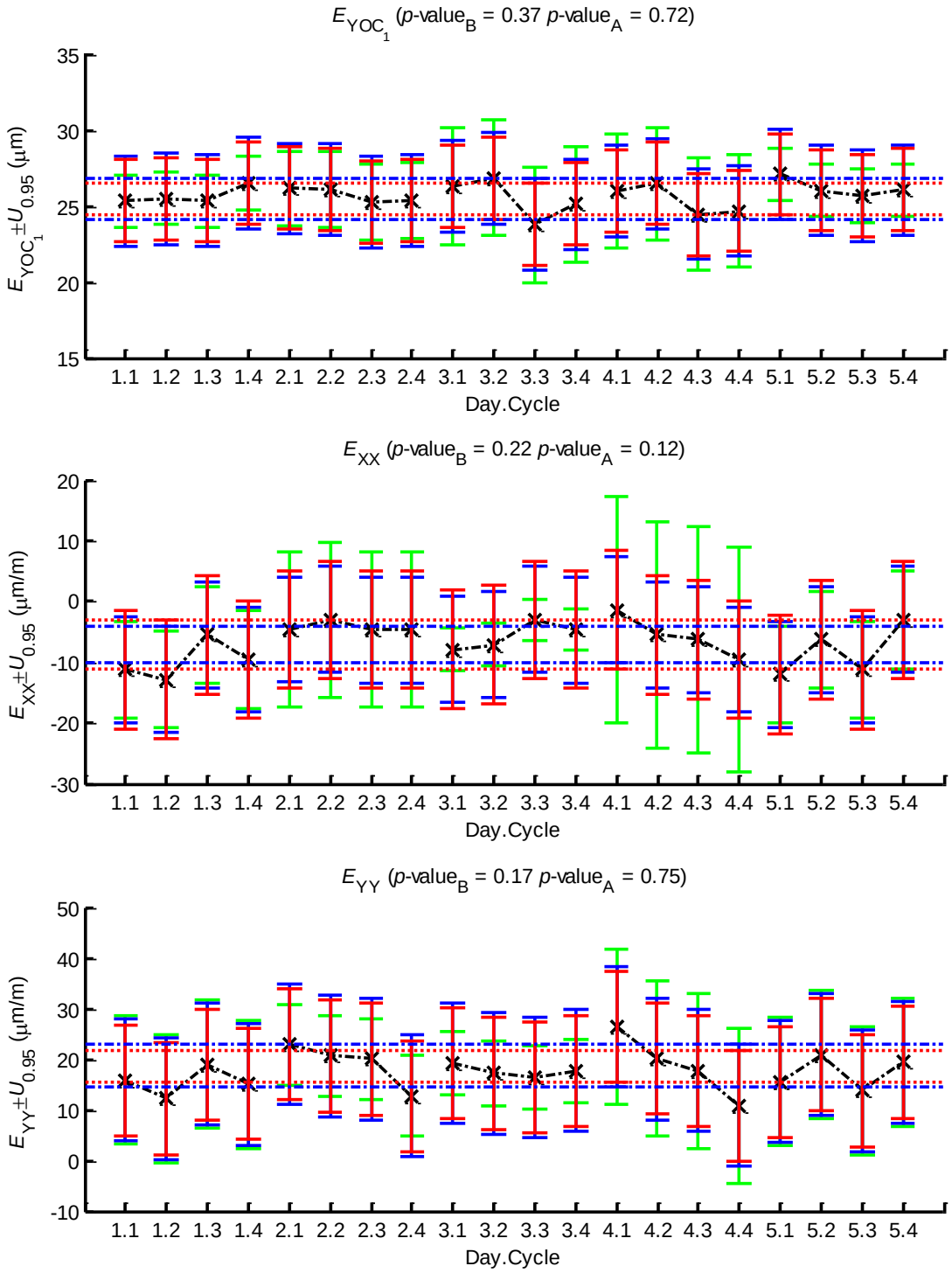

Figure 5.4 (continued): Calibration uncertainty values including short- and medium-term measurand changes for the confidence level p = 0.95 with the p-value of the Bartlett's test and one-way ANOVA

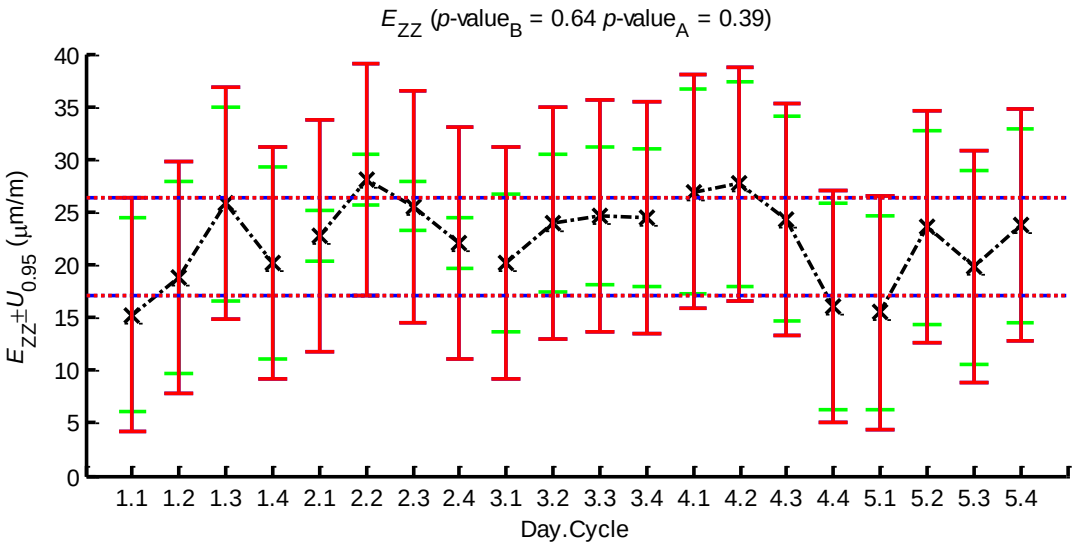

Figure 5.4 (continued): Calibration uncertainty values including short- and medium-term measurand changes for the confidence level p = 0.95 with the p-value of the Bartlett's test and one-way ANOVA

5.8 Conclusion

A detailed investigation of uncertainty in the indirect calibration of a five-axis machine tool including potential changes occurring over time as short- and medium-term are considered. Variations appearing during each day and between the days are taken into account.

The machine performance changes were estimated through repeated measurements. The results were used to calculate three uncertainties i.e. for each day u, from all of the performed cycles u_{all} and pooled by the days u_{pooled} (reflecting short- and medium-term variations) of the input probing data and were propagated on the calibration results using the adaptive Monte Carlo method. The three proposed uncertainty estimation metrics include the machine short-term variations occurring during each day (calculated for each day separately), short-term changes (estimated from the long-term data but pooled by days) or long-term changes (computed from all 20 cycles) as well as the probing repeatability for all three cases.

The input probing data of the repeated scale and master balls artefact (SAMBA) measurement over five days indicate that the machine and/or the artefact are varying during and between the days. The effect of those variations can also be observed in the calibration results. However, while a

trend can be seen in the probing data, the calibration results appear more random possibly due to the artefact self-calibrating SAMBA algorithm.

The performed tests depict the machine performance changes of systematic and apparently random nature. For most of the geometric error parameters the uncertainty pooled by days is smaller or equal to the one calculated from all the results and common uncertainty bounds can be found. Comparison of uncertainties for each day allows finding common bounds in almost each case. Nevertheless, in some cases, they differ significantly and the pooled uncertainty is a better estimate reflecting changes occurring during the day. The uncertainty calculated for all the results reflects weekly fluctuations and is an accurate uncertainty estimate when the daily mean measurand values are not equal.

Since SAMBA is a reconfigurable artefact, the proposed uncertainty method could be used to optimize the artefact configuration as well as the number of measurement points and the rotary axes indexations.

The performed measurement and the identified machine geometric error parameter depicts the machine tool performance impact on the calibration results. The variations occurring in the probing data and the calibration results, demonstrate the necessity of considering the calibration uncertainties (which include machine performance) when the decision about machine geometric errors correction and/or compensation is made. That way we can evaluate the machine tool geometry, not only from the metrologist's point of view (at the time of measurement) but from the machine user's as well (between machine working cycles and days).

Furthermore, the obtained machine geometric results can be used with their covariance as the input quantity for the uncertainty estimation of the volumetric errors mapping and/or prediction of workpiece feature errors.

5.9 Acknowledgments

This research was supported by the NSERC Canadian Network for Research and Innovation in Machining Technology (NSERC CANRIMT; www.nserc canrimt.org).

5.10 References

[1] H. Schwenke, W. Knapp, H. Haitjema, A. Weckenmann, R. Schmitt, and F. Delbressine, "Geometric error measurement and compensation of machines-An update," CIRP Annals - Manufacturing Technology, vol. 57, pp. 660-675, 2008.

[2] J. S. Chen, T. W. Kou, and S. H. Chiou, "Geometric error calibration of multi-axis machines using an auto-alignment laser interferometer," Precision Engineering, vol. 23, pp. 243-252, 1999.

[3] S. Aguado, D. Samper, J. Santolaria, and J. J. Aguilar, "Identification strategy of error parameter in volumetric error compensation of machine tool based on laser tracker measurements," International Journal of Machine Tools and Manufacture, vol. 53, pp. 160-169, 2012.

[4] S. Moustafa, N. Gerwien, F. Haertig, and K. Wendt, "Comparison of error mapping techniques for coordinate measuring machines using the plate method and laser tracer technique," in 19th IMEKO World Congress 2009, September 6, 2009 - September 11, 2009, Lisbon, Portugal, 2009, pp. 2487-2491.

[5] B. Bringmann and W. Knapp, "Machine tool calibration: Geometric test uncertainty depends on machine tool performance," Precision Engineering, vol. 33, pp. 524-529, 2009.

[6] J. R. R. Mayer, "Five-axis machine tool calibration by probing a scale enriched reconfigurable uncalibrated master balls artefact," CIRP Annals - Manufacturing Technology, vol. 61, pp. 515-518, 2012.

[7] B. Bringmann, J. P. Besuchet, and L. Rohr, "Systematic evaluation of calibration methods," CIRP Annals - Manufacturing Technology, vol. 57, pp. 529-532, 2008.

[8] H. Schwenke, M. Franke, J. Hannaford, and H. Kunzmann, "Error mapping of CMMs and machine tools by a single tracking interferometer," CIRP Annals - Manufacturing Technology, vol. 54, pp. 475-478, 2005.

[9] S. Weikert and W. Knapp, "R-test, a new device for accuracy measurements on five axis machine tools," CIRP Annals - Manufacturing Technology, vol. 53, pp. 429-432, 2004.

[10] S. Parkinson, A. P. Longstaff, and S. Fletcher, "Automated planning to minimise uncertainty of machine tool calibration," Engineering Applications of Artificial Intelligence, vol. 30, pp. 63-72, 4// 2014.

[11] GUM, "Evaluation of measurement data – Supplement 2 to the "Guide to the expression of uncertainty in measurement" – Extension to any number of input quantities," ed, Joint Committee for Guides in Metrology, JCGM 102:2011.

[12] R. Schultschik Oe, "Components of the Volumetric accuracy," Manuf Technol, Gen Assem of CIRP, 27th, vol. 26, pp. 223-228, 1977.

CHAPTER 6 ARTICLE 3: APPLICATION OF GUF FOR A MULTI-OUTPUT ITERATIVE MEASUREMENT MODEL ESTIMATION ACCORDING TO GUM S2 IN INDIRECT FIVE-AXIS CNC MACHINE TOOL CALIBRATION

A. Los, J. R. R. Mayer

Department of Mechanical Engineering, Polytechnique Montreal, QC, Canada

* Published in *Laser Metrology and Machine Performance XI* in March 2015

6.1 Abstract

The paper looks at the problem of estimating the uncertainty of the five-axis machine tool indirect calibration method, using (generalized) GUM Uncertainty Framework (GUF) presented in Guide to the Expression of Uncertainty in Measurement Supplement 2 (GUM S2). The analysed Scale Enriched Master Balls Artefact (SAMBA) probing calibration method is solved through an iterative calculation (for each iteration the calculation model changes and depends on the previous one), which causes difficulties when the measurement model sensitivity matrix has to be defined analytically. That is why a numerical Jacobian is used. The simulated results of the machine geometric errors uncertainties estimation are presented for different number and configuration of master balls used in the SAMBA artefact.

Keywords: GUF, calibration, SAMBA

6.2 Introduction

Calibration of multi-axis machine tools requires estimating their geometric error parameters. This can be achieved through direct or indirect methods [1]. The former involve measuring each parameter separately using, for example, laser interferometry. The latter allow estimating a number of those parameters from the measurement of volumetric effects within the machine workspace. The devices used for indirect calibration are, among others, ‘chase-the-ball’ [2], SAMBA [3], self-tracking laser interferometers etc.

Calibration results can be evaluated through different means. Bringmann et al. [4] compare different calibration strategies through the uncertainty on the workpiece feature errors estimated from the calibration results using the Monte Carlo method (MCM). In [2] the calibration results are evaluated through their uncertainty obtained from the MCM simulation of the full machine model. Schwenke et al. [5] estimate the machine parametric errors from the interferometric displacement measurements. In order to calculate the calibration results uncertainty, the MCM simulations are performed with the randomly distributed noise added to the measurement results. The standard deviations of the parameters represent their standard uncertainties and are used for optimizing the measurement strategy.

Because the indirect calibration methods have a multi-output model, their uncertainty evaluation should be estimated following the GUM S2 [6] rather than the GUM [7]. In this study, the (generalized) GUM uncertainty framework is applied for the uncertainty calculation of the SAMBA method, which has a multi-output model and an iterative solution.

6.3 SAMBA

The SAMBA calibration method [3] requires probing the artefact consisting of a number of master balls and a scale bar in different machine rotary axis indexations. In Figure 6.1 (left) the artefact with 4 master balls (with a diameter of 12.7 mm) and the scale bar (with a length of 304.6686 mm) mounted on the table of the Mitsui Seiki five-axis machine tool is shown. The kinematic model of the machine is depicted in Figure 6.1 (right). During the SAMBA measurements, the balls are probed in five points which allows calculating their centre position coordinates.

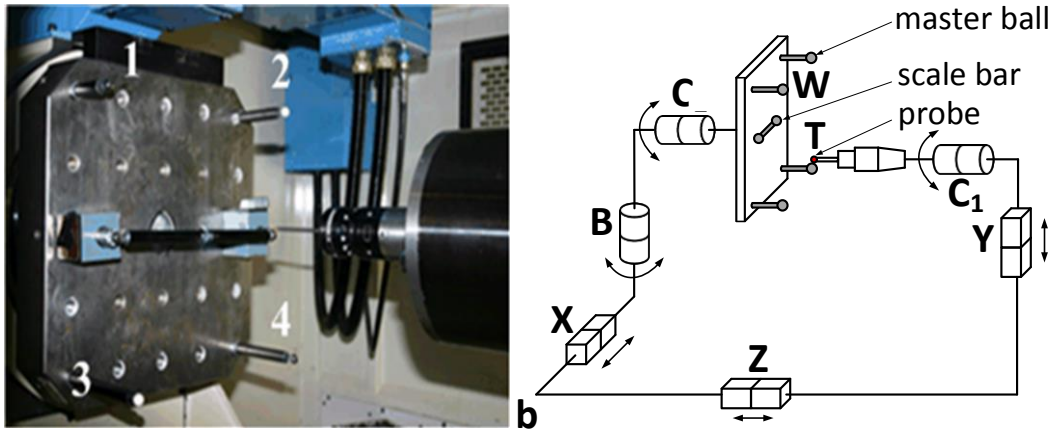

Figure 6.1: left: SAMBA artefact probed on the machine tool for [*b*, *c*]=[0, 0];
right: five-axis machine tool kinematic model with the topology WCBXbZYC$_1$T; W - workpiece, T - tool, b - machine base, B, C – rotary axes around the Y and Z axes respectively, X, Y, Z – machine linear axes, C$_1$ – spindle

Figure 6.2 shows the SAMBA method algorithm for identifying the *m* output quantities $\boldsymbol{Y}$ with the estimate $\boldsymbol{y}=(y_1,...,y_m)$ from the *N* input quantities $\boldsymbol{X}$ with the estimate $\boldsymbol{x}=(x_1, y_1, z_1,.., x_{(N-1)/3}, y_{(N-1)/3}, z_{(N-1)/3,}, L)$, where *x*, *y*, *z* are the measured balls centers coordinates and *L* is the calibrated scale bar length.

In order to identify the geometric error parameters the machine kinematic model needs to be built [8]. That allows predicting the tool position (virtual tool position at the ball centre) and comparing it with the measured ball centre position by using the homogenous transformation matrix (HTM) ${}^{ball}\boldsymbol{T}_{tip}$, which results in calculating the residual volumetric error $\boldsymbol{X}_R$. In order to reduce this error, the Newton-Gauss approach is applied. The machine sensitivity Jacobian matrix $\boldsymbol{J}$ is used for calculating the adjustment in machine parameters $\delta\boldsymbol{y}$ from the equation:

$$\boldsymbol{X}_R + J \cdot \delta\boldsymbol{y} = 0 \tag{6.1}$$

The calculations are continued until $\delta\boldsymbol{y}_i$ is smaller than the set threshold value τ.

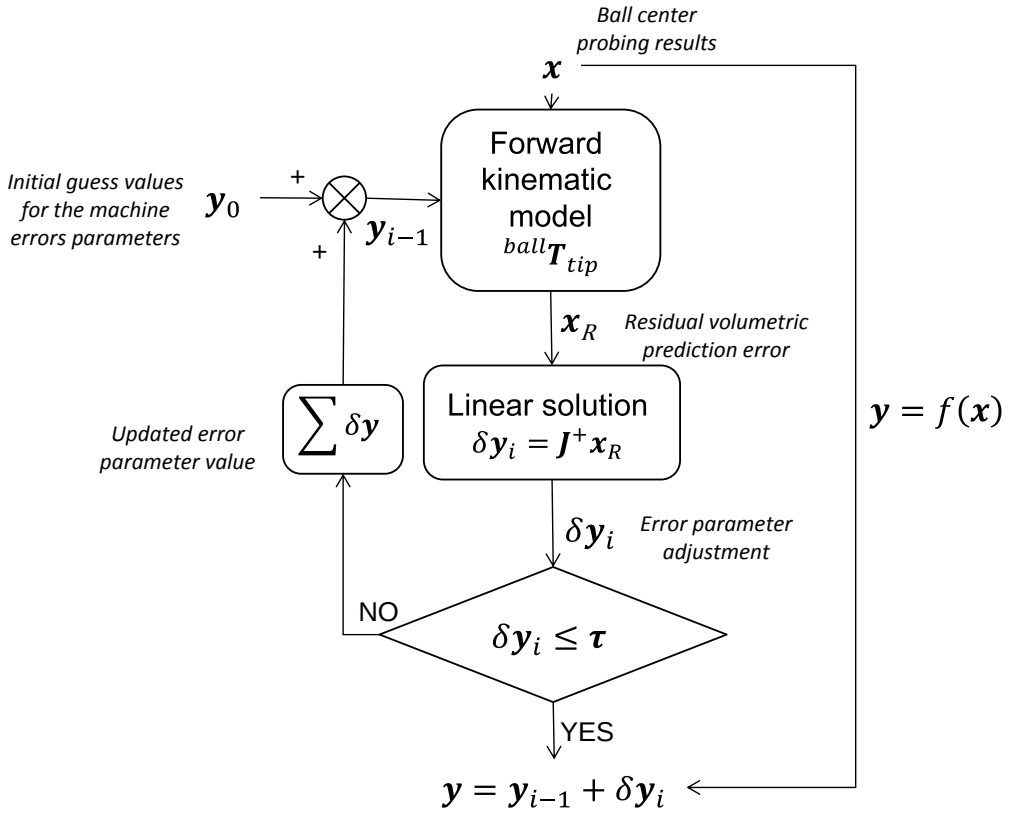

Figure 6.2: SAMBA flow chart

6.4 Uncertainty estimation

Since the analysed calibration model is a multi-output model, the uncertainty is estimated according to GUM S2 [6]. The uncertainty is calculated for all the parameters simultaneously. The correlation between the parameters is also calculated. In order to obtain the uncertainty at the required confidence level *p* the coverage factor is estimated.

6.4.1 GUM Uncertainty Framework (GUF)

The GUF method presented in GUM S2 [6] allows estimating the output quantities covariance matrix $\boldsymbol{U}y$ from the equation:

$$\boldsymbol{U}_y = \boldsymbol{C}_x \boldsymbol{U}_x \boldsymbol{C}_x^{\mathrm{T}} \tag{6.2}$$

where:

$\boldsymbol{C}_x$ is the sensitivity measurement matrix,

$$\boldsymbol{C}_x = \begin{bmatrix} \frac{\partial f_1}{\partial x_1} & \frac{\partial f_1}{\partial x_2} & \cdots & \frac{\partial f_1}{\partial x_N} \\ \frac{\partial f_2}{\partial x_1} & \frac{\partial f_2}{\partial x_2} & & \frac{\partial f_2}{\partial x_N} \\ \vdots & & \ddots & \vdots \\ \frac{\partial f_m}{\partial x_1} & \frac{\partial f_m}{\partial x_2} & \cdots & \frac{\partial f_m}{\partial x_N} \end{bmatrix} \tag{6.3}$$

$\boldsymbol{U}_x$ is the input data covariance (uncertainty) matrix,

$$\boldsymbol{U}_x = \begin{bmatrix} u(x_1, x_1) & \ldots & u(x_1, x_N) \\ \vdots & \ddots & \vdots \\ u(x_N, x_1) & \ldots & u(x_N, x_N) \end{bmatrix} \tag{6.4}$$

where each element *(i,j)* is

$$u(x_i, x_j) = r(x_i, x_j) u(x_i) u(x_j) \tag{6.5}$$

with $r(x_i, x_j)$ the correlation coefficient associated with x_i and x_j.

6.4.2 Numerical Jacobian

Due to the iterative character of the identification procedure the function $\boldsymbol{y}=f(\boldsymbol{x})$ cannot be expressed analytically. Nevertheless, its sensitive matrix can be estimated as the *N*x*m* numerical Jacobian:

$$\boldsymbol{C}_x \approx \boldsymbol{J}_{num} \tag{6.6}$$

Each element (*n*, *k*) in $\boldsymbol{J}_{num}$ equals:

$$\boldsymbol{J}_{num(n,k)} = \frac{\partial f_k}{\partial x_n} = \frac{f_k(x_1,\ldots,x_n+\Delta x_n,\ldots,x_N) - f_k(x_1,\ldots,x_N)}{\Delta x_n} \tag{6.7}$$

Adding the Δx_n to each of the *N* input quantities consecutively allows building the numerical Jacobian column by column.

6.5 Measurements and simulation

The uncertainty calculation is performed using MATLAB®. The simulation is ran in order to calculate the numerical Jacobian and calculate the uncertainty. However, the input data covariance

$\boldsymbol{U}_x$ is estimated from 44 repeated SAMBA measurements performed over a 24 hour period. It assures that the correlation between the input data is considered. It also includes any changes in the measurands over that period.

The SAMBA calibration method is performed for the thirteen geometric error parameters listed in Table 6.1 with the values obtained during the previous calibration [3]. The measurement is simulated for the seven different rotary axis indexation pairs: [*b*, *c*] = [90, 270], [60, 180], [30, 90], [0, 0], [-90, -270], [-60, -180] and [-30, -90] deg. The obtained values allow identifying the calibration results using different number and configuration of master balls. The uncertainty for one master ball used in the artifact is estimated for each of the four balls. When two balls are used it is obtained for all of the six combinations of the balls: 1 and 2; 1and 3; … ; 3 and 4. The same for the four configurations of the three balls: 1, 2 and 3; 1,2 and 4; 1, 3 and 4; 2,3 and 4.

Table 6.1: Identified machine geometric parameters [3]

Symbol	Description	Calibration result
E_{AOB}	out-of-squareness of the B-axis relative to the Z-axis (μrad)	0.9
E_{COB}	out-of-squareness of the B-axis relative to the X-axis (μrad)	-1.5
E_{XOC}	distance between the B and C axes (μm)	-102.2
E_{AOC}	out-of-squareness of the C-axis relative to the B-axis (μrad)	3.9
E_{BOC}	out-of-squareness of the C-axis relative to the X-axis (μrad)	19.9
E_{BOZ}	out-of-squareness of the Z-axis relative to the X-axis (μrad)	-37.5
E_{AOY}	out-of-squareness of the Y-axis relative to the Z-axis (μrad)	-8.8
E_{COY}	out-of-squareness of the Y-axis relative to the X-axis (μrad)	23.9
E_{XOC1}	X offset of the spindle relative to the B-axis (μm)	-97.1
E_{YOC1}	Y offset to the spindle relative to the C-axis (μm)	15.7
E_{XX}	positioning linear error term of the X-axis (μm/m)	-45.2
E_{YY}	positioning linear error term of the Y-axis (μm/m)	5.3
E_{ZZ}	positioning linear error term of the Z-axis (μm/m)	-20.5

6.6 Results

The maximum and minimum parameter uncertainty values obtained for different number and combinations of master balls are depicted in Figure 6.3. The configuration ball numbers corresponding to the uncertainties are not shown due to the graph clarity but will be introduced in the discussion. All the uncertainties are calculated for the rectangular coverage regions for the

coverage probability p=0.95, so, depending on the master balls used, the coverage factor varies from 2.9 to 3.0.

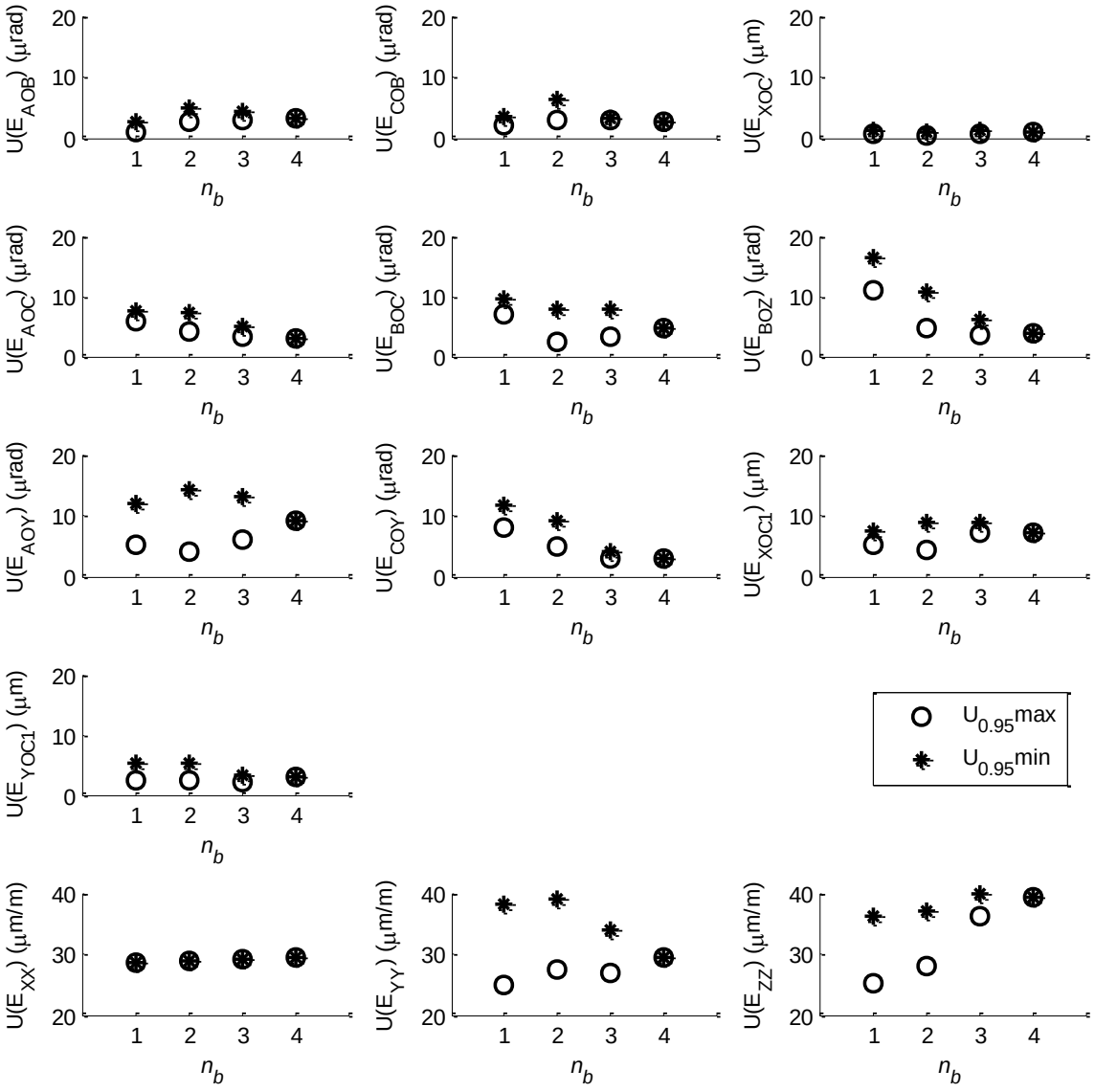

Figure 6.3: Uncertainty values for different numbers and configurations of SAMBA artefact for the confidence level p = 0.95

No clear trend in the influence of the number or combination of master balls on the uncertainty value can be observed for the E_{XX}. This parameter is estimated only from the length of the scale bar L and the measurement of the scale bar balls, so that it cannot be influenced by measurement of the master balls 1, 2, 3, 4. Almost negligible difference for the uncertainty is also observed for the E_{XOC}.

The biggest impact of the number and configuration of the master balls can be observed for the scale errors E_{YY} and E_{ZZ}. In both cases, a larger number of the master balls reduces the uncertainty range and, when one ball is used, the smallest uncertainty value is obtained for the balls 3 and 4 and the largest for the ball number 1. For the E_{ZZ} the $U_{0.95min}$ and $U_{0.95max}$ values are increasing when more balls are added and the $U_{0.95max}(E_{ZZ})$ for 1 and 2 balls is close to the $U_{0.95min}(E_{ZZ})$ for 3 balls.

The range and the mean values of $U_{0.95}$ are decreasing significantly for the E_{AOC}, E_{BOZ}, E_{COY}, E_{YOC1} when more master balls, larger n_b, are used in the artefact. On the contrary $U(E_{AOB})$ increases with the larger n_b. However, this gain is not as significant as the decrease of the uncertainty of other parameters for higher values of n_b.

6.7 Conclusion

A method for the uncertainty estimation of the multi-output calibration method has been proposed. The calculation of numerical Jacobian allowed estimating the model sensitivity matrix without defining the analytical equation of the model. This method has a relatively short computation time, compared to the Monte Carlo method, and allows giving the uncertainty result within few minutes although the number of the input and output variables is large.

The uncertainty estimation performed for different SAMBA configurations allowed comparing them and verifying if it is always necessary to use more balls, since measurement takes valuable machining time. The results showed that the uncertainty depends on the number and combination of the balls used. Since there is no best set or a ball that would give the lowest uncertainty for all the parameters, the number of balls should be chosen as the smallest number of the master balls used that gives the results with the uncertainty not lower than the demanded one. With this method the results within the desired uncertainty can be obtained for the shortest possible calibration time.

The artefact with two master balls requires half of the measuring time comparing to the one with four balls. Moreover, the uncertainty for two balls (for most of the parameters) is not significantly lower than for the four balls. Taking those factors into consideration, calibration using SAMBA with two master balls gives satisfactory results.

6.8 Acknowledgement

This research was supported by the NSERC Canadian Network for Research and Innovation in Machining Technology (NSERC CANRIMT; www.nserc-canrimt.org).

6.9 References

[1] H. Schwenke, W. Knapp, H. Haitjema, A. Weckenmann, R. Schmitt, and F. Delbressine, "Geometric error measurement and compensation of machines-An update," CIRP Annals - Manufacturing Technology, vol. 57, pp. 660-675, 2008.

[2] B. Bringmann and W. Knapp, "Model-based 'Chase-the-Ball' Calibration of a 5-Axes Machining Center," CIRP Annals - Manufacturing Technology, vol. 55, pp. 531-534, 2006.

[3] J. R. R. Mayer, "Five-axis machine tool calibration by probing a scale enriched reconfigurable uncalibrated master balls artefact," CIRP Annals - Manufacturing Technology, vol. 61, pp. 515-518, 2012.

[4] B. Bringmann, J. P. Besuchet, and L. Rohr, "Systematic evaluation of calibration methods," CIRP Annals - Manufacturing Technology, vol. 57, pp. 529-532, 2008.

[5] H. Schwenke, M. Franke, J. Hannaford, and H. Kunzmann, "Error mapping of CMMs and machine tools by a single tracking interferometer," CIRP Annals - Manufacturing Technology, vol. 54, pp. 475-478, 2005.

[6] GUM, "Evaluation of measurement data – Supplement 2 to the "Guide to the expression of uncertainty in measurement" – Extension to any number of input quantities," ed, Joint Committee for Guides in Metrology, JCGM 102:2011.

[7] GUM, "Evaluation of measurement data - Guide to the expression of uncertainty in measurement," ed, Joint Committee for Guides in Metrology, JCGM 100:2008.

[8] Y. A. Mir, J. R. R. Mayer, and C. Fortin, "Tool path error prediction of a five-axis machine tool with geometric errors," Proceedings of the Institution of Mechanical Engineers, Part B: Journal of Engineering Manufacture, vol. 216, pp. 697-712, 2002.

CHAPTER 7 GUM UNCERTAINTY FRAMEWORK VALIDATION WITH A MONTE CARLO METHOD

Monte Carlo Method (MCM) is a very useful technique when the uncertainty of a measurement result has to be evaluated and the model cannot be expressed analytically or the distributions of the results are needed. Moreover, with a large enough number of MC trials gives a simulation results reflecting the impact of the input quantities variations on the output quantity that is close to reality. However, it can be time consuming. On the other hand, the GUM uncertainty framework (GUF) is faster to implement but requires the analytical function of the model, so that the partial derivatives can be calculated, or the linearization of the model.

In this chapter, the GUF presented in Chapter 6 is validated using the MCM described in Chapter 4 and Chapter 5. The input uncertainty presented in Chapter 4 for the *Cold-Cold* test (without the warm-up cycle) is used. The validation is performed according to GUM S2 (GUM, Joint Committee for Guides in Metrology, JCGM 102:2011).

The MCM results are depicted for different number of *M* MC trials, so that the converging of the estimated values can be observed.

7.1 Validation procedure

The comparison of the results obtained by GUF and MCM is necessary to validate the former with the later. Both of the methods results in the output quantity $\boldsymbol{Y}$ values with the estimate $\boldsymbol{y} = (y_1, \dots, y_m)$, their covariance matrix $\boldsymbol{U_y}$ (that includes standard uncertainties $u(y)$ and correlation matrix $\boldsymbol{R_y}$) and the k_p and k_q coverage factors for hyper-rectangular and hyper-ellipsoidal coverage regions.

In order to perform the validation, the absolute difference *d* between the output quantity estimates (d_y), their uncertainties estimates ($d_{u(y)}$,), the maximum eigenvalues of the results correlation matrices ($d_{\lambda_{max}}$), and the coverage factors (d_{k_p}, d_{k_q}) are calculated from the both methods results using the eq. 7-11 from [GUM S2, 2011]:

$$d_{y_j} = \left| y_j^{GUF} - y_j^{MCM} \right|, \qquad j = 1, \dots, m \tag{7.1}$$

$$d_{u(y_j)} = \left|u(y_j^{GUF}) - u(y_j^{MCM})\right|, \qquad j = 1, \dots, m \tag{7.2}$$

$$d_{\lambda_{max}} = \left|\lambda_{max}^{GUF} - \lambda_{max}^{MCM}\right| \tag{7.3}$$

$$d_{k_p} = \left|k_p^{GUF} - k_p^{MCM}\right| \tag{7.4}$$

$$d_{k_q} = \left|k_q^{GUF} - k_q^{MCM}\right| \tag{7.5}$$

Those values must be no larger than their corresponding numerical tolerances, which should be at least five times greater than adaptive MCM numerical tolerances. Those tolerances are chosen arbitrarily depending on the stability demanded by the user.

7.2 Results

In order to validate the GUF, the uncertainties on the eleven geometric error parameters were estimated through MCM and GUF using the input uncertainty estimated in Chapter 4 during the test without the warm-up cycle. The MCM simulations were performed for $M = [10^3, 10^4, 10^5, 10^6]$. The results for $M = 10^5$ represent the ones obtained for adaptive MCM. The absolute differences between the GUF and MCM results are calculated for MCM with $M = 10^6$. The percentage value of the computed values *d* relatively to the MCM (reference in the validation process) are presented, as well. The estimation results are listed with an exaggerated precision and uncertainties are rounded to three significant digits, in order to show the evolution of the parameters for different *M* values.

Firstly, the output value estimates (machine geometric error parameters) are compared and depicted in Table 7.1. Already for $M = 10^4$, the results are almost equal. In general, the closest results are obtained when GUF is compared to MCM with $M = 10^6$. The highest relative difference in estimated parameters equals 0.2%, which is insignificant. Thus, the output quantity estimation results are validated with MCM.

The next step is the comparison of the obtained uncertainties (Table 7.2). Similarly to the output values parameters, the GUM and MCM methods are very close starting with the $M = 10^4$. When only MCM results for $M = 10^6$ are considered, the highest relative difference between GUF and MCM equals 0.6%. The estimated GUF uncertainties values are validated with MCM.

Table 7.1: GUF and MCM machine geometric errors results comparison

y	GUF	MCM				d_y for M= 10^6	$\frac{d_y}{y^{MCM_{M=10^6}}}$ 100%
		M = 10^3	M = 10^4	M = 10^5	M = 10^6		
E_{AOB}	-79	-79.052	-79.002	-79.001	-79.003	0.003	0 %
E_{COB}	-210	-209.889	-209.991	-210.000	-209.999	0.001	0 %
E_{XOC}	-93	-93.001	-93.001	-92.999	-93.000	0	0 %
E_{AOC}	100	100.007	100.018	100.001	100.000	0	0 %
E_{BOC}	-18	-17.923	-17.979	-18.001	-18.000	0	0 %
E_{BOZ}	-87	-86.882	-86.977	-87.005	-86.998	0.002	0 %
E_{AOY}	20	19.918	19.984	20.000	19.996	0.004	0 %
E_{COY}	-97	-96.863	-96.982	-96.999	-97.000	0	0 %
E_{XX}	33	33.036	32.856	32.958	32.982	0.018	0.1%
E_{YY}	94	93.904	93.809	93.952	93.975	0.025	0 %
E_{ZZ}	13	12.856	12.752	12.938	12.969	0.031	0.2%

Table 7.2: GUF and MCM machine geometric errors results uncertainties comparison

$u(y)$	GUF	MCM				$d_{u(y)}$ for M=10^6	$\frac{d_{u(y)}}{u(y^{MCM_{M=10^6}})}$ 100%
		M = 10^3	M = 10^4	M = 10^5	M = 10^6		
$u(E_{AOB})$	1.78	1.81	1.79	1.78	1.79	0.01	0.6%
$u(E_{COB})$	1.05	1.06	1.05	1.05	1.05	0	0 %
$u(E_{XOC})$	0.237	0.230	0.235	0.237	0.237	0	0 %
$u(E_{AOC})$	0.882	0.876	0.884	0.882	0.881	0.001	0.1%
$u(E_{BOC})$	1.15	1.19	1.17	1.16	1.15	0	0 %
$u(E_{BOZ})$	1.76	1.87	1.77	1.77	1.76	0	0 %
$u(E_{AOY})$	2.53	2.57	2.54	2.53	2.53	0	0 %
$u(E_{COY})$	1.32	1.35	1.32	1.32	1.32	0	0 %
$u(E_{XX})$	8.92	8.83	8.98	8.89	8.92	0	0 %
$u(E_{YY})$	12.0	11.9	12.1	12.0	12.0	0	0 %
$u(E_{ZZ})$	15.5	15.4	15.6	15.5	15.5	0	0 %

Finally, the coverage factors and correlation matrices are compared (Table 7.3). The relative difference between the hyper-ellipsoidal coverage factors k_p is 1.2% and allows its validation. The maximum eigenvalues obtained for GUF and MCM are almost equal, so this parameter can also be validated. When the coverage factors for hyper-rectangular coverage regions k_q are compared, the difference is significant. The relative difference is 10%, it means that the coverage regions

calculated with GUF estimations would be 10% wider than those calculated with MCM. However, the GUM S2 refers to the k_q and k_p estimated with MCM as their minimal values. This situation (when k_q is not validated) can be observed in most the examples presented in GUM S2 (GUM, Joint Committee for Guides in Metrology, JCGM 102:2011).

Table 7.3: GUF and MCM coverage factors and correlation matrix maximum eigenvalue results comparison

v	GUF	MCM				d_v for M=10^6	$\frac{d_v\ 100\%}{v^{MCM_{M=10^6}}}$
		$M = 10^3$	$M = 10^4$	$M = 10^5$	$M = 10^6$		
λ_{max}	18.42	18.41	18.46	18.42	18.43	0.01	0 %
k_p	6.52	6.64	6.60	6.61	6.61	0.08	1.3%
k_q	3.13	2.82	2.86	2.86	2.85	0.30	9.8%

The λ_{max} allows comparison of the correlation matrices. The output quantity correlation coefficients, depicted in Table 7.4, Table 7.5 and Table 7.6 respectively for GUF, MCM with $M = 10^3$ and MCM with $M = 10^6$, allow a closer look at each value in correlation matrices. All three presented matrices have very close correlation coefficients for all the combinations of the estimated parameters. The biggest difference between the GUF and MCM correlations coefficients equals 0.05 (correlation) and 0.06 for $M = 10^5$ and $M = 10^6$, respectively. Therefore, the GUF results correlations are in accordance with MCM ones.

Table 7.4: Output quantity correlations for GUF results

E_{AOB}	-0.25	-0.34	-0.24	-0.13	-0.49	0.92	-0.53	0.75	0.75	0.75
	E_{COB}	0.09	-0.24	0.40	0.38	-0.26	0.68	0.02	0.03	0.05
		E_{XOC}	-0.23	-0.22	-0.01	-0.39	0.17	-0.27	-0.23	-0.27
			E_{AOC}	0.11	0.22	-0.08	-0.05	-0.38	-0.41	-0.41
				E_{BOC}	0.74	-0.16	0.44	-0.24	-0.25	-0.20
					E_{BOZ}	-0.48	0.55	-0.42	-0.42	-0.38
						E_{AOY}	-0.60	0.77	0.77	0.76
							E_{COY}	-0.44	-0.43	-0.41
								E_{XX}	1.00	0.99
									E_{YY}	0.99
										E_{ZZ}

Table 7.5: Output quantity correlations for MCM results obtained for $M = 10^3$

E_{AOB}	-0.30	-0.38	-0.21	-0.13	-0.51	0.92	-0.55	0.72	0.73	0.73
	E_{COB}	0.07	-0.21	0.41	0.44	-0.30	0.67	0.01	-0.01	-0.01
		E_{XOC}	-0.22	-0.21	0.04	-0.40	0.18	-0.28	-0.28	-0.24
			E_{AOC}	0.09	0.16	-0.05	-0.04	-0.39	-0.36	-0.39
				E_{BOC}	0.75	-0.19	0.46	-0.21	-0.25	-0.26
					E_{BOZ}	-0.50	0.59	-0.37	-0.42	-0.41
						E_{AOY}	-0.62	0.74	0.75	0.75
							E_{COY}	-0.45	-0.48	-0.47
								E_{XX}	0.99	0.99
									E_{YY}	1.00
										E_{ZZ}

Table 7.6: Output quantity correlations MCM results obtained for $M = 10^6$

E_{AOB}	-0.25	-0.34	-0.25	-0.13	-0.49	0.92	-0.53	0.75	0.75	0.75
	E_{COB}	0.09	-0.24	0.40	0.38	-0.26	0.68	0.05	0.02	0.03
		E_{XOC}	-0.23	-0.22	-0.01	-0.39	0.17	-0.27	-0.27	-0.23
			E_{AOC}	0.12	0.22	-0.08	-0.05	-0.41	-0.38	-0.41
				E_{BOC}	0.74	-0.16	0.44	-0.20	-0.24	-0.25
					E_{BOZ}	-0.48	0.55	-0.38	-0.42	-0.42
						E_{AOY}	-0.60	0.76	0.77	0.77
							E_{COY}	-0.41	-0.44	-0.43
								E_{XX}	0.99	0.99
									E_{YY}	1.00
										E_{ZZ}

7.3 Conclusion

The applied GUF uncertainty estimation method has been validated with MCM results for the iterative multi-input multi-output SAMBA calibration method in the terms of the estimated values and their uncertainties, the results correlation matrix and its maximum eigenvalue, and the coverage factor the hyper-ellipsoidal coverage regions. However, the coverage factor for the hyper-rectangular coverage regions has not been validated. Nevertheless, the results obtained using

GUF can be used with their standard uncertainties and covariance as the input uncertainty when the machine geometric errors are used for estimation, e.g., of the volumetric error. The calculation of the expanded uncertainties using the coverage factors calculated with GUF would results in the coverage regions larger by 10% comparing to the MCM results.

Moreover, The MCM simulations results show that for $M > 10^4$ there is no significant changes in the machine geometric errors and their uncertainties estimation.

CHAPTER 8 GENERAL DISCUSSION

In this chapter, the general discussion of the thesis is presented. The main approaches and methods used are explained in the context of machine calibration uncertainty estimation.

Machine tool performance can be tested using various calibration methods. Those methods significantly vary in terms of equipment used and information about the machine obtained. The machine geometric errors can be estimated using a wide range of measuring devices and methods. Starting with the highly precise laser interferometer, through the calibrated gauge and finally with an uncalibrated artefact. Each of the available device would result in different measurement uncertainty. However, many researchers have proven that the calibration is significantly impacted by the machine performance and therefore, should be considered in the uncertainty budget. Since the machine is the uncertainty source and the measurand at the same time, it is difficult to estimate its uncertainty. Moreover, the machine performance changes over the time and due to the environmental conditions. The standards for machine performance testing do not give guidance in this matter, nor the standards for uncertainty estimation. Some researchers propose to use the standard or given by the machine manufacturer geometric errors ranges in uncertainty analysis. However, it is not known if the machine performance variations have not changed comparing to those predicted in its specifications.

In this thesis, firstly the SAMBA calibration measurement (probing) uncertainty sources were defined as the probe, uncalibrated artefact (only within one cycle) and the machine itself. The probing is registered when the probe mounted in the spindle approaches the ball touches it and sends the signal to the machine. Thus, not only the probe repeatability influences the result but machine performance as well (respond time of the machine axis encoders and drives, positioning accuracy, etc.). The uncalibrated artefact geometry changes as well. However, since it is being calibrated in the SAMBA identification along with the machine geometric error parameters, those changes influence the calibration result, only when they occur during the test but not between the tests. In order to estimate all those effects, the repeated SAMBA measurement was proposed as the probing uncertainty estimate. The input data was modeled using the normal distribution with the mean and variance obtained from the repeated measurement. The joint probability density function was modeled using Gaussian copula for correlated distribution with the correlations coefficients obtained from the correlation matrix of the repeated SAMBA measurement. That way the MC

sampling was reflecting the reality of the probing. The calibrated scale bar uncertainty was considered as non-correlated uncertainty source and was included in the covariance matrix.

In order to expand the investigation area of the machine performance variations, SAMBA repeated test were conducted considering various factors. The first part of the calibration series was conducted with and without the warm-up cycle before the measurements. Each series was performed for 24 hours (with forty four repetitions). That allowed the analysis of the machine variations when it was cooling down and when it was slightly warming up. Performing a warm-up cycle caused significant changes in the machine geometry, which within few hours stabilized to the machine "cold" state. Repeated calibration conducted from the "cold" state resulted in smaller geometry changes. However, a trend, due to slight warming up caused by the axis movements during probing, was visible. The uncertainties for the test with warm-up were few times wider than those for the one without.

The second part was focusing on the short- and medium-term variations rather than the environmental conditions. Therefore, four measurement cycles were performed each day for five days. That brought the information about machine daily changes and changes between the days. The mean values and variations of each day were compared. The uncertainty was calculated in three ways: from all the data, for each day and pooled by the day. The last one reflected the daily changes in machine performance but disregarded the changes of the mean.

In the next step the uncertainty on the probing had to be propagated on the calibration results – machine geometric error parameters. The propagation had to be appropriate for a multi-input and a multi-output calibration model. Since SAMBA has an iterative solution (the analytical function of the output is not known), the (adaptive) Monte Carlo method according to GUM S2 was chosen. Moreover, the MCM is considered as a good estimator of the model input variations (which were measured during the repeated calibration) propagation on the output results.

Although, MCM gave satisfactory results and allowed estimating the uncertainties with all its parameters, it showed to be time-consuming. On average, one SAMBA simulation programmed in MATLAB® took around one second, with $M = 10^5$ runs the simulation time came to almost, without and with the MATLAB® parallel computing toolbox, 28 hours and 7 hours, respectively. The faster method GUM uncertainty framework (GUF) requires the partial derivatives of the model output to

its input. In the lack of the information about the calibration model analytical function, those derivatives were estimated from the calculated numerical Jacobian.

The GUF method was used to calculate the calibration uncertainty for different subsets of one, two or three master balls and for the set of four master balls in the SAMBA artefact. The results depicted the impact of the master balls and their configuration on the uncertainty. The lowest uncertainties were obtained when four balls were used. It showed that uncertainty on the calibration results also depends on the artefact configuration and therefore, should be considered when the SAMBA strategy is optimized.

Finally, the GUF validation using MCM was performed according to the GUM S2 standard, where it is recommended to use both methods and compare the results. If the results do not differ more than required by the user numerical tolerances, the GUF method can be used in future for uncertainty estimation when similar measuring systems are considered. If not, MCM is recommended.

CHAPTER 9 CONCLUSION AND RECOMMENDATIONS

In this chapter the conclusions coming from the research presented in chapters 4-7 and the recommendations for the future work are listed.

9.1 Conclusion and contributions of the work

In this thesis, a complex approach for a multi-input multi-output uncertainty estimation of a calibration method with an iterative solution and an uncalibrated artefact was presented. The probing (input) uncertainty was estimated through the repeated SAMBA calibration. That way the input uncertainty reflected the variations of the machine-probe-artefact system. The machine performance and its changes were analysed considering different factors. The estimated probing uncertainties were propagated on the calibration results (output) with consideration of correlations between them. The (adaptive) Monte Carlo method, which simulates the effect of the model input changes on the output values, and the time-efficient GUM uncertainty framework were applied. The probing and calibration results were analysed in terms of their estimates, standard deviations, correlations and trend. The appropriate for a multi-output model uncertainty coverage factors were calculated.

The results proved that the calibration outcome depends on the machine performance, which varies over the time, and due to the environmental conditions. Analysis of the trend and identified machine geometric error parameters values depicted that calibration pre-conditions may change the calibration results significantly. The machine changes occurring during the short- and medium-term influence the calibration results as well. The uncertainty estimation methods reflecting the environmental conditions and the time-dependent changes were proposed. Moreover, the pooled uncertainty was proposed to estimate the daily variations from the data gathered over few days without including the changes of the mean between the days.

When the calibration is performed, the information obtained reflects the machine state at the moment of the calibration test. Within a few hours (or the next day) the machine geometry may be in a very different state, so that the calibration results uncertainties have to be considered. It is a crucial information from the machine user point of view, who has to make a decision about the error correction or compensation.

Moreover, the uncertainty was estimated for different number of the master balls in SAMBA artefact. That demonstrated that SAMBA artefact configuration has an impact on the calibration uncertainty. Thus, the uncertainty can be used as one of the SAMBA optimization parameters.

Finally, the machine geometric errors estimates, their uncertainties, correlation coefficients and hyper-ellipsoidal coverage factor calculated using GUF were validated with the MCM results.

Applied uncertainty estimation methods allowed calculating the machine geometric error parameters with the full uncertainty structure including the standard uncertainties and the covariance matrix. That way the results can be used as the input quantity, when, for example, the volumetric error is predicted with its uncertainties in the machine volume.

9.2 Future works

The proposed SAMBA calibration uncertainty estimation method can be further developed. This method can be applied to evaluate the SAMBA (and other methods) calibration strategy (artefact geometry. number of master balls. order and values of the rotary axes indexations). As a result, the SAMBA strategy could be optimized in terms of the uncertainty minimization.

Additional calibration tests could be performed that would include different environmental effects on machine performance, such as the shop temperature and humidity (for some, the temperature can vary between around 10 to 40°C). This method could also be used to regularly monitor a pool of machines. A significant change in the uncertainty results might highlight the wear of certain components of a machine. By then, the check of the different uncertainties may be helpful in determining worn or defective part or device of the machine.

Since proposed method gives the full uncertainty structure, it can be used as the input uncertainty for the next stages of machine performance evaluation, such as volumetric and workpiece feature errors prediction. The machine volumetric error maps can be depicted with their uncertainties. Thus, the workpiece feature errors can be minimized.

The presented calibration uncertainty evaluation reflects the effect of the machine and performed measurement. This approach could be enriched by the model uncertainty estimation. In this research the machine errors model was considered as optimized. However, the model has its uncertainty which reflects the errors interpolation and the effect of not modeled errors. This can be

estimated, for example, through the prediction uncertainty. That way the calibration would be evaluated not only as the measurement method but as the machine modeling.

BIBLIOGRAPHY

(BIPM), B. I. d. P. e. M. (2017). JCGM Working Group on the Expression of Uncertainty in Measurement (GUM). Retrieved from http://www.bipm.org/en/committees/cc/wg/jcgm-wg1.html

Abbaszadeh-Mir, Y., Mayer, J. R. R., Cloutier, G., & Fortin, C. (2002). Theory and simulation for the identification of the link geometric errors for a five-axis machine tool using a telescoping magnetic ball-bar. International Journal of Production Research, 40(Copyright 2003, IEE), 4781-4797. Retrieved from http://dx.doi.org/10.1080/00207540210164459

Abbaszadeh-Mir, Y., Mayer, J. R. R., & Fortin, C. (2003). Methodology and simulation of the calibration of a five-axis machine tool link geometry and motion errors using polynomial modelling and a telescoping magnetic ball-bar. Paper presented at Sixth International Conference on Laser Metrology, Machine Tool, CMM and Robot Performance LAMDAMAP 2003, July 1, 2003 - July 3, 2003, Huddersfield, United Kingdom (pp. 527-543).

Aguado, S., Samper, D., Santolaria, J., & Aguilar, J. J. (2012). Identification strategy of error parameter in volumetric error compensation of machine tool based on laser tracker measurements. International Journal of Machine Tools and Manufacture, 53(1), 160-169. doi: http://dx.doi.org/10.1016/j.ijmachtools.2011.11.004

Andolfatto, L., Mayer, J. R. R., & Lavernhe, S. (2011). Adaptive Monte Carlo applied to uncertainty estimation in five axis machine tool link errors identification with thermal disturbance. International Journal of Machine Tools and Manufacture, 51(7–8), 618-627. doi: http://dx.doi.org/10.1016/j.ijmachtools.2011.03.006

Antonio, P. (2010). Copulas for uncertainty analysis. Metrologia, 47(3), 262. Retrieved from http://stacks.iop.org/0026-1394/47/i=3/a=017

ASME. (B5.54:2005). Methods for Performance Evaluation of Computer Numerically Controlled Machining Centers.

Bringmann, B., Besuchet, J. P., & Rohr, L. (2008). Systematic evaluation of calibration methods. CIRP Annals - Manufacturing Technology, 57(1), 529-532. doi: http://dx.doi.org/10.1016/j.cirp.2008.03.114

Bringmann, B., & Knapp, W. (2006a). Model-based `Chase-the-Ball' Calibration of a 5-Axes Machining Center. CIRP Annals - Manufacturing Technology, 55(1), 531-534. doi: Doi: 10.1016/s0007-8506(07)60475-2

Bringmann, B., & Knapp, W. (2006b). Model-based 'Chase-the-Ball' Calibration of a 5-Axes Machining Center. CIRP Annals - Manufacturing Technology, 55(1), 531-534. doi: http://dx.doi.org/10.1016/S0007-8506(07)60475-2

Bringmann, B., & Knapp, W. (2009). Machine tool calibration: Geometric test uncertainty depends on machine tool performance. Precision Engineering, 33(4), 524-529. doi: DOI: 10.1016/j.precisioneng.2009.02.002

Bringmann, B., Kung, A., & Knapp, W. (2005). A Measuring Artefact for true 3D Machine Testing and Calibration. CIRP Annals - Manufacturing Technology, 54(1), 471-474. Retrieved from http://www.sciencedirect.com/science/article/pii/S0007850607601474

Byrne, G., Dornfeld, D., & Denkena, B. (2003). Advancing Cutting Technology.

Castro, H. F. F. (2008). Uncertainty analysis of a laser calibration system for evaluating the positioning accuracy of a numerically controlled axis of coordinate measuring machines and machine tools. Precision Engineering, 32(2), 106-113. doi: http://dx.doi.org/10.1016/j.precisioneng.2007.05.001

Chen, J. S., Kou, T. W., & Chiou, S. H. (1999). Geometric error calibration of multi-axis machines using an auto-alignment laser interferometer. Precision Engineering, 23(4), 243-252. doi: Doi: 10.1016/s0141-6359(99)00016-1

Eichstadt, S., Link, A., Harris, P., & Elster, C. (2012). Efficient implementation of a Monte Carlo method for uncertainty evaluation in dynamic measurements. Metrologia, 49(3), 401-410. doi: 10.1088/0026-1394/49/3/401

Erkan, T. (2010). Méthodes de suivi de l'état des machines-outils par palpage d'artefacts. (Doctorate, Université de Montréal, Montreal).

Erkan, T., Mayer, J. R. R., & Dupont, Y. (2011). Volumetric distortion assessment of a five-axis machine by probing a 3D reconfigurable uncalibrated master ball artefact. Precision Engineering, 35(Compendex), 116-125. Retrieved from http://dx.doi.org/10.1016/j.precisioneng.2010.08.003

Givi, M., & Mayer, J. R. R. (2014). Validation of volumetric error compensation for a five-axis machine using surface mismatch producing tests and on-machine touch probing. International Journal of Machine Tools and Manufacture, 87 89-95. doi: http://dx.doi.org/10.1016/j.ijmachtools.2014.08.001

GUM. (Joint Committee for Guides in Metrology, JCGM 100:2008). Evaluation of measurement data - Guide to the expression of uncertainty in measurement.

GUM. (Joint Committee for Guides in Metrology, JCGM 101:2008). Evaluation of measurement data – Supplement 1 to the "Guide to the expression of uncertainty in measurement" – Propagation of distributions using a Monte Carlo method.

GUM. (Joint Committee for Guides in Metrology, JCGM 102:2011). Evaluation of measurement data – Supplement 2 to the "Guide to the expression of uncertainty in measurement" – Extension to any number of input quantities.

GUM. (Joint Committee for Guides in Metrology, JCGM 104:2009). Evaluation of measurement data – An introduction to the "Guide to the expression of uncertainty in measurement" and related documents.

GUM. (Joint Committee for Guides in Metrology, JCGM 107:In preparation). Evaluation of measurement data – Applications of the least-squares method.

GUM. (Joint Committee for Guides in Metrology, JCGM 200:2012). International Vocabulary of Metrology – Basic and General Concepts and Associated Terms (VIM 3rd edition).

Haesselbarth, W., & Bremser, W. (2004). Correlation between repeated measurements: bane and boon of the GUM approach to the uncertainty of measurement. Accreditation and Quality Assurance, 9(10), 597-600. doi: 10.1007/s00769-004-0821-2

Ibaraki, S., Iritani, T., & Matsushita, T. (2013). Error map construction for rotary axes on five-axis machine tools by on-the-machine measurement using a touch-trigger probe. International

Journal of Machine Tools and Manufacture, 68(0), 21-29. doi: http://dx.doi.org/10.1016/j.ijmachtools.2013.01.001

ISO. (230-2:2014). Test code for machine tools -- Part 2: Determination of accuracy and repeatability of positioning of numerically controlled axes.

Jae Pahk, H., Sam Kim, Y., & Hee Moon, J. (1997). A new technique for volumetric error assessment of CNC machine tools incorporating ball bar measurement and 3D volumetric error model. International Journal of Machine Tools and Manufacture, 37(11), 1583-1596. Retrieved from http://www.sciencedirect.com/science/article/pii/S0890695597000291

Jamshidi, A., Maropoulos, P., Chappell, M., & Cave, J. (2015). Implementation of a machine tool performance measurement and diagnostic system and its impact on parts verification. Sustainable Design Manufacturing 2015.

Jokiel Jr, B., Ziegert, J. C., & Bieg, L. (2001). Uncertainty propagation in calibration of parallel kinematic machines. Precision Engineering, 25(1), 48-55. Retrieved from http://www.sciencedirect.com/science/article/pii/S0141635900000556

Knapp, W. (2002). Measurement Uncertainty and Machine Tool Testing. CIRP Annals - Manufacturing Technology, 51(1), 459-462. doi: Doi: 10.1016/s0007-8506(07)61560-1

Lamikiz, A., López de Lacalle, L. N., & Celaya, A. (2009). Machine Tool Performance and Precision. In L. N. López de Lacalle & A. Lamikiz (Eds.), Machine Tools for High Performance Machining (pp. 219-260). London: Springer London.

Lee, K.-I., & Yang, S.-H. (2013). Measurement and verification of position-independent geometric errors of a five-axis machine tool using a double ball-bar. International Journal of Machine Tools and Manufacture, 70(0), 45-52. doi: http://dx.doi.org/10.1016/j.ijmachtools.2013.03.010

Lei, W. T., & Hsu, Y. Y. (2003). Error measurement of five-axis CNC machines with 3D probe ball. Journal of Materials Processing Technology, 139(1-3), 127-133. Retrieved from http://www.sciencedirect.com/science/article/pii/S0924013603001936

Liang, Y., Chen, G., Chen, W., Sun, Y., & Chen, J. (2013). Analysis of Volumetric Error of Machine Tool Based on Monte Carlo Method. Journal of Computational and Theoretical Nanoscience, 10(5), 1290-1295. doi: 10.1166/jctn.2013.2845

Liebrich, T., Bringmann, B., & Knapp, W. (2009). Calibration of a 3D-ball plate. Precision Engineering, 33(1), 1-6. doi: DOI: 10.1016/j.precisioneng.2008.02.003

Linares, J.-M., Chaves-Jacob, J., Schwenke, H., Longstaff, A., Fletcher, S., Flore, J., . . . Wintering, J. (2014). Impact of measurement procedure when error mapping and compensating a small CNC machine using a multilateration laser interferometer. Precision Engineering, 38(3), 578-588. doi: http://dx.doi.org/10.1016/j.precisioneng.2014.02.008

Lira, I., & Grientschnig, D. (2010). Bayesian assessment of uncertainty in metrology: a tutorial. Metrologia, 47(3), R1-R14. Retrieved from http://dx.doi.org/10.1088/0026-1394/47/3/R01

López de Lacalle, L. N., & Lamikiz, A. (2009). Machine Tools for Removal Processes: A General View. In L. N. López de Lacalle & A. Lamikiz (Eds.), Machine Tools for High Performance Machining (pp. 1-45). London: Springer London.

Mayer, J. R. R. (2012). Five-axis machine tool calibration by probing a scale enriched reconfigurable uncalibrated master balls artefact. CIRP Annals - Manufacturing Technology, 61(1), 515-518. doi: 10.1016/j.cirp.2012.03.022

Mayer, J. R. R., Rahman, M. M., & Los, A. (2015). An uncalibrated cylindrical indigenous artefact for measuring inter-axis errors of a five-axis machine tool. CIRP Annals - Manufacturing Technology, 64(1), 487-490. doi: http://dx.doi.org/10.1016/j.cirp.2015.04.015

Mchichi, N. A., & Mayer, J. R. R. (2014). Axis Location Errors and Error Motions Calibration for a Five-axis Machine Tool Using the SAMBA Method. Procedia CIRP, 14 305-310. doi: http://dx.doi.org/10.1016/j.procir.2014.03.088

Mir, Y. A., Mayer, J. R. R., & Fortin, C. (2002). Tool path error prediction of a five-axis machine tool with geometric errors. Proceedings of the Institution of Mechanical Engineers, Part B: Journal of Engineering Manufacture, 216 697-712. Retrieved from http://dx.doi.org/10.1243/0954405021520391

Moustafa, S., Gerwien, N., Haertig, F., & Wendt, K. (2009). Comparison of error mapping techniques for coordinate measuring machines using the plate method and laser tracer technique. Paper presented at 19th IMEKO World Congress 2009, September 6, 2009 - September 11, 2009, Lisbon, Portugal (Vol. 4, pp. 2487-2491).

Okafor, A. C., & Ertekin, Y. M. (2000). Vertical machining center accuracy characterization using laser interferometer: Part 1. Linear positional errors. Journal of Materials Processing Technology, 105(3), 394-406. doi: Doi: 10.1016/s0924-0136(00)00661-0

Parkinson, S., Longstaff, A. P., & Fletcher, S. (2014). Automated planning to minimise uncertainty of machine tool calibration. Engineering Applications of Artificial Intelligence, 30(0), 63-72. doi: http://dx.doi.org/10.1016/j.engappai.2014.02.002

Ramesh, R., Mannan, M. A., & Poo, A. N. (2000). Error compensation in machine tools a review: Part I: geometric, cutting-force induced and fixture-dependent errors. International Journal of Machine Tools and Manufacture, 40(9), 1235-1256. Retrieved from http://www.sciencedirect.com/science/article/pii/S0890695500000092

Santolaria, J., & Ginés, M. (2013). Uncertainty estimation in robot kinematic calibration. Robotics and Computer-Integrated Manufacturing, 29(2), 370-384. doi: http://dx.doi.org/10.1016/j.rcim.2012.09.007

Schultschik Oe, R. (1977). Components of the Volumetric accuracy. Manuf Technol, Gen Assem of CIRP, 27th, 26(1 - 2), 223-228.

Schwenke, H., Franke, M., Hannaford, J., & Kunzmann, H. (2005). Error mapping of CMMs and machine tools by a single tracking interferometer. CIRP Annals - Manufacturing Technology, 54(1), 475-478. Retrieved from http://www.sciencedirect.com/science/article/pii/S0007850607601486

Schwenke, H., Knapp, W., Haitjema, H., Weckenmann, A., Schmitt, R., & Delbressine, F. (2008). Geometric error measurement and compensation of machines-An update. CIRP Annals - Manufacturing Technology, 57(2), 660-675. doi: DOI: 10.1016/j.cirp.2008.09.008

Schwenke, H., Schmitt, R., Jatzkowski, P., & Warmann, C. (2009). On-the-fly calibration of linear and rotary axes of machine tools and CMMs using a tracking interferometer. CIRP Annals - Manufacturing Technology, 58(1), 477-480. Retrieved from http://www.sciencedirect.com/science/article/pii/S0007850609000110

Seng Khim, T., & Chin Keong, L. (March 17-19, 2010, MArch 17-19). Modeling the volumetric errors in calibration of five-axis CNC machine. Paper presented at International MultiConference of Enigneers and Computer Scientists, IMECS 2010, Hong Kong (Vol. III).

Viprey, F., Nouira, H., Lavernhe, S., & Tournier, C. (2016). Novel multi-feature bar design for machine tools geometric errors identification. Precision Engineering, 46 323-338. doi: http://dx.doi.org/10.1016/j.precisioneng.2016.06.002

Weikert, S., & Knapp, W. (2004). R-test, a new device for accuracy measurements on five axis machine tools. CIRP Annals - Manufacturing Technology, 53(1), 429-432.

Zargarbashi, S. H. H., & Mayer, J. R. R. (2009). Single setup estimation of a five-axis machine tool eight link errors by programmed end point constraint and on the fly measurement with Capball sensor. International Journal of Machine Tools and Manufacture, 49(Compendex), 759-766. Retrieved from http://dx.doi.org/10.1016/j.ijmachtools.2009.05.001